Relevance of the phosphatase subunit PR130 for checkpoint kinase signaling

Dissertation

zur Erlangung des Grades

„Doktor der Naturwissenschaften“

im Promotionsfach Chemie

am Fachbereich Chemie, Pharmazie,

Geografie und Geowissenschaften

der Johannes Gutenberg-Universität Mainz

Melanie Woods

[redacted]

Mainz, 2024

1. Betreuer: [redacted]
2. Betreuer: [redacted]

1 Curriculum vitae

Personal Details

[redacted]

Education

[redacted]

Publications

- **Dzulko M**, Pons M, Henke A, Schneider G, Krämer OH. *The PP2A subunit PR130 is a key regulator of cell development and oncogenic transformation*. Biochim Biophys Acta Rev Cancer. 2020 Dec;1874(2):188453.

- Nguyen A, **Dzulko M**, Murr J, Yen Y, Schneider G, Krämer OH. *Class 1 Histone Deacetylases and Ataxia-Telangiectasia Mutated Kinase Control the Survival of Murine Pancreatic Cancer Cells upon dNTP Depletion*. Cells. 2021 Sep 23;10(10):2520.

- Wachholz V, Mustafa AM, Zeyn Y, Henninger SJ, Beyer M, **Dzulko M**, Piée-Staffa A, Brachetti C, Haehnel PS, Sellmer A, Mahboobi S, Kindler T, Brenner W, Nikolova T, Krämer OH. *Inhibitors of class I HDACs and of FLT3 combine synergistically against leukemia cells with mutant FLT3*. Arch Toxicol. 2022 Jan;96(1):177-193.

2 Abbreviations

Abbreviation	Name
(γ)H2AX	(pS139)-Histone 2A variant
53BP1	p53 Binding Protein
AIF	Apoptosis-Inducing Factor
APAF-1	Apoptotic Protease-Activating Factor-1
APC	Adenomatous Polyposis Coli
APS	Ammonium Persulfate
Ara-C	Cytarabine
ATM	Ataxia-Telangiectasia Mutated
ATMi	ATM inhibitor
ATR	Ataxia-Telangiectasia Mutated and RAD3-related
ATRi	ATR inhibitor
ATRIP	ATR-Interacting Protein
Bcl-2	B-cell lymphoma protein 2
BRCA1/2	Breast Cancer 1/2
BSA	Bovine Serum Albumin
CAK	CDK-Activating Kinase
CBP	CREB Binding Protein
Cdc25	Cell division cycle 25
Cdc6	Cell division control 6 protein
CDK	Cyclin-Dependent Kinase
CDK2i	CDK2 inhibitor
CHK1	Checkpoint Kinase 1
CHK1i	CHK1 inhibitor
CHK2	Checkpoint Kinase 2
CK1	Casein Kinase 1

CREB	cAMP-Response Element Binding protein
CtIP	CtBP-Interacting Protein
Ctrl	Control/untreated
dATP	deoxyadenosine triphosphate
DDR	DNA Damage Response
dHJ	double Holliday junction
DMEM	Dulbecco’s Modified Eagle’s Medium
DNA	Deoxyribonucleic Acid
DNA-PKcs	DNA-dependent Protein Kinase (catalytic subunit)
dNTPs	Deoxyribonucleotide(s)
DSB	DNA Double Strand Break/Double-Stranded DNA break
dsDNA	double stranded DNA
DTT	Dithiothreitol
E. coli	Escherichia coli
ECL	Enhanced Chemiluminescence
EDTA	Ethylenediaminetetraacetic Acid
EGFR	Epidermal Growth Factor Receptor
EtOH	Ethanol
FADD	Fas-Associated protein with Death Domain
FasR	Fas Receptor
FAT(C)	FRAP-ATM-TRRAP (carboxy-terminal)
FCS	Fetal Calf Serum
FITC	Fluorescein Isothiocyanate
FSC	Forward Scatter
G	Gap
GCN5	General Control of Nuclear-5-related N-acetyl transferase
GSK3β	Glycogen Synthase Kinase 3β

H	Histone
h	Hour
HA	Hemagglutinin
HAT	Histone Acetyltransferase
HCl	Hydrochloric acid
HDAC	Histone Deacetylase
HDACi	Histone Deacetylase Inhibitor
HEAT	Huntington-Elongation factor 3-protein phosphatase 2A-TOR1
HEPES	Hydroxyethyl Piperazineethanesulfonic acid
HR	Homologous Recombination
HRP	Horseradish Peroxidase
HSP90	Heat Shock Protein 90
HtrA2	High temperature requirement A2
HU	Hydroxyurea
IAP	Inhibitor of Apoptosis Protein
IN	Input
IP	Immunoprecipitation
kDa	Kilodalton
KU	KU-60019
LPP	LIM-protein Lipoma Preferred Partner
Lys (K)	Lysine residue
M	Mitosis
MDC1	Mediator of DNA Damage Checkpoint 1
MDM2	Mouse Double Minute 2
min	minute
miRNA	microRNA
MK	MK-8776/MK-1775

MOZ	Monocytic leukemia Zinc-finger protein
MRN	MRE11-RAD50-NBS1
Ms	Mouse
MYC	Myelocytomatosis
NAD^+	Nicotinamide Adenine Dinucleotide
NBS1	Nijmegen Breakage Syndrome 1
NHEJ	Non-Homologous End-Joining
NKD	Naked cuticle
ORC	Origin Recognition Complex
PBS	Phosphate-Buffered Saline
Pen/Strep	Penicillin/Streptomycin
PFA	Paraformaldehyde
PI	Propidium Iodide
PP2A	Protein Phosphatase 2A
Pre	Pre-immune serum
Rb	Rabbit
RB	Retinoblastoma protein
RIF1	Replication Timing Regulatory Factor 1
RNA	Ribonucleic acid
RNAi	RNA interference
RNAse	Ribonuclease
RNF	Ring Finger protein
RNR	Ribonucleotide Reductase
ROS	Reactive Oxygen Species
RPA	Replication Protein A
RS	Replicative Stress/Replication Stress
RT	Room Temperature

SAS3/2	Something About Silencing 3/2
SCAI	Suppressor of Cancer cell Invasion
SD	Standard Deviation
SDS	Sodium Dodecyl Sulfate
SDSA	Synthesis-Dependent Strand Annealing
SDS-PAGE	Sodium Dodecyl Sulphate Polyacrylamide Gel Electrophoresis
SEM	Standard Error of Mean
Ser/Thr (S/T)	Serine/Threonine residues
SHIP1/2	Src-Homology domain-containing Inositol Polyphosphate 5'-phosphatase 1 and 2
shRNA	small hairpin RNA
siRNA	small interfering RNA
SIRT	Sirtuins
Smac/DIABLO	Second mitochondria-derived activator of caspase/Direct Inhibitor of Apoptosis Protein (IAP)-Binding protein with Low pI
SMAPs	Small-Molecule Activators of PP2A
SRC	Steroid Receptor Coactivators
SSB	Single Strand Break
SSC	Side Scatter
ssDNA	single stranded DNA
TEMED	Tetramethylethylenediamine
TIP60	Tat-Interactive Protein 60
TNF-R	TNF receptor
TNF-α	Tumor Necrosis Factor-α
TopBP1	Topoisomerase II-Binding Protein
TRADD	TNF Receptor type 1 Associated Death Domain protein

Tyr (Y)	Tyrosine residue
US FDA	United States Food and Drug Administration
VE	VE-821
wt	wild-type
XRCC4	X-ray cross-complementing protein 4
YBF2	Yeast Binding Factor 2
Zn^{2+}	Zinc

3 Abstract

Cancer cells depend on continuous cell proliferation and efficient cell cycle checkpoints to prevent the induction of cell death. In the clinic, there are different strategies to eliminate cancer cells effectively. The strong dependence on cell proliferation can be exploited by inhibition of Cyclin-Dependent Kinases (CDKs), the main drivers of cell cycle progression, which force cancer cells into cell cycle arrest. In this context, the two CDK inhibitors WEE1 and p21 play a major role by regulating CDK activity. Another method is the induction of replication stress since cancer cells are very susceptible to it due to their fast cell division rate. Sensing replication stress and DNA damage involves phosphorylation and therefore activation of the checkpoint kinases Ataxia telangiectasia mutated (ATM), ATM and RAD3-related (ATR), Checkpoint Kinase 2 (CHK2) and CHK1, which slow down the cell cycle and initiate Deoxyribonucleic Acid (DNA) repair, or if the damage cannot be repaired, induce apoptosis.

Phosphorylation and acetylation are posttranslational modifications, which control not only signaling pathways but also gene expression. The two histone deacetylases (HDAC), HDAC1 and HDAC2, have been found to control the expression of the Protein Phosphatase 2A (PP2A) B-type subunit PR130, which is involved in the regulation of various cellular processes such as DNA repair, apoptosis, cell proliferation and autophagy. Moreover, the PP2A-PR130 complex plays an important role in the DNA damage response since it deactivates ATM via dephosphorylation of S1981 upon replication stress. Recent studies showed that colorectal cancer cells devoid of PR130 had higher levels of pCHK1 and arrested earlier at the G1/S phase boundary than wild-type cells upon replication stress. Combinatorial treatment with the HDAC inhibitor (HDACi) entinostat, however, reduced phosphorylation of CHK1 independent of the PR130 status of the cells. This shows that the PP2A-PR130 complex is indirectly involved in the regulation of CHK1 phosphorylation.

In this thesis it was investigated how CHK1 phosphorylation is controlled by PR130 and HDACi. Proteome and RNA sequencing analyses revealed higher levels of the cell cycle regulator p21 in PR130-deficient cells compared to wild-type cells. Moreover, it was shown that the ATM-p53-axis controls the expression of p21. Additionally, class I HDACi increased levels of p21, which binds and deactivates CDK2, leading to diminished CHK1 phosphorylation upon replication stress. Furthermore, two novel targets of the PP2A-PR130 complex, pp21-S130 and pWEE1-T190, were identified. Both proteins are directly connected to higher CDK2 activity: pp21-S130 cannot bind to CDK2 and pWEE1-T190 is not able to phosphorylate it. The results showed that PR130 controls CHK1

phosphorylation twofold, on a transcriptional level via p21 and by posttranslational modifications via dephosphorylation of pp21-S130 and pWEE1-T190.

Furthermore, it was shown that class I HDACi dysregulate DNA repair proteins important for homologous recombination, thereby promoting non-homologous end-joining, resulting in Replication Timing Regulatory Factor 1 (RIF1) foci formation in a PR130-dependent manner. This gives new insights into how HDACi and PR130 control the DNA repair pathway choice upon DNA replication stress.

All in all, the results demonstrate that the PP2A-PR130 complex is a key player in cell cycle regulation, DNA damage signaling and DNA repair pathways. This versatility explains the frequent mutation of the B-type subunit in cancer and underlines it as a potentially interesting target in clinical research.

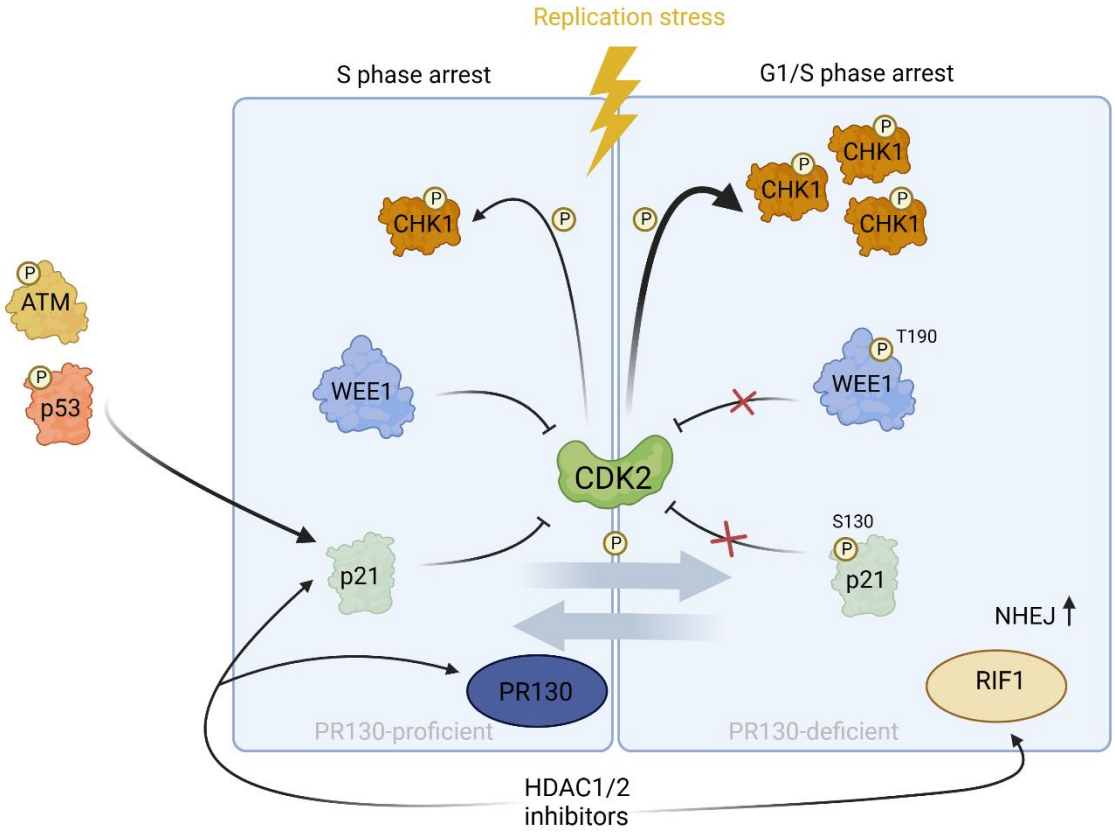

4 Zusammenfassung

Krebszellen sind auf eine kontinuierliche Zellvermehrung und effiziente Zellzykluskontrollpunkte angewiesen, um den Zelltod zu verhindern. In der Klinik gibt es verschiedene Strategien, um Krebszellen wirksam zu eliminieren. Die starke Abhängigkeit von der Zellproliferation kann durch die Hemmung von Cyclin-abhängigen Kinasen (CDKs), den Haupttreibern der Zellzyklusprogression, ausgenutzt werden, wodurch Krebszellen in einen Zellzyklusstillstand gezwungen werden. In diesem Zusammenhang spielen die beiden CDK-Inhibitoren, WEE1 und p21, eine wichtige Rolle, da sie die CDK-Aktivität regulieren. Eine weitere Methode ist die Induktion von Replikationsstress, da Krebszellen aufgrund ihrer schnellen Zellteilungsrate sehr empfindlich sind. Das Erkennen von Replikationsstress und Desoxyribonukleinsäure (DNA)-Schäden beinhaltet die Phosphorylierung und damit die Aktivierung der Checkpoint-Kinasen *Ataxia telangiectasia mutated* (ATM), *ATM and RAD3-related* (ATR), Checkpoint-Kinase 2 (CHK2) und CHK1, die den Zellzyklus verlangsamen und die DNA-Reparatur einleiten oder, wenn der Schaden nicht repariert werden kann, die Apoptose induzieren.

Phosphorylierung und Acetylierung sind posttranslationale Modifikationen, die nicht nur Signalwege, sondern auch Genexpression steuern. Es wurde festgestellt, dass die beiden Histondeacetylasen (HDAC) HDAC1 und HDAC2 die Expression der Protein-Phosphatase 2A (PP2A)-Untereinheit, PR130, steuern, welche an der Regulierung verschiedener zellulärer Prozesse wie DNA-Reparatur, Apoptose, Zellproliferation und Autophagie beteiligt ist. Darüber hinaus spielt der PP2A-PR130-Komplex eine wichtige Rolle bei der Reaktion auf DNA-Schäden, da er bei Replikationsstress ATM durch Dephosphorylierung von S1981 deaktiviert. Jüngste Studien haben gezeigt, dass Darmkrebszellen ohne PR130 höhere pCHK1-Werte aufweisen und bei Replikationsstress früher an der G1/S-Phasengrenze zum Stillstand kommen als Wildtypzellen. Eine kombinatorische Behandlung mit dem HDAC-Inhibitor (HDACi) Entinostat reduzierte jedoch die Phosphorylierung von CHK1 unabhängig vom PR130-Status der Zellen. Dies zeigt, dass der PP2A-PR130-Komplex indirekt an der Regulierung der CHK1-Phosphorylierung beteiligt ist.

In dieser Arbeit wurde untersucht, wie die CHK1-Phosphorylierung durch PR130 und HDACi gesteuert wird. Proteom- und RNA-Sequenzierungsanalysen ergaben, dass der Zellzyklusregulator p21 in PR130-defizienten Zellen im Vergleich zu Wildtyp-Zellen erhöht ist. Außerdem wurde gezeigt, dass die ATM-p53-Achse die Expression von p21 kontrolliert. Darüber hinaus erhöhten Klasse-I-HDACi die Konzentration von p21, welches CDK2 bindet und deaktiviert, was zu einer verminderten CHK1-Phosphorylierung bei

Replikationsstress führt. Ebenfalls wurden zwei neue Targets des PP2A-PR130-Komplexes, pp21-S130 und pWEE1-T190, identifiziert. Beide Proteine stehen in direktem Zusammenhang mit einer höheren CDK2-Aktivität: pp21-S130 kann nicht an CDK2 binden und pWEE1-T190 ist nicht in der Lage, es zu phosphorylieren. Die Ergebnisse zeigten, dass PR130 die CHK1-Phosphorylierung in zweifacher Weise kontrolliert, auf transkriptioneller Ebene über p21 und durch posttranslationale Modifikationen über die Dephosphorylierung von pp21-S130 und pWEE1-T190.

Darüber hinaus konnte gezeigt werden, dass HDACi der Klasse I DNA-Reparaturproteine, die für die homologe Rekombination wichtig sind, deregulieren und dadurch die nicht-homologe Endverknüpfung fördern, was zur Bildung von Replikationszeitpunkt Regulatorischer Faktor 1 (RIF1)-Foci in einer PR130-abhängigen Weise führt. Dies liefert neue Erkenntnisse darüber, wie HDACi und PR130 die Wahl des DNA-Reparaturweges nach DNA-Replikationsstress kontrollieren.

Alles in allem zeigen die Ergebnisse, dass der PP2A-PR130-Komplex eine Schlüsselrolle bei der Regulierung des Zellzyklus, der DNA-Schadensantwort und bei DNA-Reparaturmechanismen spielt. Diese Vielseitigkeit erklärt die häufige Mutation der Untereinheit bei Krebs und unterstreicht, dass sie ein potenziell interessantes Ziel für die klinische Forschung darstellt.

Table of contents

1 Introduction

The world population's average age increases from year to year. In 2050, more than 20% of the people will be older than 60 years. For this reason, diseases like cancer, which mainly affect older human beings, increasingly get into the focus of our healthcare system (Fane and Weeraratna 2020).

According to D. Hanahan and R. Weinberg, cancer cells are characterized by common features, the so-called hallmarks of cancer (Figure 1.1) (Hanahan and Weinberg 2000, Hanahan and Weinberg 2011, Hanahan 2022).

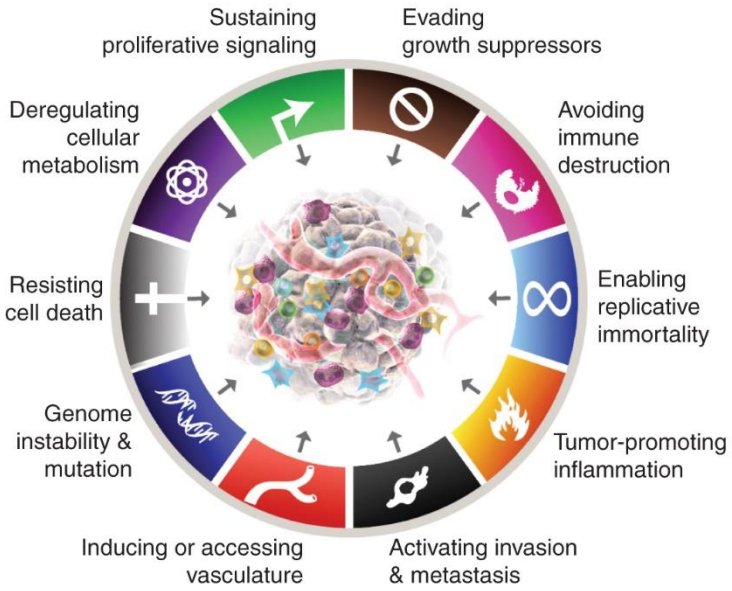

Figure 1.1: Hallmarks of cancer defined by Hanahan and Weinberg (Hanahan 2022).

Cells rely on the maintenance of genomic stability to ensure the correct transmission of their genetic material (Matos-Rodrigues et al. 2020). Whereas normal cells have various control mechanisms regarding their growth and division, cancer cells often have defects in those. During cell cycle progression, cell cycle checkpoints should prevent replication of genetic errors, which can lead to cancer development. In cancer cells however, these control mechanisms are often perturbed allowing uncontrolled division, which results in genomic instability (Matthews et al. 2022). From a clinical point of view, it is important to understand basic signaling pathways and protein networks in more detail to allow development of novel, precise cancer treatment options.

1.1 The DNA damage response

The Deoxyribonucleic Acid (DNA) Damage Response (DDR) allows cells to react to various exogenous (e.g., UV light, ionizing radiation, chemicals) and endogenous (e.g., replication errors, oxidative damage by reactive oxygen species) stimuli causing DNA damage (Chatterjee and Walker 2017, Gasser and Raulet 2006). As a consequence, cells arrest in their cell cycle (see chapter 1.2) and decide whether they can repair the damaged DNA (see chapter 1.3). If the damage level is too high, cells instead undergo apoptosis (see chapter 1.4) to prevent replication of genetic errors (Gasser and Raulet 2006).

The three serine (S)/threonine (T) kinases Ataxia telangiectasia mutated (ATM), ATM and RAD3-related (ATR), and DNA-dependent protein kinase catalytic subunit (DNA-PKcs) play a central role during the DDR. They are similar in their structure but are activated upon different types of DNA damage. While ATM and DNA-PKcs get activated by binding to ends of double-stranded DNA breaks (DSBs), ATR is activated by single-stranded DNA (ssDNA; upon DNA damage also known as SSBs) bound to Replication Protein A (RPA) (Figure 1.2). All three kinases prefer to phosphorylate S/T sites adjacent to glutamine (Fedak et al. 2021, Goodwin and Knudsen 2014).

To better understand the activity of the three kinases, it is necessary to take a closer look at their structure. ATM, ATR, and DNA-PK consist of Huntington-Elongation factor 3-protein phosphatase 2A-TOR1 (HEAT) repeats and a kinase domain enclosed by a FRAP-ATM-TRRAP (FAT) and FAT carboxy-terminal (FATC) domain. HEAT repeats mediate interactions with proteins that regulate kinase activity in case of ATM Nijmegen Breakage Syndrome 1 (NBS1), in case of ATR ATR-Interacting Protein (ATRIP) and in case of DNA-PKcs KU70 and KU80 (Maréchal and Zou 2013, Blackford and Jackson 2017).

In the absence of DNA damage, the FAT and kinase domains of ATM interact with each other, preventing ATM activity (Bakkenist and Kastan 2003). Upon DNA damage, the MRE11-RAD50-NBS1 (MRN) complex acts as a DSB sensor and recruits ATM to the DNA breaks (Uziel et al. 2003, Lee and Paull 2005). This leads to ATM autophosphorylation at S1981 (located near the FAT domain) and dissociation of the ATM homodimer resulting in activation of the kinase (Bakkenist and Kastan 2003). ATM is further activated by binding of the Histone Acetyltransferase (HAT) Tat-Interactive Protein 60 (TIP60) to its FATC domain resulting in its acetylation at lysine 3016 (Schleicher et al. 2022, Maréchal and Zou 2013, Sun et al. 2007). Nevertheless, ATM can also be activated independent of the MRN complex. Upon treatment with the replication stress inducer hydroxyurea (HU) or UV irradiation, it was found that ATR

phosphorylates ATM at S1981. This stimulated phosphorylation of Checkpoint Kinase 2 (CHK2) and G2/M phase arrest (Stiff et al. 2006). Treatment with Reactive Oxygen Species (ROS) increased phosphorylation of ATM as well without need of the MRN complex (Paull 2015).

Autophosphorylation of ATR at T1989 within its FAT domain stimulates Topoisomerase II-Binding Protein 1 (TopBP1) binding and kinase activation (Liu et al. 2011). Furthermore, ATR forms a complex with ATRIP, which is essential for ATR activation through ATRIP-mediated stabilization of ATR (Cortez et al. 2001). This promotes its localization to RPA-ssDNA (Zou and Elledge 2003). ATRIP further contains a TopBP1-interacting region, which mediates interaction between TopBP1 and ATR (Mordes et al. 2008). DNA-PKcs has multiple autophosphorylation sites, which are mainly located within the HEAT repeats. Phosphorylation at T3950 activates kinase activity. However, S2056 and T2609 phosphorylation are not important for activation but are more involved in DNA repair (Blackford and Jackson 2017).

Activated ATM phosphorylates a variety of substrates, such as CHK2, p53 (encoded by the *TP53* gene), and Histone 2A variant (H2AX) and is mainly involved in activation of the G1/S checkpoint (Figure 1.2). Phosphorylation of CHK2 at T68 stimulates its dimerization and activation. Active CHK2 phosphorylates the kinases Cell division cycle 25 a (Cdc25a) and c (Cdc25c) leading to their inactivation and thereby cell cycle arrest by inhibition of Cyclin-Dependent Kinase (CDK) activity (see chapter 1.2). CHK2, as well as ATM, ATR and CHK1 phosphorylate p53 at S15 and S20 causing p53 stabilization and activation through inactivation of the ubiquitin ligase Mouse Double Minute 2 (MDM2). Active p53 promotes transcription of p21 (encoded by the *CDKN1A* gene) and the pro-apoptotic genes *PUMA*, *NOXA*, *BAX* and *APAF-1* (Smith et al. 2020). Phosphorylation of H2AX at S139 (γH2AX) is propagated by Mediator of DNA Damage Checkpoint 1 (MDC1), which directly interacts with γH2AX, and leads to the formation of γH2AX foci (Ruff et al. 2020). Phosphorylation of H2AX promotes histone unwinding, which allows repair of damaged DNA by enabling better access of repair proteins (Fedak et al. 2021). Through phosphorylation of p53-binding protein 1 (53BP1), ATM is involved in the induction of the DSB repair pathway Non-Homologous End-Joining (NHEJ). However, it also controls phosphorylation of Breast Cancer 1 (BRCA1), MRE11, and the endonuclease CtBP-Interacting Protein (CtIP), which are important for Homologous Recombination (HR) (Smith et al. 2020, Wang et al. 2021, Kijas et al. 2015).

ATR activation plays a crucial role especially during S and G2/M phase. Upon replication stress and DNA damage, ATR phosphorylates CHK1 at S345 and S317 causing autophosphorylation at S296 and thereby full activation of the checkpoint kinase (Figure

1.2) (Smith et al. 2020, Zhao and Piwnica-Worms 2001). However, this activation depends on the adaptor protein claspin, which is phosphorylated by ATR and recruits inactive CHK1 in close proximity to the DDR kinase (Kumagai and Dunphy 2000, Smits et al. 2019). The replication stress response only occurs during S phase and should prevent induction of DNA damage and entry of damaged cells into mitosis. The endonuclease MUS81 forms heterodimeric complexes with EME1/EME2 and recognizes branched DNA structures, which occur during replication or HR. CDK1 and CDK2 activate MUS81-EME1/2 complexes to recover stalled replication forks. Upon DNA damage, the WEE1 kinase protects replication forks as it phosphorylates both CDKs to prevent activation of the endonuclease. Loss of WEE1 activity results in a slowed replication progression and an increased genomic instability (Di Ghelli Luserna Rorà et al. 2020, Martín et al. 2011). Activated CHK1 phosphorylates and inactivates Cdc25a and Cdc25c resulting in their proteasomal degradation, and phosphorylates and activates WEE1 resulting in inhibitory CDK1 phosphorylation (Sanchez et al. 1997, Smith et al. 2020). ATR, CHK1 and WEE1 are mainly involved in HR. ATR promotes the recruitment of RAD51 to DSBs in a BRCA-independent manner. Moreover, CHK1 phosphorylates RAD51 and BRAC2 (Smith et al. 2020). Both CHK1 and WEE1 inhibition cause an accumulation of DNA breaks and a slowed replication fork speed and were thought to act in the same manner. However, a combinatorial treatment with CHK1i and WEE1i shows additive effects suggesting that both proteins have different roles during replication (Martín et al. 2011).

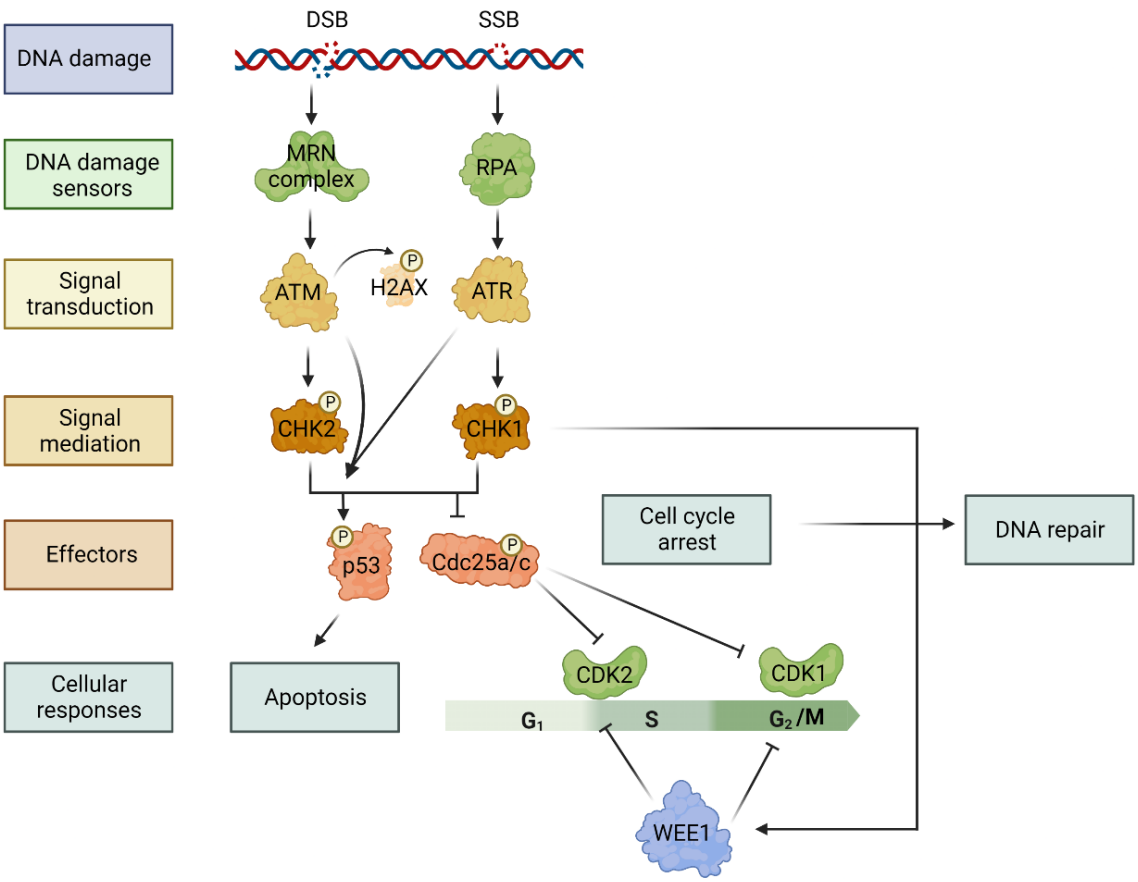

Figure 1.2: Scheme of the DNA damage response. ATM and ATR are activated by DSBs or SSBs and phosphorylate a variety of targets resulting in cell cycle arrest and DNA repair or apoptosis. Figure created with BioRender (Aleem and Arceci 2015, Jackson et al. 2018, Li et al. 2013, Smith et al. 2020).

For DNA-PK-promoted NHEJ, KU binds to the DSB, which recruits DNA-PKcs and subsequently proteins such as Artemis, DNA ligase IV and X-ray repair cross-complementing protein 4 (XRCC4), which play a major role for NHEJ-dependent DNA-end ligation (Blackford and Jackson 2017).

The complex regulation of the DDR is necessary to allow cells to respond to stress and guarantee subsequent cell cycle progression.

1.2 Cell cycle control

Every dividing cell undergoes a tightly regulated cell cycle. This cell cycle is divided into four major phases (Figure 1.3). During the synthesis (S) phase, DNA replication occurs. Throughout the mitosis (M) phase, cells divide into two identical daughter cells. The two gap (G) phases, G1- and G2, separate S and M phases and are key periods for cell cycle regulation (Matthews et al. 2022). Checkpoints at the borders from G1 to S and G2 to M phases are necessary to react to various exogenous and endogenous stimuli causing potential errors in the DNA (Matthews et al. 2022, Chatterjee and Walker 2017). During the G1 phase, cells can also exit into a non-proliferative, quiescent state (G0). Cancer cells are characterized by an abnormal cell division behavior, primarily caused by inhibition of apoptosis, errors in cell cycle exit, or dysregulated cell cycle regulator proteins in these cells (Matthews et al. 2022, Suski et al. 2021).

The main cell cycle regulators, which push cells from one cell cycle phase to the next one, are CDKs. CDKs are S/T kinases, which form complexes with cell cycle phase-specific cyclins (Schafer 1998). Complex formation leads to a conformational change of residues responsible for ATP binding. This results in CDK activation and stimulates cell cycle entry, progression or completion (Malumbres 2014, Matthews et al. 2022). CDKs important for cell cycle regulation are CDK4, CDK6, CDK2 and CDK1. Additionally, there are other CDKs, which carry out transcriptional (CDK7, CDK8, and CDK9) or post-mitotic (CDK5) functions (Asghar et al. 2015).

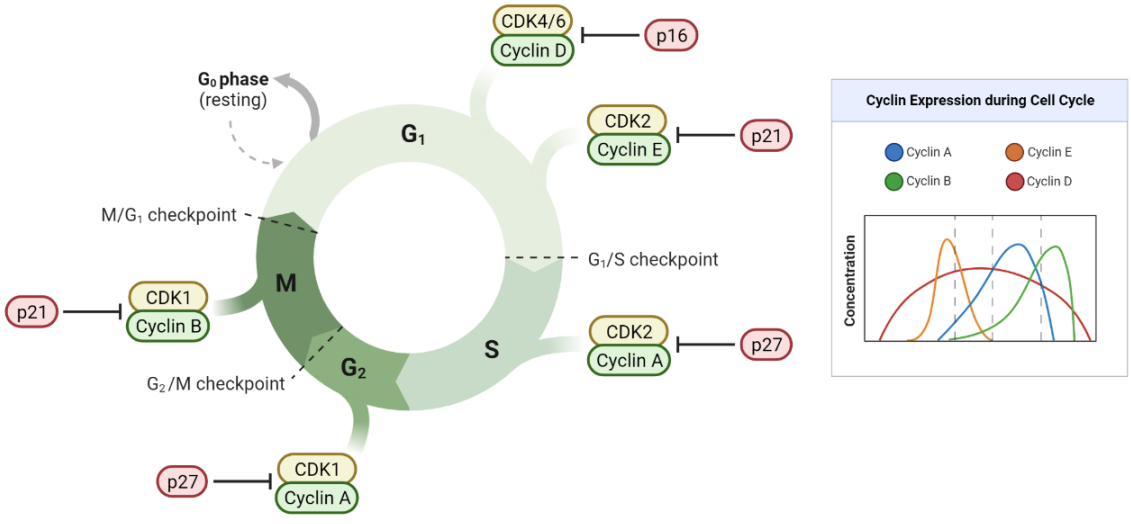

Figure 1.3: The cell cycle and its regulators. The cell cycle consists of the four major phases G1, S, G2, and M. CDKs together with their cell cycle phase-specific cyclins drive the cells into the next cell cycle phase. Inhibitors of the CIP/KIP or the INK4 family (p21, p16, p27) regulate the activity of CDK-cyclin complexes. Figure was created using BioRender. Modified after Yang (2018) and García-Osta et al. (2022).

Whereas levels of CDKs remain quite constant, levels of cyclins differ during the cell cycle phases, which allows specific activation of CDKs needed in each phase (Morgan 1995). Cyclins contain a PEST sequence, which targets them for ubiquitination. Before entering the next cell cycle phase, cyclins not needed anymore get degraded by the proteasome and the synthesis of the next cell cycle phase-specific cyclin starts (Schafer 1998). During G1 phase, D-type cyclins (D1, D2, D3) are upregulated and bind to CDK4 or CDK6. These complexes are stabilized by proteins of the CIP/KIP family such as $p21^{CIP1}$, $p27^{KIP1}$ and $p57^{KIP2}$. However, proteins of the INK4 family ($p16^{INK4A}$, $p15^{INK4B}$, $p18^{INK4C}$, $p19^{INK4D}$) inhibit the activity of CDK4/6-cyclin D complexes (Suski et al. 2021, Sherr and Roberts 2004). To promote cell cycle progression, CDK4/6-cyclin D complexes phosphorylate Retinoblastoma protein (Rb) causing dissociation of Rb from transcription factor E2F. E2F stimulates transcription of genes, which are important for DNA synthesis, and also leads to an increase in cyclin E levels at the end of the G1 phase, resulting in activation of CDK2 (Bertoli et al. 2013). CDK2-cyclin E complexes hyperphosphorylate Rb further and drive cells into the S phase (Sherr and Roberts 1999). While cyclin E levels decrease with progressing replication, cyclin A levels increase at the same time. Cyclin A can activate CDK2 as well as CDK1 and is therefore not only important during the S phase, but also for the transition from the G2 to M phase as it activates cyclin B complexes (Martínez-Alonso and Malumbres 2020). CDK2-cyclin A complexes stimulate the transcription factor FOXM1, which is essential for the transcription of mitotic genes (Lim and Kaldis 2013). Proteins of the CIP/KIP family inhibit CDK2 and CDK1 complexes (Malumbres 2014, Sherr and Roberts 2004). Upon DNA damage, activation of p53 increases levels of p21. Binding of p21 to CDKs inactivates their kinase activity. Therefore, unphosphorylated Rb still binds to E2F, which prevents cell cycle progression from the G1 to S phase (Matthews et al. 2022).

To understand CDK-mediated cell cycle progression in more detail, it is necessary to have a closer look on CDK regulation. CDKs are regulated by different mechanisms such as phosphorylation on threonine and tyrosine residues, or as already mentioned, binding of cyclins and cyclin-dependent kinase inhibitors of the CIP/KIP or INK4 family (Schafer 1998). Important CDK-regulators are proteins of the WEE1 family, which consists of the three different S/T kinases WEE1, PKMYT1 and WEE2. WEE1 and PKMYT1 are mainly connected to mitosis and, especially WEE1, more recently to regulation of replication. WEE2 plays a major role during meiosis. The WEE1 kinase is located in the nucleus, the PKMYT1 kinase in the endoplasmic reticulum and the Golgi apparatus (Di Ghelli Luserna Rorà et al. 2020). Both proteins regulate CDK1 activity via an inhibitory phosphorylation at tyrosine (Y) 15 and T14 thereby reducing its substrate affinity, which stops cell cycle progression. WEE1 additionally phosphorylates CDK2 at Y15 (Di Ghelli Luserna Rorà et

al. 2020). However, inhibitory phosphorylation of CDK1 and CDK2 can be counteracted by different isoforms of the Cdc25 phosphatase (Malumbres 2014, Elbæk et al. 2020). Cdc25a and b are important for G1 to S phase transition, whereas Cdc25c plays a major role for G2 to M phase transition (Sur and Agrawal 2016, Smith et al. 2020). Moreover, the CDK-Activating Kinase (CAK) complex, comprising the proteins CDK7, cyclin H1 and MAT1, phosphorylates CDK1 at T161. Cyclin B1 activates CDK1 further via phosphorylation, leading to nuclear import of the complex and the beginning of mitosis (Di Ghelli Luserna Rorà et al. 2020). Besides that, CDK1 has a feedback mechanism to inhibit WEE1 and Cdc25 activity (Ferrell et al. 2009). Phosphorylation of WEE1 at S123 results in binding of polo like kinase 1 and casein kinase 2, which phosphorylate the kinase further and tag it for degradation by the ubiquitin ligase $SCF^{\beta\text{-}TrCP}$ (Di Ghelli Luserna Rorà et al. 2020).

Beside cell cycle regulation, CDKs and cyclins also play a role in the repair of damaged DNA. Cyclin E1 accumulates at stalled replication forks to impede Cell division control 6 protein (Cdc6) dissociation, and thereby enhances activation of CHK1 (Lu et al. 2009). Moreover, using the yeast model *Saccharomyces cerevisiae* it was found that CDK1 phosphorylates the nucleases Dna2 and Sae2, which triggers their recruitment to DSBs and initiates HR (Chen et al. 2011, Huertas et al. 2008). Additionally, BRCA2-dependent cyclin D1 recruitment induces recruitment of RAD51 to DSBs, which also triggers HR (Jirawatnotai et al. 2011). Another study showed that CDK2 phosphorylates Werner syndrome protein at S426, which stabilizes its affinity for RPA and causes a switch from NHEJ to HR (Lee et al. 2021). Complexes of CDK2/cyclin A as well as CDK1/cyclin B were also found to phosphorylate BRCA2 at S3291, which is necessary for RAD51 binding (Satyanarayana and Kaldis 2009).

1.3 Repair mechanisms

DSBs are formed if both strands of the DNA double-helix are broken (Chapman et al. 2012). They are difficult to handle because the cells do not have a correct template to repair the damaged DNA. Considering that genomic stability is extremely important for cells, unrepaired DSBs have a large impact on the maintenance of DNA stability. For this reason, cells choose between two major repair mechanisms (Figure 1.4) to handle the damage: HR or NHEJ (Lieber 2010). NHEJ is the main pathway because it occurs cell cycle independent in dividing and not-dividing cells. However, it is favored in the G1 phase. HR only takes place during S or G2/M phase, since it needs an identical sister chromatid as a template for repair (Helleday et al. 2007, Chapman et al. 2012). Whereas HR is mostly error-free and the more accurate repair mechanism, NHEJ is faster, but often mutagenic (Mao et al. 2008). The interplay between the two proteins 53BP1 and BRCA1 has been identified as a mechanism to decide whether the cells repair via the HR or NHEJ pathway (Escribano-Díaz et al. 2013).

1.3.1 Homologous Recombination

The initial step of HR is DNA end resection to create 3’ ssDNA overhangs at the site of the DSB. Hereby, the MRN complex plays a major role as it recognizes the break and recruits the co-factor CtIP (in case of short-range resection) stimulating the endonuclease activity of the MRN complex. The nucleases EXO1 and DNA2 are required for long-range resection. To protect ssDNA from degradation, the overhangs are rapidly coated by RPA (Escribano-Díaz et al. 2013). BRCA1 and BRCA2 facilitate loading of RAD51 onto the ssDNA, which leads to the formation of a presynaptic filament. This filament searches for a homologous dsDNA and mediates pairing with the ssDNA forming a D-loop. The synthesis of the new strand is carried out by DNA polymerases, which extend the invading 3’ end of the ssDNA and synthesize a new strand using the homologous dsDNA as a template. The D-loop is stabilized by the formation of a Holliday junction, linking the ssDNA with the homologous dsDNA (Ranjha et al. 2018). To resolve the Holliday junction, there are two different pathways: the Synthesis-Dependent Strand Annealing (SDSA) pathway leading to non-crossover products or the double Holliday junction (dHJ) pathway resulting in crossover or non-crossover products. HR creates a precisely repaired DSB (Brandsma and Gent 2012).

1.3.2 Non-Homologous End-Joining

NHEJ is only active if the DSB ends are minimally processed (Escribano-Díaz et al. 2013). For initiation of NHEJ, the KU heterodimer binds to the ends of the DSB to stabilize the break and protect the ends from exonucleases. Afterwards, DNA-PKcs is recruited, which activates the XRCC4 ligase (Ackerson et al. 2021, Chang et al. 2017). If the DNA ends are blunt, XRCC4 and DNA ligase IV bind to and directly ligate the ends. If 5' or 3' DNA overhangs are present, DNA-PKcs activates the endonuclease Artemis, which removes overhangs before the ligation step. Another mechanism for incompatible 3' ends is the activity of the polymerases Pol μ and Pol λ which are recruited to the KU-DNA complex. Whereas Pol μ primarily works template-independent and adds nucleotides to generate regions of microhomology, Pol λ needs a template to fulfill its task. Other NHEJ factors such as XRCC4-like factor (XLF) or paralogue of XRCC4 and XLF (PAXX) share structural similarity to XRCC4 and support the ligation by ligase IV (Chang et al. 2017). One key player that promotes NHEJ is 53BP1 (Lei et al. 2022). Upon DSBs, the MRN complex phosphorylates ATM, which itself phosphorylates H2AX at S139. This leads to the formation of γH2AX foci at the damage site and recruitment of MDC1, E3 ubiquitin ligase Ring Finger protein (RNF) 8 and RNF168. Together with E2 ubiquitin-conjugation enzyme, RNF8 and RNF168 ubiquitinate H2AX, which allows binding of 53BP1 and leads to 53BP1 foci formation (Lei et al. 2022). Phosphorylation of 53BP1 by ATM results in recruitment of Replication Timing Regulatory Factor 1 (RIF1) and the Shieldin complex. This prevents accumulation of BRCA1 and leads consequently to protection of the DNA ends from resection. Therefore, 53BP1 and BRCA1 are important key players for the decision between the two repair mechanisms (Lei et al. 2022, Isobe et al. 2021, Chapman et al. 2013). However, RIF1 can be counteracted by Suppressor of Cancer cell Invasion (SCAI), which binds to 53BP1 and promotes repair by HR (Isobe et al. 2017). RIF1 is also involved in the intra-S-phase checkpoint, timing of replication firing, and replication of heterochromatin upon DNA damage or at stalled replication forks (Chapman et al. 2013, Buonomo et al. 2009, Silverman et al. 2004, Yamazaki et al. 2012).

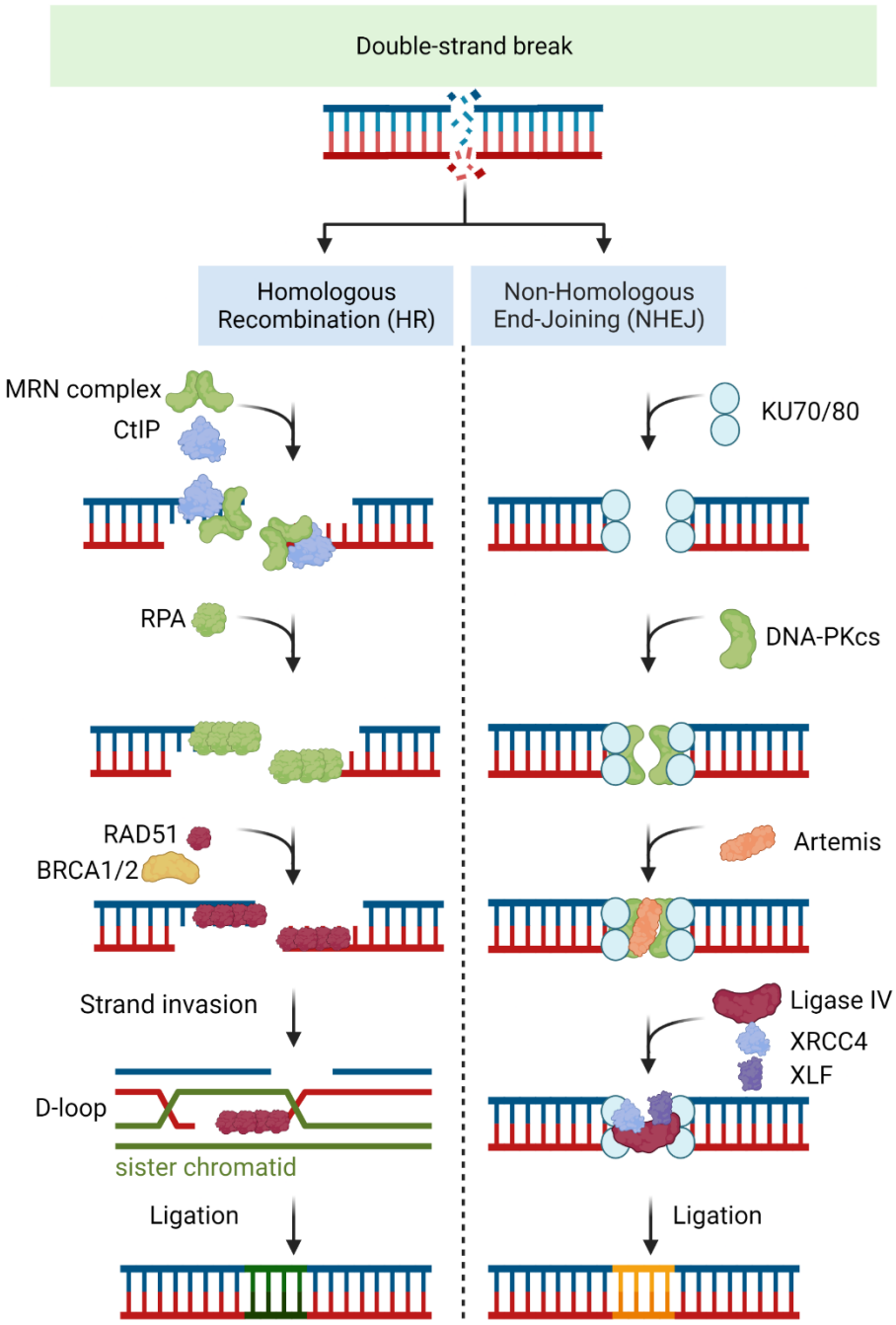

Figure 1.4: The DSB repair pathways Homologous Recombination (HR) and Non-Homologous End-Joining (NHEJ). HR (left) is initiated by the MRN-CtIP complex, which creates 3' single-stranded DNA (ssDNA) overhangs, NHEJ (right) by binding of the KU70/80 heterodimer to the DSB ends. Figure was created using BioRender. Modified after Brandsma and Gent (2012) and Christmann et al. (2003).

1.4 Apoptosis

Apoptosis, which is also referred to as programmed cell death, is a process that occurs during normal cellular development and aging, but also in response to damaging agents (Elmore 2007). It is an important self-destruction mechanism to eliminate damaged or infected cells in the body without causing inflammation reactions (Haanen and Vermes 1995). The morphology of apoptotic cells is characterized by cell shrinkage, pyknosis (which is the result of chromatin condensation), and DNA fragmentation (Elmore 2007).

Apoptosis is induced via an extrinsic or an intrinsic pathway (Figure 1.5). The intrinsic pathway, also referred to as the mitochondrial pathway, is primarily activated by intracellular stress signals, such as DNA damage, oxidative stress, unfolded protein response, or the absence of certain growth factors and hormones (D'Arcy 2019, Singh and Lim 2022). The tumor suppressor p53 plays an important role in the induction of apoptosis as it regulates proteins of the B-cell lymphoma protein 2 (Bcl-2) family, such as anti-apoptotic Bcl-xl, Bcl-xs, Bcl-w, Mcl-1 and BFL-1/A1, pro-apoptotic Bax, Bak, and Bok, and pro-apoptotic BH3-only Bad, Bid, Bik, Bim, HRK, NOXA, and PUMA (Elmore 2007, Kashyap et al. 2021). These proteins can change the inner mitochondrial membrane and therefore the permeability of the mitochondrial pore, leading to a release of the pro-apoptotic proteins cytochrome c, Second mitochondria-derived activator of caspase/Direct Inhibitor of Apoptosis protein (IAP)-Binding protein with Low pI (Smac/DIABLO), and High temperature requirement A2 (HtrA2)/Omi into the cytoplasm. Cytochrome c binds to Apoptotic Protease-Activating Factor-1 (APAF-1), which together with deoxyadenosine triphosphate (dATP) and Pro-caspase-9 forms the apoptosome complex. This triggers caspase-9 and downstream the activation of various effector caspases, such as caspase-3. As a result, endonucleases and proteases are activated, chromosomes and nuclear proteins degraded, which finally ends in apoptosis. Smac/DIABLO and the serine protease HtrA2/Omi promote apoptosis by IAP proteins (XIAP, cIAP1, cIAP2) (D'Arcy 2019, Singh and Lim 2022). Moreover, Apoptosis-Inducing Factor (AIF) and endonuclease G are released from the inner mitochondrial membrane into the cytoplasm in a caspase-independent manner, resulting in DNA fragmentation (Elmore 2007).

The extrinsic pathway is also referred to as the death receptor pathway. It depends on binding of specific ligands to their corresponding death receptors. There are several ligand-receptor pairs, such as CD95/Fas Receptor (FasR), Tumor Necrosis Factor-α (TNF-α)/TNF Receptor (TNF-R) 1, Apo2L/DR4, or Apo2L/DR5. Ligand binding leads to recruitment and dimerization of the death receptors and subsequently the recruitment of the adaptor proteins Fas-Associated protein with Death Domain (FADD) and TNF

Receptor type 1 Associated Death Domain protein (TRADD), Pro-caspase-8, and Pro-caspase-10. Activation of caspase-8 and -10 causes cleavage and activation caspase 3, 6 and 7 (Kashyap et al. 2021). In general, caspases are extremely important for apoptosis and are further divided into initiator caspases (caspase 2, 8, 9 and 10) and effector caspases (caspase 3, 6 and 7). Whereas the initiator caspases are autoactivated, the effector caspases are activated by cleavage at specific sites by the initiator caspases (Shi 2002).

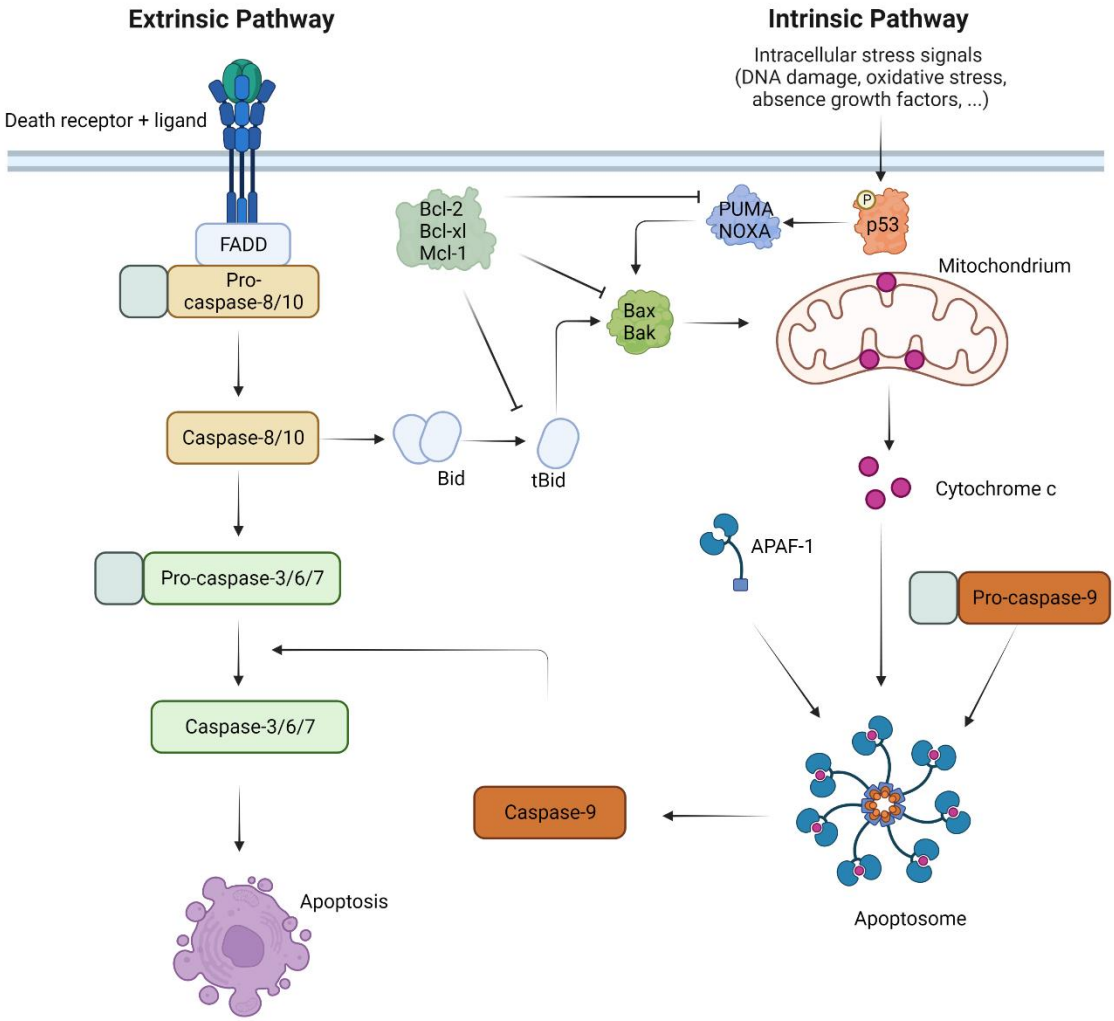

Figure 1.5: The intrinsic and extrinsic apoptosis pathways. The extrinsic pathway is initiated by binding of an extrinsic ligand to a death receptor. The intrinsic pathway is initiated by various intracellular stress signals, such as DNA damage or oxidative stress and is also referred to as the mitochondrial pathway. Figure was created using BioRender. Modified after Kashyap et al. (2021) and Wanner et al. (2020).

1.5 Protein phosphatase 2A

Posttranslational modifications of proteins such as phosphorylation, ubiquitination, SUMOylation, acetylation, or methylation are important to maintain genomic stability (Dzulko et al. 2020). Especially protein phosphorylation and dephosphorylation are essential processes affecting the division, signaling, and survival of normal cells. Cancer cells often show aberrant protein phosphorylation which can lead to gain-of- or loss-of-function (Singh et al. 2017). The main phosphorylation residues are serine (85%), threonine (11.8%), and tyrosine (1.8%) (Ardito et al. 2017). One important protein phosphatase, Protein phosphatase 2A (PP2A), is a trimeric major serine/threonine phosphatase, which is involved in the regulation of various cellular processes, including apoptosis, autophagy, cell proliferation, and DNA repair.

Active PP2A complexes consist of a structural A- (PP2A-A), a catalytic C- (PP2A-C), and a regulatory B-type (PP2A-B) subunit (Figure 1.6). There are four different classes of B-type subunits (B, B’, B’’, B’’’) comprising about 24 different isoforms and splice variants. The regulatory subunits define the substrate specificity and the subcellular localization of the holoenzyme (Dzulko et al. 2020).

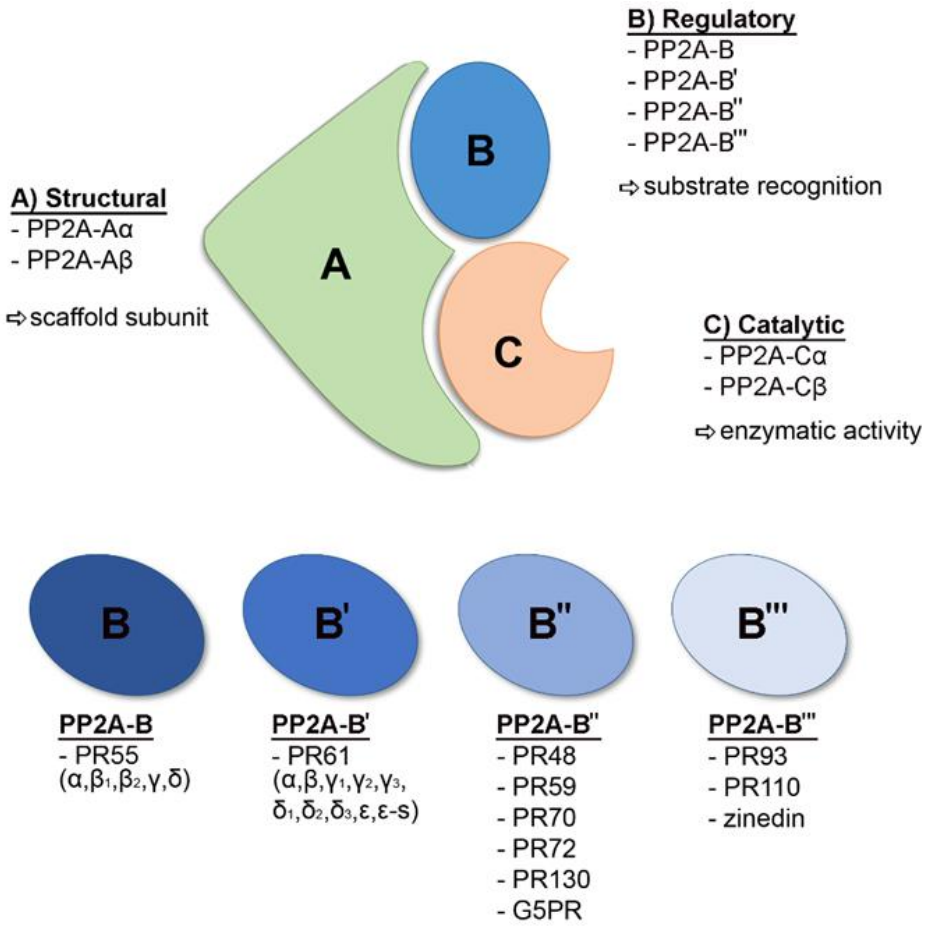

Figure 1.6: Schematic overview of the PP2A subunits. The trimeric PP2A complex consists of structural (PP2A-A), regulatory (PP2A-B), and catalytic (PP2A-C) subunits. The B-type subunits fall into four classes (B, B', B'', B''') with 24 different isoforms and splice variants (PR59 is mouse-specific; PR70/PR48 are human-specific; PR61 is also referred to as PR56) (Dzulko et al. 2020).

Binding of PP2A phosphatase activator leads to conformational change and activation of the C-type subunit. This is followed by dimerization with the structural A-type subunit (Mazhar et al. 2019). Methylation on leucine-309 at the C-type subunit by leucine carboxyl methyltransferase 1 triggers binding of the regulatory B-type subunits (Khan et al. 2021). Protein phosphatase methylesterase 1 can counteract methylation and prevent assembly of the PP2A holoenzyme complex (Mazhar et al. 2019). PP2A-related pathways are not only perturbed in cancer, but also in cardiovascular disease, diabetes, and neurodegenerative Alzheimer's and Parkinson's disease. PP2A is often inactivated due to recurring mutations, suppression of one of the subunits, or up-regulation of its endogenous inhibitors such as SET, CIP2A or TIPRL (Mazhar et al. 2019, Sangodkar et al. 2016).

The PP2A complex is tightly regulated by various activators and inhibitors as it is involved in a plethora of cellular pathways and therefore a key player in the maintenance of genomic stability. One activator is the sphingolipid ceramide, causing PP2A-induced apoptosis through induction of p27 (Kim et al. 2010). There are also synthetic Small-Molecule Activators of PP2A (SMAPs), which can bind to and stabilize PP2A complexes. SMAPs inhibit tumor growth and decrease Myelocytomatosis (MYC) oncogene expression (Farrington et al. 2020). MYC is a transcription factor important for the expression of proliferation-related genes, for example cyclin A2, cyclin D2 and cyclin E. However, MYC also decreases expression of the cell cycle regulators p21 and p15 to allow uncontrolled growth of cancer cells (Miller et al. 2012). Phenothiazine drugs, such as chlorpromazine, activate PP2A as well. Nevertheless, they are not used for cancer therapy as they cause harsh side-effects through activation of G protein-coupled receptors and amine transporters (Clark and Ohlmeyer 2019).

The endogenous inhibitor SET is frequently overexpressed in cancer and can bind to the C-type subunit of the PP2A complex (Sangodkar et al. 2016, Switzer et al. 2011). However, drugs like OP449 or FTY720 can bind to SET and counteract its inhibitory effect (Mazhar et al. 2019, Neviani and Perrotti 2014, Vicente et al. 2020). Inhibition of SET via FTY720 for example impairs expression of BCR-ABL resulting in less proliferation and enhanced apoptosis of chronic myeloid leukemia cells (Manley et al. 2011). Furthermore, CIP2A overexpression, which confers high aggressiveness of the tumor, interacts with the A-type subunit of PP2A, stabilizes MYC and activates transcription factor E2F1 and AKT. High expression of CIP2A is associated with increased proliferation and inhibited apoptosis (Soofiyani et al. 2017, Mazhar et al. 2019). Other PP2A inhibitors are okadaic acid, binding to the PP2A C-type subunit (Seshacharyulu et al. 2013, Fujiki et al. 2018), and the viral protein Simian Virus 40 (SV40), which binds to the A-type subunit and displaces the B-type subunits (Cho et al. 2007). However, due to its toxicity, okadaic acid is not used in clinical trials and small molecule inhibitors of PP2A, for example LB-100, or phendione, are used instead (Hong et al. 2015, Yue et al. 2020, Ho et al. 2018).

The PP2A complex is involved in the regulation of various pathways. It has a positive regulatory function in apoptosis as it regulates proteins of the Bcl-2 family (van Hoof and Goris 2003). It dephosphorylates pro-apoptotic proteins like Bad and Bim resulting in their activation. Additionally, the complex dephosphorylates anti-apoptotic proteins such as Bcl-2, which inactivates them and causes apoptosis (Seshacharyulu et al. 2013, Perrotti and Neviani 2013).

It has also been shown that the PP2A complex regulates the cell proliferation-promoting Wnt signaling pathway context-dependent in a positive or negative manner (Thompson and Williams 2018). Wnt pathway activation increases and stabilizes β-catenin, which facilitates the transcription of several genes important for cell proliferation, for example cyclin D1 and MYC. In non-activated state, a complex of Glycogen Synthase Kinase 3β (GSK3β), axin, Casein Kinase 1 (CK1) and Adenomatous Polyposis Coli (APC) protein destabilizes β-catenin, resulting in its degradation (Wlodarchak and Xing 2016). PP2A dephosphorylates and thereby activates GSK3β, resulting in phosphorylation and proteasomal degradation of β-catenin (Wu and Pan 2010, Thompson and Williams 2018). The PP2A B-type subunit B56 can also interact with the N-terminus of APC, supporting β-catenin degradation (Townsley 1999). Contrary, B55α was shown to dephosphorylate β-catenin directly at S33, S37 and T41, which results in its stabilization (Zhang et al. 2009). Moreover, the PP2A-B56α complex dephosphorylates the proto-oncoprotein MYC at S62 resulting in its proteasomal degradation (Arnold and Sears 2006). The AKT kinase is important for cell proliferation, angiogenesis and apoptosis and is dephosphorylated at T308 (one of its full activation sites) by PP2A-B55α (Kuo et al. 2008). This leads to indirect activation of GSK3β because AKT is known to inactivate GSK3β. The PP2A complex is further involved in direct cell cycle regulation. Whereas the B-type subunit B55α was shown to interact with p107 and p130, PR70/B''γ interacted with p130 and Rb (Kolupaeva and Janssens 2013). The complex is also involved in DNA synthesis and regulation of the Origin Recognition Complex (ORC). During the late G1 and early S phase, Cdc6 binds to ORC. Cdc6 is important for correct origin firing and replication. It is phosphorylated by cyclin E/CDK2 on S54 and S74 causing its stabilization, and dephosphorylated by the PP2A-PR70 complex, resulting in Anaphase Promoting Complex/Cyclosome-promoted proteasomal degradation (Wlodarchak and Xing 2016). In addition, PP2A-B55 dephosphorylates the cell cycle regulators WEE1 and Cdc25 to control mitotic entry (Wlodarchak and Xing 2016).

1.5.1 The regulatory B-type subunit PR130

PR130 (B''α1) is one regulatory B-type subunit of the PP2A complex. PR130 and its splice variant PR72 (B''α2) are derived from the same gene (*PPP2R3A*) and share the same 486 amino acid long C-terminus. However, their N-termini are different and are encoded by alternatively spliced exons (45 and 664 amino acids). The C-termini contain two Ca^{2+}-binding EF-hand motifs, which mediate interaction with the PP2A-A subunit and promote phosphatase activity, two A subunit binding domains, and a conserved hydrophobic motif (Figure 1.7) (Dzulko et al. 2020). PR130 is expressed in several tissues, whereas PR72 is expressed in heart and skeletal muscle tissue (Zwaenepoel et al. 2008, Hendrix et al. 1993).

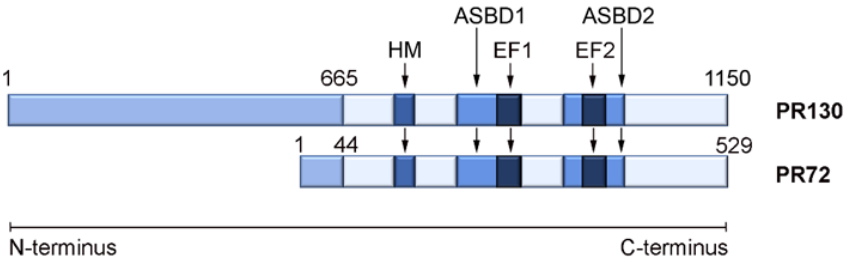

Figure 1.7: Domain structure of PR130 and PR72. The two different splice variants are derived from the same gene and share the same C-terminus with two A subunit binding domains (ASBD1/2), two Ca^{2+}-binding EF-hand (EF1/2) motifs, and a hydrophobic motif (HM) (Dzulko et al. 2020).

In a meta-analysis of 85 different sequencing studies with 9759 tumor samples, the B-type subunit PR130 was the second most frequently mutated PP2A subunit (12% mutation rate), and the highest amongst all B-type subunits. Mutations in B-type subunits mostly result in decreased expression of the subunit and are related to cancer progression and metastasis. For example, a mutation in the B-type subunit B55γ disrupted its interaction with p53, preventing its role as a tumor suppressor. Moreover, B55α dephosphorylates and inactivates the AKT kinase, which is important for cell proliferation (Sangodkar et al. 2016).

PR130 is important for proliferation and survival of cells. In Renal Cancer (RCC) it was shown that PR130 knockdown increases phosphorylation of AKT at S473, and expression of MYC. On the other hand, β-catenin expression was decreased (Sablina et al. 2010). PR130 is also directly involved in the promotion of the Wnt pathway as it interacts with the Wnt-antagonist Naked cuticle (NKD) and recruits the PP2A-A and -C-subunits in close proximity (Creyghton et al. 2006). However, PR72 displayed an

inhibitory effect on Wnt signaling (Creyghton et al. 2005). PR130 is further involved in the regulation of the replicative stress response and cell cycle regulation. CRISPR-Cas9-generated cells devoid of PR130 showed a slowed G1/S phase transition, higher phosphorylation of CHK1, which was decreased upon treatment with the class I Histone Deacetylase inhibitor (HDACi) MS-275, and higher levels of the cell cycle regulator p21. Moreover, MS-275-treated cells displayed a decrease in the repair protein RAD51. Another discovery was that phosphorylated ATM at S1981 is a direct target of the PP2A-PR130 complex (Figure 1.8) (Göder et al. 2018).

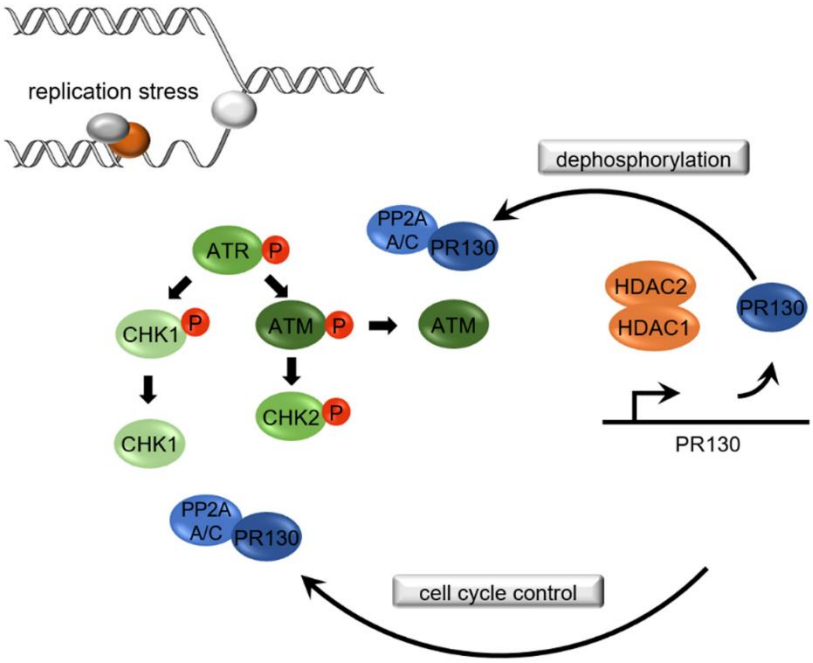

Figure 1.8: The PP2A-PR130 complex controls replication stress-induced checkpoint kinase signaling. Upon replication stress (e.g., HU treatment), ATR gets activated via phosphorylation. This leads to downstream activation of CHK1 and ATM, which itself phosphorylates CHK2. The PP2A-PR130 complex binds directly to phosphorylated ATM and dephosphorylates it. Histone deacetylase 1 and 2 (HDAC1/2) control checkpoint kinase phosphorylation upon replication stress via PR130. They bind to the *PPP2R3A* promotor and suppress *PPP2R3A* expression. PR130 also has an indirect control of CHK1 phosphorylation and an impact of cell cycle control (Dzulko et al. 2020).

Furthermore, PR130 regulates growth, invasion, and migration processes. Hepatocellular carcinoma cells with silenced *PPP2R3A* expression showed a reduction of the cell cycle regulator and proliferation marker Ki-67. Those cells also had high levels of p53, although the authors did not further analyze the posttranslational modifications, such as phosphorylation status, or target genes of the tumor suppressor (Chen et al. 2019a). The PP2A-PR130 complex was also shown to interact with Src-Homology domain-containing Inositol Polyphosphate 5'-phosphatase 1 and 2 (SHIP1/2) in cervical carcinoma cells via its EF-hand motifs (Zwaenepoel et al. 2010). The SHIP1/2

phosphatases interact with proteins, which are involved in adhesion, proliferation and apoptosis (Thomas et al. 2017). It was further discovered that PR130 mediates the stability of the Epidermal Growth Factor Receptor (EGFR) (Zwaenepoel et al. 2010). Additionally, the PP2A-PR130 complex negatively regulates cell adhesion and positively regulates migration by interacting with the LIM-protein Lipoma Preferred Partner (LPP) via a Zn^{2+}-finger-like motif in its N-terminus (Janssens et al. 2016).

PR130 is regulated by both endogenous proteins and synthetic drugs. In prostate cancer cells, microRNAs (miRNA), which regulate gene expression on post-translational level, are often overexpressed. miRNA-652 was found to decrease *PPP2R3A* mRNA levels and increase the activity of AKT, resulting in tumor growth and migration as well as epithelial-to-mesenchymal transition, exemplified by the expression of mesenchymal markers such as N-cadherin and epithelial markers such as E-cadherin (Nam et al. 2018). Another PR130 regulator is MS-275, as colorectal cancer cells and pancreatic ductal adenocarcinoma cells (8248, S411) treated with this HDACi showed an increase in the regulatory subunit (Göder et al. 2018, Nguyen et al. 2021), identifying HDAC1 and HDAC2 as main regulators of PR130 expression (Göder et al. 2018). Moreover, the Ca^{2+}-dependent protease calpain was found to degrade PR130 into a 45-58 kDa proteolysis-resistant fragment (PR45). PR45 could be detected in apoptotic cells, but its exact function remains to be investigated (Janssens et al. 2009). Another PR130 regulator is Absent In Melanoma 2 (AIM2), which has been described to be important for inflammatory responses and cell death (Lee et al. 2012). It increases the expression of the B-type subunit and controls AKT signaling (Chen et al. 2019b).

1.6 Histone deacetylases

The DNA is wound around histones to store it in the nucleus in a space-saving manner. Post-translational modifications of histones, such as methylation, phosphorylation, ubiquitylation or acetylation modulate the accessibility of the DNA as they open or close its structure (Millán-Zambrano et al. 2022). In this thesis, the focus is mainly on deacetylation processes as HDACi are combined with replicative stress inducers.

Histone acetyltransferases (HATs) acetylate the ε-amino group of lysine residues on histones using acetyl-coenzyme A as acetyl group source. This neutralizes or decreases the histones' positive charge and weakens binding to the negatively charged DNA, which causes an open and accessible DNA structure to which transcription factors can bind easily. HDACs are counterparts of HATs and remove acetyl groups (Glozak and Seto 2007, Camilo and Jerónimo 2020). There is a balance of HATs and HDACs in normal

cells, however, cancer cells often show an aberrant behavior, which affects transcription of genes that are important for the maintenance of genomic stability (Wu et al. 2020).

HATs can be divided into two classes, whereas type A HATs are in the nucleus and acetylate histones and other chromatin-associated proteins and type-B HATs are in the cytoplasm, acetylating newly synthesized histones. Type A HATs consist of the four subfamilies GNAT (GCN5 (General Control of Nuclear-5)-related N-acetyl transferase), MYST (MOZ (Monocytic leukemia Zinc-finger protein), YBF2 (Yeast Binding Factor 2), SAS3 (Something About Silencing 3)/SAS2, TIP60 (Tat Interactive Protein-60)), p300/CBP (CREB (cAMP-Response Element Binding protein), and Steroid Receptor Coactivators (SRC). There are also other HATS, which do not belong to any of other subfamilies, such as TAF1, TFIIIC, and CLOCK (Figure 1.9) (Guo 2012, Kopytko et al. 2021, Lee and Workman 2007).

HDACs fall into four classes (Figure 1.9), whereas class I, II, and IV are zinc (Zn^{2+})-dependent and class III is Nicotinamide Adenine Dinucleotide (NAD^{+})-dependent. Class I comprises the ubiquitously expressed HDAC1, 2, 3 and 8, which are mainly located in the nucleus. Class II can be divided into class IIa (HDAC4, 5, 7, 9) and IIb (6, 10). Class IIa HDACs are expressed in a tissue-specific manner and shuttle between the nucleus and the cytoplasm. Class IIb HDAC6 is in the cytoplasm, whereas HDAC10 can be found in the nucleus and in the cytoplasm. Class III comprises the Sirtuins (SIRT) 1-7, class IV includes the nuclear-located HDAC11 (Ho et al. 2020).

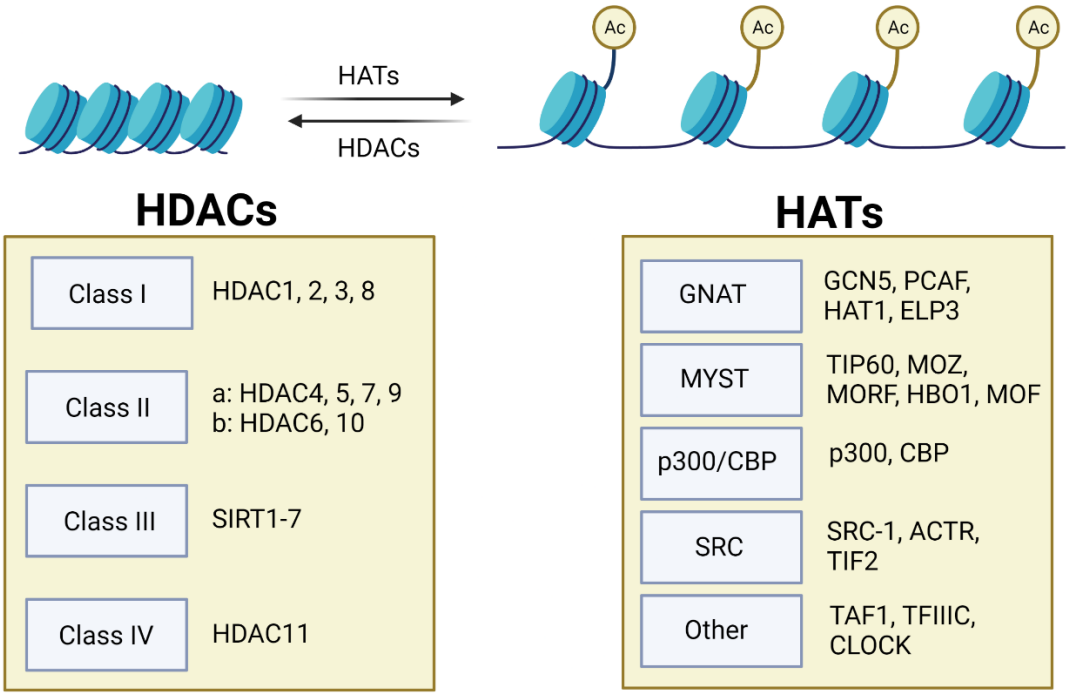

Figure 1.9: Histone Acetyltransferase (HAT) and Histone Deacetylase (HDAC) families. HATs acetylate lysin residues on histones; HDACs antagonize this modification step. Figure was created using BioRender. Modified after Kopytko et al. (2021) and Schneider et al. (2013).

HATs and HDACs have not only been found to regulate acetylation of histones, but also other proteins and targets, which have been linked to cell cycle regulation, DNA damage repair, apoptosis, and cellular differentiation (Glozak and Seto 2007, Wu et al. 2020). p53 for example can be acetylated by p300/CBP, TIP60, or PCAF at various sites increasing its ability to bind to the DNA. This increases transcription of the cell cycle regulator p21, leading to cell cycle arrest, or pro-apoptotic proteins such as Bax, resulting in apoptosis. Moreover, acetylation also enhances p53 stability as it protects it from ubiquitination and degradation (Glozak and Seto 2007). Other acetylated proteins are cytoskeletal proteins such as α-tubulin, or protein-folding chaperones such as HSP90 (Movafagh and Munson 2019).

In this thesis I mainly focus on the activity of class I HDACs as they were shown to regulate the expression of the PP2A regulatory B-type subunit PR130 (Göder et al. 2018). HDAC1 and 2 share over 80% homology, HDAC1 and HDAC3 over 64%. Therefore, it is very challenging to design specific inhibitors for each of them (Luo and Li 2020). They are mainly located in the nucleus in complexes together with the transcriptional repressor complexes NuRD, Sin3A, coREST, MiDAC, and MIERT (Ho et al. 2020). Among others they deacetylate proteins such as p53 (LeBoeuf et al. 2010, Ito et al. 2002), E2F (Harbour and Dean 2000), ATM (Thurn et al. 2013) and CAF1 (Ho et

al. 2020, Sharma et al. 2016). Moreover, they bind to the promoters of the CDKi p21, p27 and p57 suppressing their expression, or inhibit cyclin D and cyclin A and thereby control the cell cycle (Movafagh and Munson 2019). HDAC1 and HDAC2 are also involved in the regulation of DNA repair as they promote NHEJ (Miller et al. 2010). They decrease the expression of BRCA1, RAD51, and FANCD2 causing a shift from HR to NHEJ (Zhao et al. 2017, Krumm et al. 2016).

Inhibitors of HDACs modulate gene expression, cell cycle control and cell fate decisions (Nikolova et al. 2017). HDACi carry out antiproliferative and proapoptotic effects and are popular in cancer therapy due to their low toxicity to normal cells. They are often used in combinatorial treatments with DNA damage-inducing drugs, as they sensitize cancer cells to such treatments (Miller et al. 2010, Camilo and Jerónimo 2020). HDACi can be divided into five different classes due to their structural design: short-chain aliphatic acids (e.g., valproic acid), hydroxamates (e.g., trichostatin A), benzamides (e.g., entinostat), cyclic peptides (e.g., romidepsin), and mercaptoketones (e.g., KD5170) (Camilo and Jerónimo 2020). The classical HDACi consist of a zinc-binding group, a hydrophobic cap region, a connecting unit and a hydrophobic linker in between (Figure 1.10) (Asfaha et al. 2021, Camilo and Jerónimo 2020). The Zn^{2+}-binding group chelates the zinc ion at the active site of the HDAC, the connecting unit interacts with the substrate binding tunnel, and the cap region binds to the HDAC and nearby complexes and serves as surface binding domain (Camilo and Jerónimo 2020, Asfaha et al. 2021).

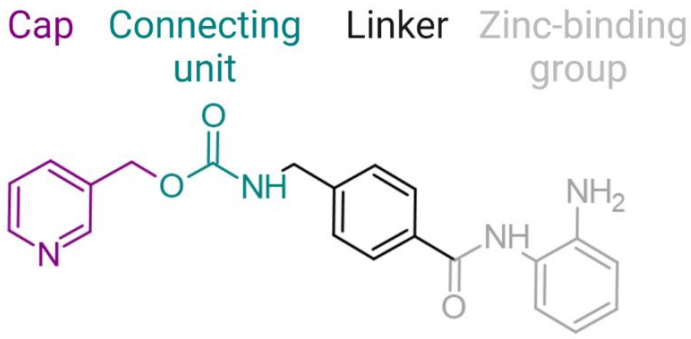

Figure 1.10: Structural design of a HDACi. It is composed of a cap region (purple), a connecting unit (cyan), a linker (black), and a Zn^{2+}-binding group (grey). Shown as an example is entinostat (MS-275). Figure was created using ChemSketch and BioRender. Modified after Asfaha et al. (2021) and El-Rayes et al. (2019).

HDACi can also be distinguished based on their selectivity. Pan-HDACi, such as vorinostat or panobinostat, are often used in clinical trials in the area of hematological malignancies and inhibit a variety of HDACs (Movafagh and Munson 2019, Camilo and

Jerónimo 2020). To date, there are only four HDACi which are approved by the United States Food and Drug Administration (US FDA): romidepsin, panobinostat, belinostat, and vorinostat (Movafagh and Munson 2019). However, unspecific inhibition of different HDACs causes many side effects and a high toxicity. Therefore, class- and isoform-specific HDACi are needed. In this study the benzamide entinostat (MS-275) was used, which inhibits class I HDACs and is less potent, but more specific than other HDACi. MS-275 is currently tested in phase I, II and III clinical trials for breast, renal or pancreatic cancer as well as leukemia, often in combination with hormone therapy and DNA damaging agents (e.g., 5-azacitidine) (Camilo and Jerónimo 2020). HDACi-treated cancer cells normally arrest in the G1 phase, however the treatment can also induce G2 phase arrest of normal cells (Camilo and Jerónimo 2020). Moreover, HDACi induces upregulation of the cell cycle regulator p21 in a p53-independent manner through the transcription factor SP1 (Ocker and Schneider-Stock 2007, Owen et al. 1998).

2 Aims and Objective

HDAC1 and HDAC2 have been known to modulate checkpoint kinase signaling and cell fate upon replication stress through the PP2A-PR130 complex (Göder et al. 2018). The exact mechanism of regulation, however, has not been identified yet. Furthermore, only a few interaction partners of the PP2A-PR130 complex are known, all associated with cellular transformation and cancer development with the phosphatase complex as a tumor suppressor or promotor (Dzulko et al. 2020). Considering that the *PPP2R3A* gene has the highest mutational rate amongst 11 B-type subunit genes testing 9759 tumor samples (Sangodkar et al. 2016), its relevance as a potential tumor marker becomes clear.

To better understand the role of the PP2A-PR130 complex in checkpoint kinase signaling and other cellular pathways, the following questions have been addressed in this thesis:

- Which interaction partners does the PP2A-PR130 complex have and in which cellular pathways is the complex involved?
- Which proteins are regulated in their expression and phosphorylation by the PP2A-PR130 complex?
- Which molecular regulators control CHK1 phosphorylation and cell cycle progression in cells with different PR130 status upon replication stress and class I HDACi?
- How do class I HDAC control the DNA repair pathways HR and NHEJ in a PR130-dependent manner?

3 Materials and Methods

3.1 Chemicals

Table 3.1: Chemicals.

Name	Manufacturer
40% Acrylamide/bisacrylamide (37.5:1)	Carl Roth
5x NewBlot IR Stripping Buffer	LI-COR Biotechnology
Acetic acid	Carl Roth
Acetone	Carl Roth
Ammonium persulfate (APS)	Carl Roth
Annexin-V Fluorescein Isothiocyanate (FITC)	BD Bioscience
Bovine Serum Albumin (BSA)	Carl Roth
Bromophenol blue	Merck
Calcium chloride	Merck
cOmplete™, EDTA-free Protease Inhibitor Cocktail	Merck
Dimethyl Sulfoxide (DMSO)	Sigma-Aldrich
Dithiothreitol (DTT)	Carl Roth
Dulbecco's Modified Eagle's Medium (DMEM)	Sigma-Aldrich
Ethanol (EtOH)	Carl Roth
Ethylenediaminetetraacetic acid (EDTA)	AppliChem
Fetal Calf Serum (FCS)	Life Technologies/Sigma-Aldrich
Glycerol	Sigma-Aldrich
Glycine	Carl Roth
Hydrochloric acid (HCl)	Carl Roth
Hydroxyethyl Piperazineethanesulfonic Acid (HEPES)	Carl Roth
Isopropanol	Carl Roth
Lipofectamine® 3000	Invitrogen
Lipofectamine® RNAiMAX	Invitrogen

Name	Manufacturer
Methanol	Carl Roth
Natriumchloride (NaCl)	Sigma-Aldrich
Non-fat dry milk	Carl Roth
NP-40	Fluka
Nuclease-free water	AppliChem
Gibco OptiMEM	Thermo Fisher Scientific
PageRuler (Plus) Prestained Protein Ladder	Thermo Fisher Scientific
Paraformaldehyde (PFA)	Carl Roth
Penicillin/streptomycin (Pen/Strep)	Life Technologies
Phosphatase inhibitor cocktail II	Sigma-Aldrich
Phosphate-Buffered Saline (PBS)	Biochrom
Phosphoric acid (H_3PO_4)	Roth
Propidium Iodide (PI)	Sigma-Aldrich
Protein G Sepharose™ 4 Fast Flow	GE Healthcare
RNAseA	Carl Roth
Roswell Park Memorial Institute Medium (RPMI) 1640	Sigma-Aldrich
Sodium Dodecyl Sulfate (SDS)	Carl Roth
Tetramethylethylenediamine (TEMED)	Carl Roth
TO-PRO-3	Life Technologies
Tris base	Carl Roth
Triton X-100	Sigma-Aldrich
Trypsin/EDTA	Life Technologies
VectaShield® Antifade mounting medium	Vector laboratories

3.2 Inhibitory, cytostatic, and genotoxic drugs

Table 3.2: Inhibitory, cytostatic, and genotoxic drugs.

Name	Description	Stock [mM]	Manufacturer
Cytarabine (Ara-C)	Anti-metabolite	10	Selleck Chemicals
Colcemide	Tubulin poison	10	Sigma-Aldrich
CDK2 inhibitor cocktail II	CDK2i	5	Santa Cruz
Hydroxyurea (HU)	RNRi	100	Sigma-Aldrich
KU-60019	ATMi	1	Selleck Chemicals
MK-1775	WEE1i	1	Selleck Chemicals
MK-8776	CHK1i	1	Selleck Chemicals
Entinostat (MS-275)	HDAC1/2/3i	5	Selleck Chemicals
Nocodazole	Tubulin poison	10	Sigma-Aldrich
RI-1	RAD51i	10	EMD Millipore
Merck60	HDAC1/2i	10	Provided by Sippl group
RGFP	HDAC3i	10	Provided by Sippl group
HI 2.1	HDAC1/2/3i	10	Provided by Sippl group
HI 7.2	HDAC1/2i	10	Provided by Sippl group

3.3 Antibodies

Table 3.3: Primary antibodies.

Name	Host	Dilution	Manufacturer	Order No.
ac-Histone H4	Rb	1:500	Cell Signaling	8647
ATM	Rb	1:1,000	Abcam	ab32420
CDK2	Ms	1:250 IP: 3.5 µg	Santa Cruz	sc-6248
CHK1	Ms	1:1,000	Cell Signaling	2360

Name	Host	Dilution	Manufacturer	Order No.
Cyclin A2	Ms	1:500	Abcam	ab38
Cyclin B1	Rb	1:500	Cell Signaling	4138
Cyclin D1	Rb	1:1,000	Abcam	ab134175
Cyclin E1	Ms	1:500	Santa Cruz	sc-377100
HA	Ms	IP: 3.5 µg	Santa Cruz	sc-7392
HDAC1	Rb	1:1,000	Cell Signaling	34589S
HDAC2	Rb	1:1,000	Santa Cruz	sc-7899
HDAC3	Rb	1:1,000	Abcam	ab32369
HSP90	Ms	1:5,000	Santa Cruz	sc-23119
p21	Rb	1:1,000	Abcam	ab109520
p53 (DO-1)	Ms	1:2,000	Santa Cruz	sc-126
p-ATM (S1981)	Rb	1:750	Abcam	ab81292
p-CDK1 (Y15)	Rb	1:1,000	Cell Signaling	4539S
p-CHK1 (S296)	Rb	1:500	Cell Signaling	2349
p-CHK1 (S345)	Rb	1:500	Cell Signaling	2348
p-p21 (S130)	Rb	1:1,000	ThermoFisher	PA5-12644
p-p53 (S15)	Rb	1:5,000	Cell Signaling	9284
PR130	Rb	1:1,000	Novus Biologicals	NBP1-87233
RAD51	Rb		Abcam	ab63801
RIF1	Rb	IF: 1:400	Bethyl Laboratories	A300-569A
RRM2	Rb	1:1,000	Thermo Fisher	PA5-13570
Vinculin	Ms	1:1,000	Santa Cruz	sc-73614
WEE1	Rb	1:500	Cell Signaling	4936
α-tubulin	Rb	1:1,000	Abcam	ab176560
γH2AX (S139)	Rb	1:1,000	Santa Cruz	sc-101696

Table 3.4: Secondary antibodies.

Name	Host	Dilution	Manufacturer	Order No.
Goat IgG	-	-	Santa Cruz	sc-2028
Mouse IgG	-	-	Santa Cruz	sc-2025
Rabbit IgG	-	-	Santa Cruz	sc-2027
IRDye® 680RD anti-mouse IgG	Gt	1:10,000	LI-COR	926-68070
IRDye® 680RD anti-rabbit IgG	Gt	1:10,000	LI-COR	926-68071
IRDye® 800CW anti-mouse IgG	Gt	1:10,000	LI-COR	926-32210
IRDye® 800CW anti-rabbit IgG	Gt	1:10,000	LI-COR	926-32211
Alexa Fluor® 488 F(ab'2) anti-mouse IgG (H+L)	Gt	1:300	Life Technologies	A11017
Cy3 anti-rabbit IgG (H+L)	Gt	1:300	Dianova	111-165-144

3.4 Kits

Table 3.5: Kits.

Name	Manufacturer	Order No.
High Pure RNA Isolation Kit	Roche	11828665001
Malachite green phosphate detection kit	Cell Signaling	12776S
RNeasy® Mini Kit (50)	QIAGEN	74104

3.5 siRNAs

Table 3.6: siRNAs.

Name	Supplier	Order No.
control siRNA A	Santa Cruz	SC-37007
control siRNA B	Santa Cruz	SC-44230
control siRNA C	Santa Cruz	SC-44321
p21 siRNA	Dharmacon	L-003471-00-0005
p53 siRNA	ThermoFisher	Cat# AM51331; ID106141
RRM2 siRNA	Dharmacon	L-010379-00-0005
WEE1 siRNA	Dharmacon	L-005050-00-0005

3.6 Plasmids

Table 3.7: Plasmids.

Name	Supplier
FLAG-p21	Kind gift by Prof. Dr. Yuping Juan (Department of Gynecology and Obstetrics, J. W. Goethe-University Frankfurt)
FLAG-p21 S130 A	Kind gift by Prof. Dr. Yuping Juan (Department of Gynecology and Obstetrics, J. W. Goethe-University Frankfurt)
FLAG-p21 S130 D	Kind gift by Prof. Dr. Yuping Juan (Department of Gynecology and Obstetrics, J. W. Goethe-University Frankfurt)
HA-PR130	Kind gift by Dr. Claudia Emmerich (Friedrich Schiller University Jena)
pcDNA3.1	Kind gift by Dr. Claudia Emmerich (Friedrich Schiller University Jena)

3.7 Equipment

Table 3.8: Equipment.

Name	Manufacturer
Autoclave 5075 ELV	Tuttnauer
BD FACS Canto II	BD Biosciences
Cell counter TC20TM	BioRad
Electronic repeating pipette, HandyStep®	Brand
Freezer -20 °C	LIEBHERR
Freezer -80 °C	SANYO
Fresco 21 centrifuge	VWR
Heracell™ 150i CO2 incubator	Thermo Fisher Scientific
LaminAir® HB 2472 workbench	Heraeus Instruments
Laser Scanning Microscope LSM 710	Carl Zeiss
(Zeiss Axio Observer.Z1 confocal microscope)	
LI-COR Odyssey 9120	LI-COR Biotechnology
Megafuge 16 centrifuge	Heraeus Instruments
Microplate reader Sunrise™	Tecan
Mini Star table centrifuge	VWR
Mini Trans-Blot® Cell	BioRad
NanoDrop 2000	Thermo Fisher Scientific
Orbital shaker Certomat R	Braun
pH meter FiveEasy™	Mettler Toledo
Pipetboy acu 2	Integra
Pipet-Lite™ XLS™ (various sizes)	VWR
PowerPac™ HC High-Current Power Supply	Bio-Rad
Primovert microscope	Zeiss
Rocking platform RS-RS 5	PHOENIX Instrumental
Roller mixer SRT9	Stuart

Name	Manufacturer
Thermomixer 5436	Eppendorf
Ultrasonic processor UP200Ht	Hielscher
Vortex-genie 2	Scientific Industries

3.8 Consumables

Table 3.9: Consumables.

Name	Manufacturer
5/10/25 ml plastic pipettes	Greiner Bio-One
6/10 cm cell culture dishes	Greiner Bio-One/Sarstedt
0.5/1.5/2 ml tubes	Greiner Bio-One
20x20 mm Coverslips	Carl Roth
15/50 ml tubes	Greiner Bio-One
6-Well/12-Well cell culture plates	Greiner Bio-One/Sarstedt
Cell culture flasks	Greiner Bio-One/Sarstedt
Cryogenic tubes	Greiner Bio-One
FACS tubes	Sarstedt
Nitrocellulose membrane (Amersham™)	Cytiva
Pipette tips	Greiner Bio-One
Syringe	BRAUN
Whatman paper	Carl Roth

3.9 Software

Table 3.10: Software.

Name	Version	Application
BD FACSDiva™	6	Flow cytometry measurement
BioRender	2023	Creation of figures
Citavi	6.14.4.0	Citation programm
GraphPad Prism	8.0.1	Flow cytometry analysis
Image Studio Lite	5.2	Immunoblot analysis and processing
ImageJ/FIJI	1.53a	Image analysis and processing
LSM Image Browser	4.2	IF analysis
Magellan™		Breadford measurement
MS Office 365	2016	Text processing, creation of figures
Odyssey Version	3.0	Immunoblot measurement
STRING Database	11.5	Pathway and protein-protein-network analysis
WebGestalt	2019	Gene set enrichment analysis

3.10 Buffers and solutions

Table 3.11: Buffers and solutions.

Name	Contents
Bradford Assay	
Bradford reagent	50 mg Brilliant Blue G-250 50 ml H_3PO_4 25 ml EtOH ad 500 ml ddH_2O, filtrate and store at 4 °C in the dark
Cell lysate preparation	
NET-N lysis buffer	10 mM Tris-HCl pH 8.0 100 mM NaCl 10% glycerol (v/v) 1 mM EDTA 0.5% NP-40 (v/v) in ddH_2O Supplemented with: protease inhibitor (cOmplete Mini) (1 tablette/10 ml) 1:1,000 phosphatase inhibitor (cocktail 2) – added fresh
NuPAGE LDS (1x)	4x NuPAGE 100 mM DTT in ddH_2O
1 M DTT	154.25 mg DTT ad 1 ml ddH_2O
Sample buffer (6x)	375 mM Tris-HCl pH 6.8 12% SDS (w/v) 30% glycerol (v/v) 500 mM dithiothreitol (DTT) spatula tip bromophenol blue in ddH_2O

Name	Contents
SDS gel electrophoresis	
5x Lämmli buffer	30 g (0.25 M) Tris 144 g (1.92 M) glycine ad 1000 ml ddH_2O
1x SDS-PAGE running buffer	200 ml 5x Lämmli buffer 10 ml 10% SDS ad 1000 ml ddH_2O
10% APS	1 g ammonium persulfate ad 10 ml ddH_2O Aliquots: storage at -20 °C
10% SDS	10 g SDS (sodium dodecyl sulfate) ad 100 ml ddH_2O
Western Blot	
1x Transfer buffer	100 ml 5x Lämmli buffer 200 ml ethanol ad 1000 ml ddH_2O
Tris-buffered saline (TBS) (10x)	200 mM Tris-HCl pH 7.6 1.4 M NaCl in ddH2O
TBS-T (TBS + Tween-20) (1x)	1/10 TBS (10x) 0.05% Tween-20 in ddH_2O
FACS measurements	
Annexin binding buffer (10x)	100 mM HEPES pH 7.4 1.4 M NaCl 25 mM $CaCl_2$ in ddH_2O

Name	Contents
Immunofluorescence	
Blocking solution	5% BSA (w/v) 0.3% Triton-X (v/v) in PBS
Immunoprecipitation	
Fixing solution	1% Paraformaldehyde (v/v) in PBS
Quenching solution	1 M Glycine in PBS
Final washing buffer	20 mM Tris-HCl pH 8.0 100 mM NaCl 1mM EDTA 0.5% NP-40 in ddH_2O
HA-IP lysis buffer	200 mM HEPES pH 7.4 150 mM NaCl 1 mM EDTA 0.5% NP-40 in ddH_2O
IP lysis buffer	50 mM Tris pH 8.0 120 mM NaCl 0.5% NP-40 in ddH_2O
High salt washing buffer	20 mM Tris-HCl pH 8.0 900 mM NaCl 1 mM EDTA 0.5% NP-40 in ddH_2O

Name	Contents
Dephosphorylation assay	
Phosphatase reaction buffer	50 mM Tris-HCl pH 7.0 100 µM CaCl2 in ddH_2O
Phospho-proteomics	
Modified RIPA buffer	50 mM Tris-HCl 150 mM NaCl 1 mM EDTA 1% NP-40 (v/v) 0.1% Na-deoxycholate (v/v) in ddH_2O

3.11 Phosphopeptides for dephosphorylation assay.

Table 3.12: Phosphopeptides for dephosphorylation assay. Obtained from Dr. Toni Kühl (University of Bonn).

Peptides	Sequence	Molecular weight [g/mol]
pS1981-ATM	Ac-AFEEGpSQSTTI-NH_2	1290.23
pS130-p21	Ac-EQAEGpSPGGPG-NH_2	1106.00
pT190-WEE1	Ac-FDTPHpTPKSLL-NH_2	1376.45

4 Methods

4.1 Cell culture

All cell lines were cultured under sterile conditions using sterile reagents and solutions. The used adherent cell lines were cultured in DMEM supplemented with 5% (all HCT116 cell lines)/10% (HROC24; VH10tert) FCS and 1% penicillin/streptomycin at 37 °C/5% CO_2. The medium of VH10tert cells was additionally supplemented with 1% glutamine. Cells were cultivated to 80–90% confluency and passaged 1:5 to 1:10. Therefore, the medium was removed, and the cells were washed with sterile PBS. To detach the cells from the flask, a trypsin/EDTA solution was added for 5 min at 37 °C. The reaction was stopped by the addition of fresh DMEM medium. The excess of cells could either be thrown away or used for experiments.

The number of cells was determined via an automatic cell counter. 10 µl of the cell suspension were pipetted onto a counting slide to detect the numbers of cells/ml. The number of cells was adjusted depending on the experiment and size of the cell dishes.

Cells were long-time stored in liquid nitrogen. Therefore, medium was removed, cells detached, and the cell pellet resuspended in 1 ml FCS supplemented with 10% DMSO. The cryogenic tube was transferred to a -80 ° C deep freezer and later in liquid nitrogen. Cells were re-cultured by thawing in a water bath at 37 °C. The cell suspension was resuspended in 5 ml pre-warmed medium, centrifuged (5 min/1,300 rpm), and washed once with PBS. Afterwards, the cells were resuspended in another 5 ml of warm medium and transferred to cell culture flasks. Cells were cultured at least one week to ensure stable growth conditions before use for experiments.

4.2 Cell lines

Table 4.1: Cell lines used for the experiments.

Cell line	Medium	Description
HCT116^{wt}	DMEM, 5% FCS	Human colorectal carcinoma cell line (ATCC)
HCT116$^{\Delta gRNA}$	DMEM, 5% FCS	Human colorectal carcinoma cell line transfected with hSpCas9 without gRNA template (generated by Dr. Anja Göder)
HCT116$^{\Delta PR130}$	DMEM, 5% FCS	Human colorectal carcinoma cell line with depletion of PPP2R3A by CRISPR Cas9 technology (generated by Dr. Anja Göder)
HCT116$^{\Delta PR130 \Delta gRNA}$	DMEM, 5% FCS	Human colorectal carcinoma cell line transfected with GFP-Cas9 without gRNA template
HCT116$^{\Delta PR130 \Delta p21}$	DMEM, 5% FCS	Human colorectal carcinoma cell line depleted of PR130 and p21 (generated via CRISPR-Cas9)
HROC24	DMEM, 10% FCS	Colon adenocarcinoma cell line (short-term culture) (provided by Dr. Michael Linnebacher)
VH10tert	DMEM, 10% FCS, 1% Glutamin	Human diploid foreskin fibroblast cell line (provided by Prof. L. Mullenders)
HCT116$^{p21\ -/-}$	DMEM, 5% FCS	Human colorectal carcinoma cell line depleted of p21 (provided by Prof. Dr. D. Vogelstein)
HCT116$^{p53\ -/-}$	DMEM, 5% FCS	Human colorectal carcinoma cell line depleted of p53 (provided by Prof. Dr. D. Vogelstein)

4.3 Transfection of adherent cells

4.3.1 Transient transfection with plasmids

HCT116 cells were transfected with plasmids using Lipofectamine® 3000. Cells were seeded to be 70–90% confluent at day of transfection. 125 µl Opti-MEM medium and 6.25 µl Lipofectamine® 3000 were mixed, as well as 125 µl Opti-MEM medium, 2 µg plasmid, and 5 µl P3000 reagent. Both solutions were mixed at a 1:1 ratio and incubated for 10–15 min at RT before dropwise addition to the cells. The volumes referred to one well of a 6-well plate and were scaled accordingly if larger plates or more wells were used. After 24 h of transfection, cells could be additionally treated with chemical compounds.

4.3.2 Transient transfection with siRNA

Knockdown of specific proteins was carried out by using small interfering RNAs (siRNAs) and Lipofectamine® RNAiMAX. Cells were seeded to be 70–90% confluent at day of transfection. 30–40 pmol siRNA/siCtrl and 100 µl Opti-MEM as well as 5 µl Lipofectamine RNAiMAX and 100 µl Opti-MEM were mixed. Both solutions were combined at a 1:1 ratio and incubated for 10 min at RT. Afterwards, 200 µl of the mixture was added dropwise to each well and incubated for at least 24 h at 37 °C (5% CO_2). The volumes referred to one well of a 6-well plate and were scaled accordingly if larger plates or more wells were used. After 24 h of transfection, cells could be additionally treated with chemical compounds.

4.3.3 CRISPR-Cas9

Lipofectamine™ CRISPRMAX™ Cas9 transfection kit (CMAX00001, Thermo Fisher) was used to create a PR130-p21-deficient HCT116 cell line. Cas9-GFP-protein (6250 ng, CAS9GFPPRO, Sigma-Aldrich), Cas9 plus reagent (12.5 µl), two synthetic gRNAs (1200 ng each; Hs.Cas9.CDKN1A.1.AA, Hs.Cas9.CDKN1A.1.AC from IDT) and 125 µl Opti-MEM™ I Medium were mixed well in a tube. CRISPRMAX™ reagent (7.5 µl) and 125 µl Opti-MEM™ I were mixed well in another tube. Both solutions were combined and incubated for 10 min at RT. HCT116$^{\Delta PR130}$ cells were transfected around 24 h prior to sorting (~70% confluent at day of transfection). Cells were sorted at BD FACSAria™ III for GFP-positive signal. Single clones were seeded in 96-well-plates and cultivated for several weeks.

4.4 Protein analysis

4.4.1 Preparation of whole cell lysates

For preparation of whole cell lysates medium was collected in a reaction tube, cells were washed once with PBS, and treated with trypsin/EDTA. After detachment, cells were transferred in the reaction tube following centrifugation (5 min/1,300 rpm). The cell pellet was washed one more time with 1 ml PBS (5 min/13,800 rpm/4 °C) before lysis. The following steps were carried out on ice. For cell lysis, 10 ml NET-N buffer was supplemented with 1 tablet of protease inhibitor (cOmplete Mini) and 1:1,000 phosphatase inhibitor cocktail 2. The amount of lysis buffer needed was adapted to the size of cell pellet. Pellets were resuspended in lysis buffer and sonified (10 pulses/40% amplitude/0.1 sec pulse duration) following a centrifugation step (20 min/13,800 rpm/4 °C). The supernatant was transferred to new 1.5 ml reaction tubes. Lysates were stored at -20 °C or -80 °C (long-term storage).

4.4.2 Bradford assay

The quantitative, photometric Bradford assay was used to determine the protein concentration in the samples (measured absorbance is proportional to the protein concentration). Under acidic conditions, the dye Coomassie Brilliant Blue G-250 binds to cationic and non-polar sidechains of protein complexes which stabilizes the anionic form of the dye and leads to a shift of the absorbance from 470 to 595 nm. Lysates were diluted (1:10 in ddH_2O), 10 µl of the dilution transferred to a 96-well plate in duplicates, as well as a BSA standard (Table 4.2). Afterwards, 200 µl of Bradford reagent were added to each well and incubated for 5 min at RT in the dark. The absorbance was measured at 595 nm (Microplate reader Sunrise™).

Table 4.2: Pipetting scheme – Bradford assay. BSA standard = 1 mg/ml.

Concentration [µg/ml]	BSA [µl]	H_2O [µl]
0	0.0	30.0
50	1.5	28.5
100	3.0	27.0
200	6.0	24.0
300	9.0	21.0
400	12.0	18.0
500	15.0	15.0

4.4.3 SDS-PAGE

A Sodium Dodecyl Sulphate Polyacrylamide Gel Electrophoresis (SDS-PAGE) is used to separate proteins according to their molecular weight. Samples were prepared by combining 30–50 µg lysate with 6x sample buffer (final concentration: 1x) and ddH_2O. The sample buffer denaturates the proteins and masks their native charge due to its compound SDS. Lysates were boiled for 5 min at 95 °C and loaded onto polyacrylamide gels consisting of a stacking and separating gel (gel preparation see Table 4.3). A protein ladder (PageRuler™ prestained protein ladder (plus)) was used to identify proteins by their size. SDS-PAGE running buffer (Table 3.11) was filled into the gel chamber and the voltage set to 95 V. After passing the stacking gel, the voltage was increased to 125 V. Proteins move in the electrical field from the positive to the negative pole, however smaller proteins move faster than larger proteins.

Table 4.3: Pipetting scheme – SDS-PAGE.

Components	Stacking gel	Separation gel			
2 x 1.0 mm gels		**7.5%**	**10%**	**15%**	**17%**
ddH_2O	4.4 ml	6.5 ml	5.6 ml	4.2 ml	3.6 ml
1.0 M Tris (pH 6.8)	0.76 ml	-	-	-	-
1.5 M Tris (pH 8.8)	-	3 ml	3 ml	3 ml	3 ml
Acrylamide	0.76 ml	2.3 ml	3.1 ml	4.6 ml	5.2 ml
SDS (10%)	60 µl	120 µl	120 µl	120 µl	120 µl
APS (10%)	60 µl	60 µl	60 µl	60 µl	60 µl
TEMED	6 µl	6 µl	6 µl	6 µl	6 µl

4.4.4 Western Blot

Following protein separation with the SDS-PAGE, the proteins were transferred to a nitrocellulose membrane via western blot technology. Therefore, the gel was put onto the membrane between two sponges and four Whatman papers (2 at each site). Western blot was carried out at 150 mA/gel (2 h) in a MiniTransBlot® Cell system filled with transfer buffer (Table 3.11) and equipped with a cool pad. After the transfer, the membrane was rinsed with TBS-T and blocked for 1 h in 5% non-fat dry milk powder (5 g/100 ml TBS-

T). Primary antibodies were diluted in 5% BSA/milk according to manufacturer's specifications and incubated with the membrane overnight (4 °C). The next day, the membrane was washed three times with TBS-T for 5 min following an incubation with the secondary antibody. Depending on the primary antibody, a rabbit or mouse (green/red) secondary antibody was diluted (1:10,000) in 2% non-fat dry milk/TBS-T. The membrane was incubated for 2 h at RT in the dark. After three washing steps with TBS-T (5 min) the proteins could be detected using the fluorescence-dependent LI-COR® Odyssey system. Proteins could be removed from membranes by incubation with 5x LI-COR® stripping buffer for 5 min following blocking in 2% non-fat dry milk/TBS-T for 30 min. Densitometric analyses were performed with Image Studio Lite.

4.4.5 Immunoprecipitation

To analyze the interaction of CDK2, p21 and PR130 in more detail, immunoprecipitations (IP) were performed.

HCT116 cells were treated with 5 µM MS-275 to increase the amount of p21 and PR130. The cells were washed two times with PBS following a fixation with 1% paraformaldehyde for 10 min and neutralization with quenching solution (Table 3.11) for 5 min. Afterwards, cells were washed three times with PBS and lysed in appropriate amounts of IP lysis buffer (~1 ml/10 cm dish). Lysis was carried out on ice for 1 h following centrifugation (13,800 rpm/20 min/4 °C). Lysates were transferred to new reaction tubes and protein concentration was determined by Bradford assay.

For the IP of CDK2, 700–850 µg protein of each condition was incubated with 3.5 µg CDK2 (Santa Cruz, sc-6248) antibody or mouse IgG overnight under rotation (4 °C). The next day, 60 µl Protein G Sepharose™ 4 Fast Flow beads were prepared for each condition. Therefore, the beads were pipetted in a fresh reaction tube and centrifuged for 5 min at 13,800 rpm. Supernatant was removed and the beads were washed three times with 750 µl PBS (each time centrifugation: 30 s/13,800 rpm). 60 µl of the washed beads were transferred to new reaction tubes per condition. The lysates were added as well following incubation for 4 h under rotation at 4 °C. Afterwards, samples were centrifuged (30 s/ 13,800 rpm/4 °C), washed five times with high salt washing buffer and once with final washing buffer. After the last washing step, washing buffer was removed completely using a syringe. 60 µl 4x sample buffer were added to the beads of each sample and boiled for 5 min at 95 °C. Samples were centrifuged (1 min/13,800 rpm) and transferred to new reaction tubes. 30 µl of each IP was used for immunoblot detection.

4.4.6 Proteomics

HCT116$^{\Delta gRNA}$ and HCT116$^{\Delta PR130}$ cells were treated with 1 mM HU ± 5 µM MS-275 for 24 h. Afterwards, cells were harvested (5 min, 200xg, 4 °C), washed once with PBS and resuspended in 1x NuPAGE® LDS Sample Buffer (4x diluted, supplemented with 100 mM DTT). Cells were lysed for 30 min on ice, sonified (10 pulses, 40% amplitude, 0.1 sec pulse duration), and boiled for 10 min at 70 °C. Lysates were centrifuged (17,000x*g*, 25 min, 4 °C) and samples were analyzed using mass spectrometry. Global proteome analysis was kindly carried out by [redacted].

4.4.7 Phospho-peptide enrichment

HCT116$^{\Delta gRNA}$ cells were cultured in light/medium and HCT116$^{\Delta PR130}$ cells were cultured in heavy SILAC media for isotopic labeling (2 weeks). Every time cells were split, they were washed with PBS after trypsin/EDTA detachment and transferred to new plates to remove trypsin/EDTA completely. After 2 weeks of labeling, enough cells were seeded to gain at least 3 mg of protein per SILAC condition. Medium and heavy labeled cells were additionally treated with 1 mM HU for 24 h. Afterwards, medium was removed, cells were washed once with PBS and harvested by scraping in 1 ml modified RIPA buffer (Table 3.11) (supplemented with protease + phosphatase inhibitors). Samples were incubated for 15 min on ice and centrifuged (15 min/13,000 rpm/4 °C). The supernatant was transferred to new reaction tubes and the protein concentration determined by Bradford assay (Table 4.2). Inputs were taken for western blot analysis to control that the labeling did not change the DNA damage response of the cells. Hereafter, labeled lysates were combined in a 1:1:1 ratio and supplemented with 4x volume ice-cold acetone. Samples were stored at -20 °C until TiO_2-based phospho-peptide enrichment. Phospho-peptide enrichment was performed by [redacted], which are hereby kindly acknowledged.

4.4.8 In vitro dephosphorylation assay

The malachite green assay can be used to quantify the activity of phosphatases such as PP2A against phosphorylated targets. Free phosphate absorbs around 650 nm (Repen et al. 2012).

First, HA-tagged PR130 or the vector control pcDNA3.1 was transfected in HCT116 cells using Lipofectamine® 3000. After 24 h, cells were additionally treated with 5 µM MS-275 (24 h) to increase the amount of PR130. Cells were washed twice with PBS and harvested in appropriate amounts of HA-IP lysis buffer (Table 3.11) supplemented with

protease inhibitor (no addition of phosphatase inhibitor). Cells were incubated on ice for 1 h and centrifuged (10 min/13,800 rpm/4 °C). Supernatant was transferred to new reaction tubes and protein concentration was determined via Bradford assay. 900 µg protein were incubated with 3.5 µg HA-antibody (Santa Cruz, sc-7392) or the same amount of mouse IgG for 2 h (4 °C) under gentle rotation. Afterwards, 60 µl Protein G fast flow Sepharose beads were added following incubation for another 3 h. Samples were washed once with HA-IP lysis buffer and three times with TBS (pH 7.4) to remove unbound antibody and free phosphate. During the last washing step with TBS the IP was divided into three equally large samples. Beads were dried using a syringe to remove the washing buffer. 750 µM of pS1981-ATM peptide (served as positive control), pS130-p21 peptide and pT190-WEE1 peptide (synthesized by [redacted] as described in Göder et al. (2018)) in phosphatase reaction buffer (Table 3.11) were added to the IP and incubated for 30 min at 37 °C. 25 µl supernatant of each sample was transferred to a 96-well plate in triplicates and mixed with 100 µl malachite green solution following an incubation for 15 min. Afterwards, absorbance at 630 nm was measured (Microplate reader Sunrise™). A phosphate standard (50–1,600 pmol; pipetting scheme see Table 4.4) served as reference to quantify the amount of free phosphate.

Table 4.4: Pipetting scheme - In vitro dephosphorylation assay. Phosphate standard = 1 mM.

Diluted stock (0.1 mM) [µl]	ddH_2O [µl]	Phosphate [pmol]/25 ml
160	90	1600
140	110	1400
120	130	1200
100	150	1000
80	170	800
60	190	600
40	210	400
20	230	200
10	240	100
5	245	50
0	250	0

4.4.9 Flow cytometry

4.4.9.1 Cell cycle analyses

Cell cycles can be analyzed by measuring the intensity of the fluorescent dye Propidium Iodide (PI). Fixation with ethanol permeabilizes cells and allows entrance and intercalation of PI into the DNA. In the S phase, DNA synthesis takes place, hence cells in G2 phase bind the double amount of PI compared to cells in the G1 phase.

Cells were seeded in 6-well/12-well plates and treated for 24/48 h depending on experimental setup. Cells were harvested by collecting medium in reaction tubes, washed once with 1 ml PBS and detached with trypsin/EDTA. The detached cells were transferred into reaction tubes and centrifuged (5 min/1,300 rpm/RT). The cell pellet was washed one more time with 1 ml PBS. Afterwards, the cell pellet was resuspended in 100 µl PBS and fixed over night by dropwise addition of 2 ml ice-cold 80% ethanol. Fixed samples were stored at -20 °C until analysis. On the day of measurement, samples were centrifuged (5 min/1,300 rpm/RT) and resuspended in 333 µl PBS + 1 µl RNAse A following incubation for 1 h at RT. Then 165 µl PI (stock solution: 50 µg/ml) was added to each sample. Measurement was carried out on the BD FACS Canto II. Results were analyzed using FACSDiva™ Software.

4.4.9.2 Annexin V-FITC/propidium iodide staining

Cells were seeded in 6-well/12-well plates and treated for 24/48 h, depending on experimental setup. Cells were harvested in reaction tubes described as in section 4.4.9.1 for cell cycle analysis. A master mix of 50 µl 1 x annexin binding buffer and 2.5 µl annexin V-FITC per sample was prepared and cell pellets were resuspended and incubated for 20 min in the dark. Another master mix of 430 µl 1x annexin binding buffer and 10 µl PI (50 µg/ml) was prepared and transferred into the FACS tubes prior to measurement. Measurement was carried out on the BD FACS Canto II. Results were analyzed using FACSDiva™ Software.

4.4.10 Immunofluorescence

HCT116$^{\Delta gRNA}$ and HCT116$^{\Delta PR130}$ cells were seeded on 20x20 mm coverslips 24 h prior to treatment (200.000 cells/well) in a 6-well plate. Cells were treated as indicated in the experiment. After 24 h, medium was removed and the cover slips were washed carefully with 3 ml PBS for 5 min. Cells were fixed in -20 °C methanol:acetone (7:3) for 8 min. The fixing solution was immediately removed and replaced by 3 ml PBS following two additional washing steps with PBS (3x 5 min). Cover slips were placed on small sockets

and incubated with 150 µl of blocking solution (5% BSA/0.3% Triton-X in PBS) for 1 h at RT (wet chamber). Blocking was followed by incubation with 200 µl primary antibody (RIF1, 53BP1; dilution see Table 3.3; in blocking solution) overnight (4 °C). On the next day, the coverslips were washed three times with 3 ml PBS (3x 5 min) following incubation with 200 µl of the secondary antibody (AlexaFluor488/Cy3; 1:300) for 1 h at RT in the dark. The coverslips were washed two times with PBS for 5 min, once with high salt PBS for exactly 2 min and one last time with PBS (5 min). For nuclear staining, 10 µl Vectashield® + 1:100 TO-PRO3 were combined and vortexed for at least 30 s. 10 µl of the solution were put onto microscopy slides and the coverslips were carefully placed on top. Cover slips were sealed with nail polish until measurement. Analysis was performed on the Zeiss Axio Observer.Z1 confocal microscope (LSM710 laser-scanning unit) and Image J software.

4.4.11 RNA sequencing

1x 10^6 HCT116$^{\Delta gRNA}$ and HCT116$^{\Delta PR130}$ cells were seeded on 6 cm dishes per condition. Cells were treated with HU ± MS-275 for 24 h or PD for 6/24 h. Medium was removed, cells were washed with 1 ml PBS and detached by addition of trypsin/EDTA. Trypsin was inactivated by addition of fresh culture medium following centrifugation (5 min/1,300 rpm/RT). The cell pellet was washed one more time with 1 ml PBS, lysed in 350 µl RLT buffer (QIAGEN kit) and vortexed. 1x volume of 70% ethanol was added to the homogenized lysate and mixed well by pipetting. The sample was transferred to the RNeasy spin column placed in a 2 ml collection tube and centrifuged (15 s/10,000 rpm). The flow-through was discarded. Afterwards, 350 µl of RW1 buffer was added to the RNeasy spin column following centrifugation (15 s/10,000 rpm) to wash the column. The flow-through was discarded. 10 µl DNAse I stock solution (1,500 Kunitz units in 550 µl RNAse-free water) were mixed with 70 µl RDD buffer (a master mix was prepared for all samples) and added to the spin column following incubation for 15 min at RT. 350 µl RW1 buffer was added to the spin column and centrifuged again for 15 s at 10,000 rpm. The flow-through was discarded. Afterwards, 500 µl RPE buffer was added, centrifuged (15 s/10,000 rpm) and the flow-through discarded again. Another 500 µl of RPE buffer was added following centrifugation for 2 min at 10,000 rpm. The long centrifugation step should ensure that the spin column membrane is completely dry. The spin column was then placed in a new collection tube following addition of 30–50 µl RNAse-free water. It was centrifuged for 1 min at 10,000 rpm to elute the RNA. The quality of the RNA was analyzed with the NanoDrop2000. RNA sequencing analysis was kindly performed by [redacted]. [redacted] analyzed the data.

5 Results

5.1 PR130 impacts checkpoint kinase signaling and cell cycle regulation upon replication stress

Göder et al. already showed that the PP2A B-type subunit PR130 is involved in the regulation of checkpoint kinase signaling upon replication stress through dephosphorylation of ATM at S1981; cells devoid of PR130 displayed a stronger phosphorylation of ATM and CHK1, although the ATR activity was equal (Göder et al. 2018). The exact mechanism by which PR130 controls the phosphorylation status of CHK1 independent of ATR has not been identified yet. Moreover, the class I HDAC inhibitor entinostat (MS-275) was found to decrease hydroxyurea (HU)-induced phosphorylation of ATM in HCT116$^{\Delta gRNA}$, but not in HCT116$^{\Delta PR130}$ cells. CHK1 phosphorylation in contrast was decreased in both cell systems (Göder et al. 2018). Thus, PR130 must antagonize the phosphorylation of ATM and CHK1 via two independent mechanisms, which have not been identified yet.

To validate the previous findings, HCT116$^{\Delta gRNA}$ and HCT116$^{\Delta PR130}$ cells were treated with 1 mM HU ± 5 µM MS-275 for 24 h and analyzed by immunoblot and flow cytometry (Figure 5.1).

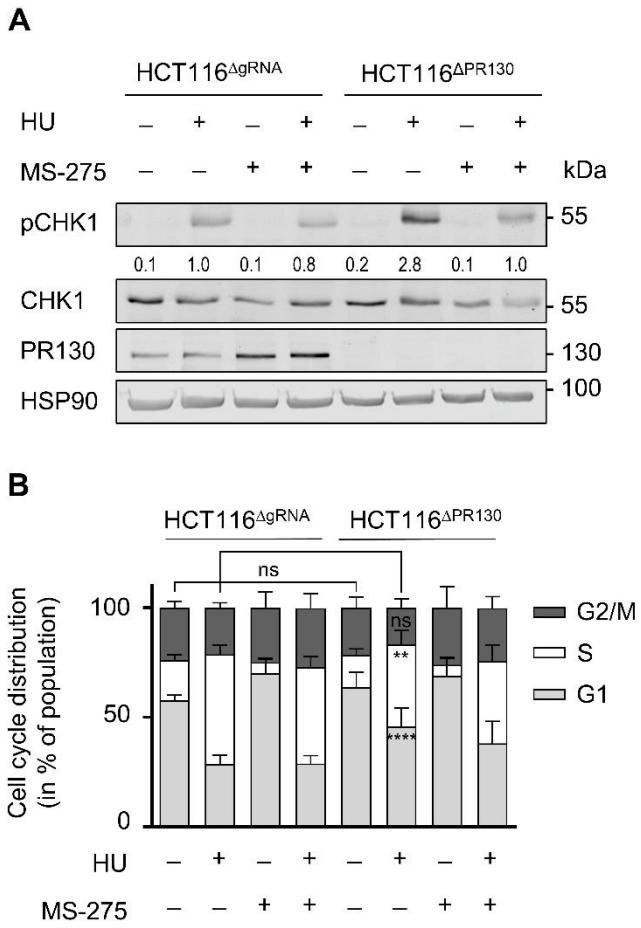

Figure 5.1: PR130 modulates cell cycle progression and phosphorylation of CHK1 during replication stress. A HCT116$^{\Delta gRNA}$ and HCT116$^{\Delta PR130}$ cells were treated with 1 mM HU ± 5 µM MS-275 for 24 h. PR130, pCHK1 and CHK1 were analyzed by immunoblot. HSP90 served as loading control. Numbers indicate densitometric values of the immunoblot signals relative to those of lysates from HU-treated wild-type cells (normalized to the respective loading control). **B** Cells were treated as stated in **A** and stained with Propidium Iodide (PI). Cell cycle distributions were analyzed using flow cytometry. Data are mean ± SD. Statistical analysis was performed using Two-way ANOVA and Tukey's Multiple Comparison Test (**p<0.01, ****p<0.0001, ns=not significant; n=7).

Genetic deletion of PR130 via CRISPR Cas9 technology increased levels of phosphorylated CHK1 (Figure 5.1 A) and significantly slowed G1/S phase transition (Figure 5.1 B) upon replication stress, which is in line with earlier experiments from our group (Göder et al. 2018). HCT116$^{\Delta PR130}$ cells showed 2.8-fold higher levels of pCHK1 compared to wild-type cells. Moreover, addition of MS-275 to HU-treated cells reduced pCHK1 levels in both cell lines (Figure 5.1 A). It should be noted that this reduction is more pronounced in PR130-deficient cells; HCT116$^{\Delta gRNA}$ cells showed around 20% less, whereas HCT116$^{\Delta PR130}$ cells displayed around 65% less CHK1 phosphorylation. The

combinatorial treatment led to a slippage of the cells from S phase to G2/M phase (Figure 5.1 B).

5.1.1 PR130 modulates CHK1 phosphorylation independent of the cell system and replicative stress inducer

The first aim of the thesis was to find the source of higher pCHK1 levels upon replication stress depending on the PR130 status of the cells. To assess the effect of genotoxic stress in both cell systems, a global proteome screen (in cooperation with Falk Butter, IMB Mainz) was conducted (Figure 5.2 A and B).

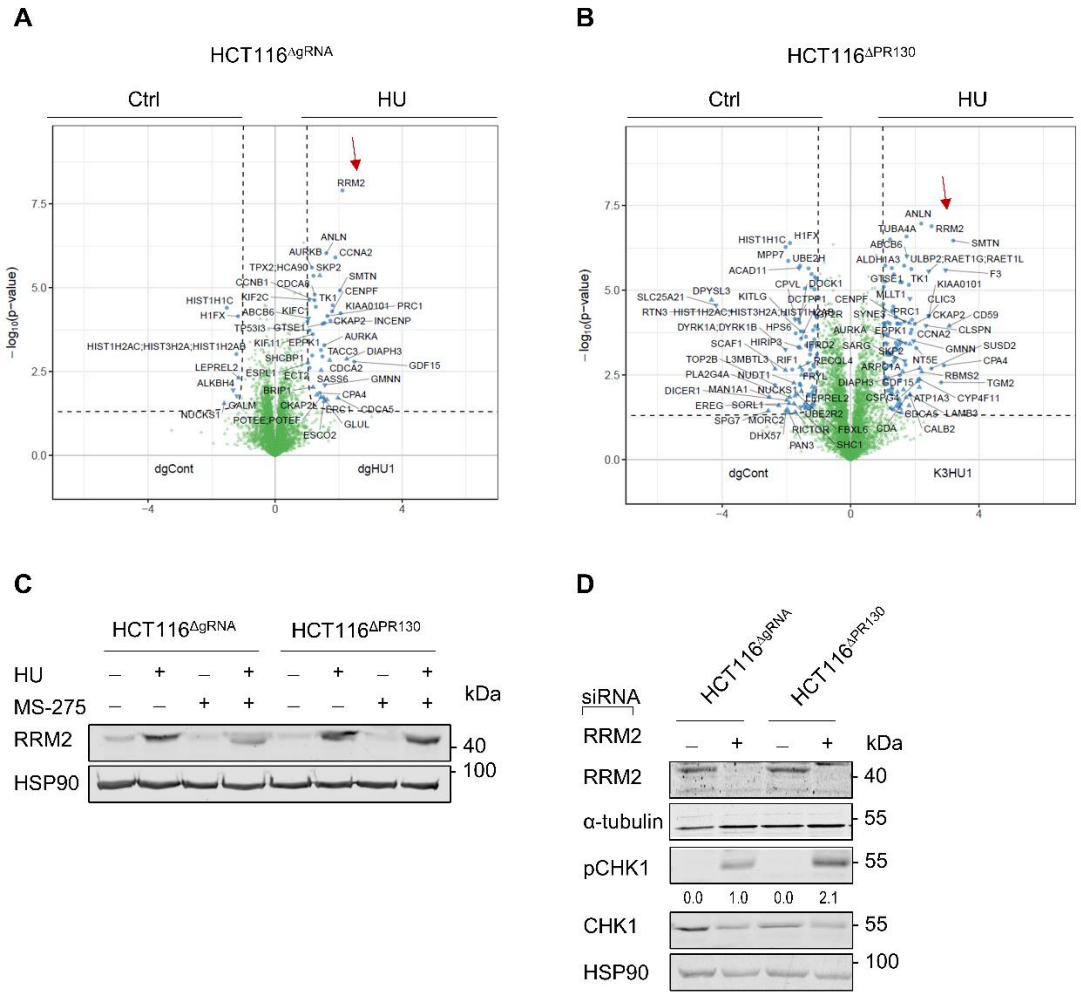

Figure 5.2: Genetic knockdown of RRM2 induces phosphorylation of CHK1. HCT116$^{\Delta gRNA}$ and HCT116$^{\Delta PR130}$ cells were treated with 1 mM HU for 24 h and analyzed by mass spectrometry. Volcano plots show the most significantly upregulated proteins for HCT116$^{\Delta gRNA}$ (**A**) and HCT116$^{\Delta PR130}$ (**B**) cells. **C** Cells were treated with 1 mM HU ± 5 µM MS-275 for 24 h. RRM2 was detected using the Odyssey Infrared Imaging System. HSP90 served as loading control. **D** Cells were transfected with 30 pmol siRNA against RRM2 or the same amount of siCtrl (48 h). Indicated proteins were analyzed by immunoblot. Numbers indicate densitometric analysis of pCHK1

signals relative to loading control. Signals are normalized to HCT116$^{\Delta gRNA}$ cells transfected with siRRM2.

The global proteome screen showed an upregulation of the ribonucleotide reductase subunit 2 (RRM2) in HCT116$^{\Delta gRNA}$ and HCT116$^{\Delta PR130}$ cells upon replication stress (Figure 5.2 A and B), which could be validated by western blot (Figure 5.2 C). This result is in line with the literature, since RRM2 is stable and accumulates constantly with a maximum peak during S phase (Zuo et al. 2024). Knockdown of RRM2 in both cell lines displayed 2.1-fold higher levels of pCHK1 in case of PR130-deficient cells compared to wild-type cells (Figure 5.2 D), in accordance with the results from the first experiment (Figure 5.1).

Since RRM2 is the molecular target of HU, it was next investigated if the effects seen in HCT116$^{\Delta gRNA}$ and HCT116$^{\Delta PR130}$ cells were HU-specific or could be also triggered by other stimuli. The antimetabolite arabinoside (cytarabine, ara-C) was used (Figure 5.3 B) due to its different mode of action (David et al. 2016). Moreover, pCHK1 levels upon HU-treatment were analyzed in the short-term colorectal cancer cell line HROC24 with different PR130-status to assess if the phosphorylation effect is cell line-specific (Figure 5.3 C).

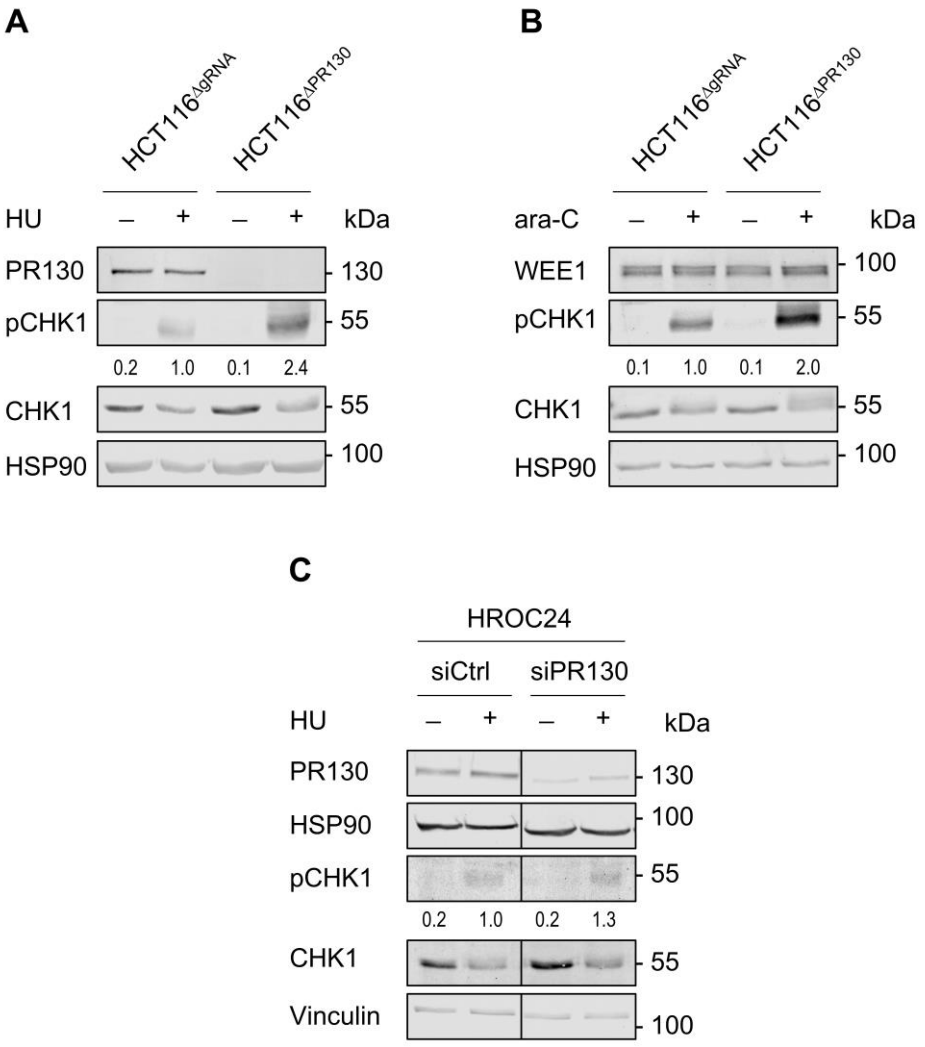

Figure 5.3: PR130 status influences phosphorylation of CHK1 upon different sources of replication stress. HCT116$^{\Delta gRNA}$ and HCT116$^{\Delta PR130}$ cells were treated with 1 mM HU (**A**) or 0.5 µM ara-C (**B**) for 24 h. HROC24 cells (**C**) were transfected with 30 pmol siCtrl or siPR130 for 24 h and then treated with 1 mM HU for 24 h. Indicated proteins were analyzed by immunoblot. HSP90 and vinculin served as loading controls. Numbers represent densitometric analysis of pCHK1 signals relative to the respective loading controls (normalized to HU-treated HCT116$^{\Delta gRNA}$ or HROC24 (siCtrl + 1 mM HU) cells). **C** All shown proteins are located on the same membrane but cut together for better comparison.

HCT116$^{\Delta PR130}$ cells showed a 2.0-fold increase in CHK1 phosphorylation upon ara-C treatment (Figure 5.3 B) compared to HCT116$^{\Delta gRNA}$ cells, which was similar to HU-treated cells (Figure 5.3 A). Moreover, transient knockdown of PR130 in short-term colorectal cancer HROC24 cells treated with HU (Figure 5.3 C) displayed a 1.3-fold increase in CHK1 phosphorylation compared to wild-type controls cells. In summary, the experiments showed that PR130-dependent phosphorylation of CHK1 is independent of the cell system and replicative stress inducer.

Next, the cell cycle distribution of HU- and ara-C treated cells was investigated (Figure 5.4), since PR130-deficient cells have been shown to arrest earlier in the cell cycle upon HU treatment than control cells (Figure 5.1 B).

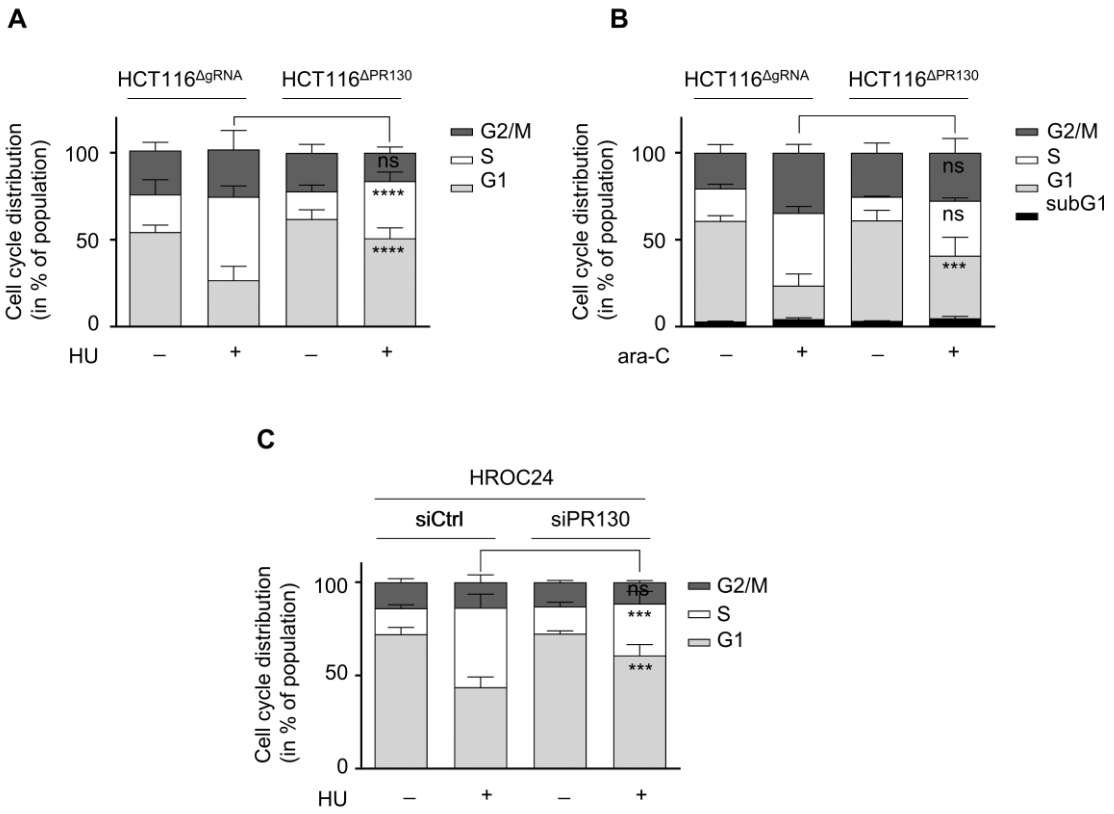

Figure 5.4: PR130 status influences cell cycle distribution of HU- and ara-C-treated cells. HCT116$^{\Delta gRNA}$ and HCT116$^{\Delta PR130}$ cells were treated with 1 mM HU (**A**) or 0.5 µM ara-C (**B**) for 24 h. HROC24 cells were transfected with 30 pmol siCtrl/siPR130 (24 h) and were afterwards treated with 1 mM HU for 24 h (**C**). Cell cycle distribution of PI-stained cells was analyzed using the BD FACS Canto II system. For **A** and **C** subG1 fractions are excluded. Data are presented as mean ± SD (**A**: HCT116$^{\Delta gRNA}$, n=18; HCT116$^{\Delta PR130}$, n=16; **B**: n=3; **C**: n=3). Statistical analysis was carried out using Two-way ANOVA and Tukey's Multiple Comparison Test (*** $p < 0.001$; **** $p < 0.0001$; ns=not significant).

Induction of replication stress led to S phase arrest of HCT116$^{\Delta gRNA}$ and control HROC24 (siCtrl) cells. In case of HU, the number of cells in S phase increased from 22% to 48% for HCT116$^{\Delta gRNA}$ cells (Figure 5.4 A), and from 14% to 43% for HROC24 cells (Figure 5.4 C). In case of ara-C, there was an increase from 19% to 42% for HCT116$^{\Delta gRNA}$ cells (G1: 58% to 19%) (B). However, HCT116$^{\Delta PR130}$ cells and HROC24 cells with PR130-knockdown (siPR130) arrested significantly earlier in G1/S phase. HU treatment increased HCT116$^{\Delta PR130}$ cells in S phase from 16% to 33% (Figure 5.4 A), and ara-C from 14% to 32% (Figure 5.4 B). In case of PR130-deleted HROC24 cells, HU treatment increased cells in S phase from 15 to 28% (Figure 5.4 C). Comparing the number of cells

in G1 phase of HU-treated HCT116$^{\Delta gRNA}$ and HCT116$^{\Delta PR130}$ cells, the wild-type showed 27% whereas the deficient cells displayed 51% (Figure 5.4 A). In case of ara-C treatment, the difference of cells in G1 phase for both cell systems was slightly smaller (HCT116$^{\Delta gRNA}$: 19%; HCT116$^{\Delta PR130}$: 36%; Figure 5.4 B). In HROC24 cells, 44% of HU-treated control cells were in G1 phase, compared to 61% of HU-treated PR130-deficient cells. Taken together, PR130 deficiency leads to stronger arrest in G1/S phase upon replication stress.

Additionally, the time (Figure 5.5 A) and dose dependency (Figure 5.5 B) of HU-induced cell cycle arrest in HCT116$^{\Delta gRNA}$ and HCT116$^{\Delta PR130}$ cells was analyzed.

A

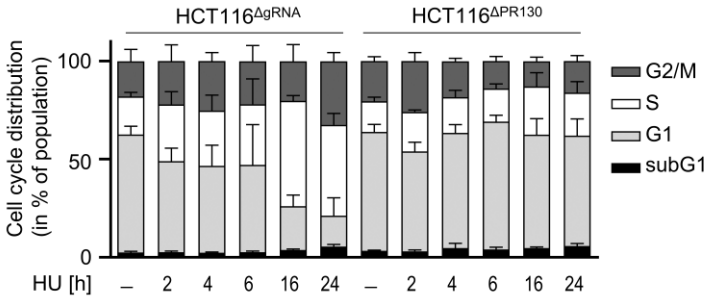

Time [h]	G1	S	G2/M
0	ns	ns	ns
2	ns	ns	ns
4	ns	ns	ns
6	**	ns	ns
16	****	****	ns
24	****	***	*

B

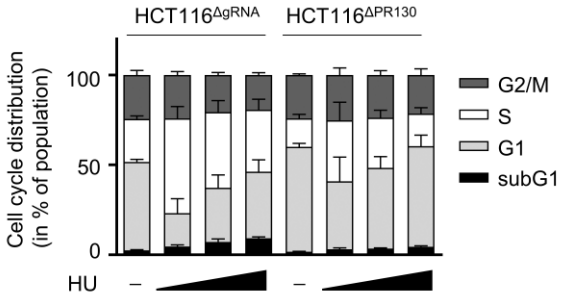

Treatment	G1	S	G2/M
con	ns	ns	ns
1 mM HU	***	***	ns
2 mM HU	**	*	ns
5 mM HU	***	**	ns

Figure 5.5: HU-induced cell cycle arrest is time- and dose-dependent. HCT116$^{\Delta gRNA}$ and HCT116$^{\Delta PR130}$ cells were treated with 1 mM HU for 2, 4, 6, 16, and 24 h (**A**). Additionally, cells were treated with increasing doses of HU (1, 2, 5 mM) for 24 h (**B**). Cell cycle distribution of PI-stained cells was measured on the BD FACS Canto II system. Data show mean ± SD (n=3). Statistical analysis was carried out using Two-way ANOVA and Tukey's Multiple Comparison Test (*p<0.05; **p<0.01; ***p<0.001; ****p<0.0001 ns=not significant). In the table, treatments of HCT116$^{\Delta gRNA}$ and HCT116$^{\Delta PR130}$ cells are directly compared to each other.

It was observed that S phase arrest increased with progressing time (2–24 h) in HCT116$^{\Delta gRNA}$ cells. After 16 h, the number of cells in S phase was the highest with 54%. Directly comparing the cell cycle distribution of HCT116$^{\Delta gRNA}$ and HCT116$^{\Delta PR130}$ cells at the same time points, there was always a higher number of PR130-deficient cells in G1 phase (Figure 5.5 A). However, there was just a trend visible until 4 h, which became significant from 6 h on. After 16 and 24 h, it could be determined that a slight S phase arrest built up in HCT116$^{\Delta PR130}$ cells, but compared to the wild-type cells, G1/S phase transition is slowed. Furthermore, increasing doses of HU shifted the number of cells progressively in G1 phase (Figure 5.5 B). The differences in cell cycle distribution were apparent regardless of drug concentration.

It was also tested if the earlier cell cycle arrest at the G1/S boundary of HU treated HCT116$^{\Delta PR130}$ compared to HCT116$^{\Delta gRNA}$ cells was caused by cells which traversed through G2/M phase and then stalled in the subsequent G1 phase. Therefore, both cell systems were treated with HU in combination with the tubulin poison nocodazole (Figure 5.6).

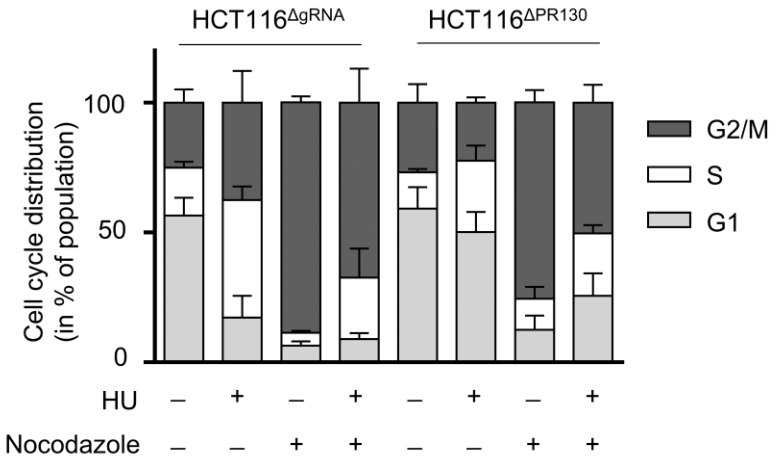

Figure 5.6: HCT116$^{\Delta PR130}$ cells arrest earlier at the G1/S phase boundary compared to HCT116$^{\Delta gRNA}$ cells. Both cell systems were pre-treated with 100 nM nocodazole for 1 h. Afterwards, cells were treated with 1 mM HU for 24 h. Cell cycle distributions were analyzed by flow cytometry (mean ± SD; n=4).

Nocodazole treatment led to an accumulation of HCT116$^{\Delta gRNA}$ and HCT116$^{\Delta PR130}$ cells in G2/M phase, whereas the combinatorial treatment with HU reduced the number of cells in this cell cycle phase for both cell systems. This indicates that cells arrested in S phase without transversal into G2/M phase.

5.1.2 PR130-deficient cells depend on CHK1 signalling for cell cycle progression upon replication stress

To determine the importance of higher pCHK1 levels upon HU treatment in PR130-deficient cells compared to wild-type cells, both cell systems were additionally stimulated with the CHK1 inhibitor MK-8668 (Figure 5.7).

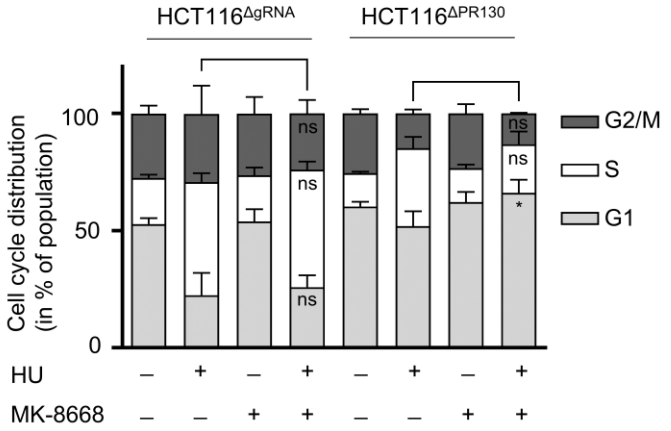

Figure 5.7: Cell cycle distribution of HCT116$^{\Delta gRNA}$ and HCT116$^{\Delta PR130}$ cells upon CHK1 inhibition and replication stress. Cells were treated with 1 mM HU ± 300 nM MK-8668 (1 h pre-treatment) for 24 h and stained with PI. Cell cycle distribution (subG1 fractions were excluded) was measured on the flow cytometer. Data are presented as mean ± SD (HCT116$^{\Delta gRNA}$: n=4; HCT116$^{\Delta PR130}$: n=3). Statistical analysis was performed by Two-way ANOVA and Tukey's multiple comparison test (*p<0.05; ns=not significant).

Whereas the cell cycle distribution of HCT116$^{\Delta gRNA}$ cells did not change upon the combinatorial treatment with HU and MK-8668, HCT116$^{\Delta PR130}$ cells showed significantly more cells in G1 phase compared to HU single treatment (Figure 5.7), indicating that CHK1 activation is involved in S phase transition in PR130-deficient cells.

It is evident that PR130-dependent CHK1 phosphorylation regulates cell cycle progression, although the molecular regulators of this phosphorylation are not sufficiently known. Therefore, global proteome-, phosphoproteome- and RNA sequencing analyses were employed to identify targets of the regulatory subunit and elucidate possible involvement in regulatory pathways.

5.2 The PP2A-PR130 complex is involved in the regulation of various pathways

5.2.1 Proteome screen identifies PR130-dependent involvement in cell cycle regulation and DNA repair

In order to identify new and previously unknown targets of the PP2A-PR130 complex in the context of the DNA damage response to exogenous stimuli, a global proteome analysis of HCT116$^{\Delta gRNA}$ and HCT116$^{\Delta PR130}$ cells treated with 1 mM HU ± 5 µM MS-275 (24 h) was carried out (Figure 5.8).

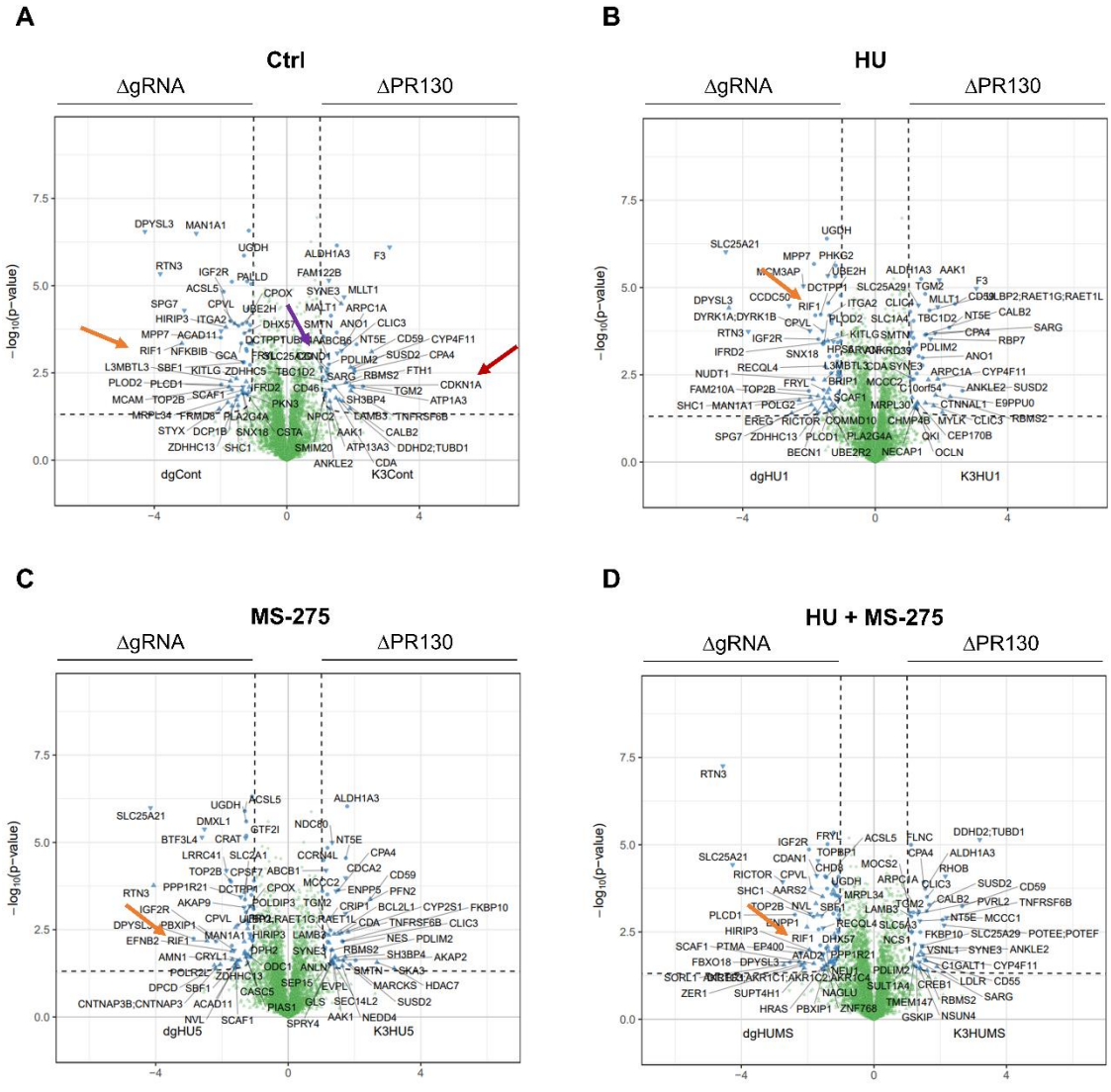

Figure 5.8: Volcano plots of HCT116$^{\Delta gRNA}$ and HCT116$^{\Delta PR130}$ cells upon replication stress and HDACi. Cells were treated with 1 mM HU ± 5 µM MS-275 for 24 h. Cell lysates were subjected to label-free mass spectrometry (n=4). The left side shows proteins enriched in HCT116$^{\Delta gRNA}$ cells, the right side shows proteins enriched in HCT116$^{\Delta PR130}$ cells. Red arrow: p21 (*CDKN1A*); purple arrow: cyclin D1 (*CCND1*); orange arrow: RIF1 (*RIF1*). Single treatments for

each cell line can be found in the supplementary (HCT116$^{\Delta gRNA}$: Supplementary Figure 8.1; HCT116$^{\Delta PR130}$: Supplementary Figure 8.2).

A STRING analysis using significantly upregulated proteins in both cell systems was performed to determine differentially regulated pathways depending on the PR130-status of the cells (Supplementary Figure 8.3 A–D). Although there was no clear pattern of proteins which belong to a certain pathway, some cell cycle regulators, such as p21 (encoded by the *CDKN1A* gene) and cyclin D1 (encoded by the *CCND1* gene), as well as DNA repair proteins, such as RIF1 (encoded by the *RIF1* gene) were upregulated as seen in the volcano plots (Figure 5.8). p21 and cyclin D1 were only significantly upregulated in untreated HCT116$^{\Delta PR130}$ cells compared to wild-type cells (Figure 5.8 A). RIF1, however, was enriched in HCT116$^{\Delta gRNA}$ cells upon all treatment conditions (Figure 5.8 A–D).

5.2.1.1 Western Blot analysis validates higher levels of cell cycle regulators in PR130-deficient cells

To validate the proteome screen, p21 and cyclin D1 levels were analyzed by immunoblot (Figure 5.9). Therefore, HCT116$^{\Delta gRNA}$ and HCT116$^{\Delta PR130}$ cells were incubated with 1 mM HU ± 5 µM MS-275 for 24 h.

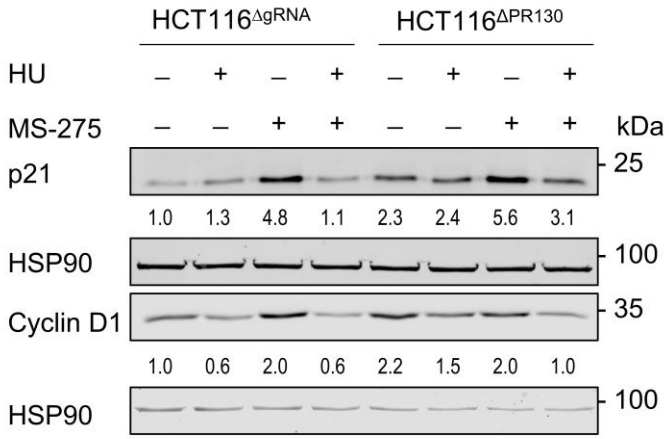

Figure 5.9: PR130-deficient cells have higher levels of p21 and cyclin D1 compared to wild-type cells. Cells were treated with 1 mM HU ± 5 µM MS-275 for 24 h. p21 and cyclin D1 levels were analyzed by immunoblot with HSP90 as loading control. Numbers indicate densitometric analysis of protein signals relative to untreated wild-type cells normalized to the respective loading controls.

About 2.3-fold higher levels of p21, and 2.2-fold higher levels of cyclin D1 were detected in untreated PR130-deficient cells compared to wild-type cells (Figure 5.9). However, HU- and/or MS-275-treated HCT116$^{\Delta PR130}$ cells also showed higher levels of p21 compared to control cells treated with the same inhibitor, which could not be seen in the proteome screen. Moreover, MS-275 treatment increased levels of p21 in both cell lines. In case of cyclin D1, there were not only twofold higher protein levels in the untreated, but also in HU-treated HCT116$^{\Delta PR130}$ cells compared to similar treated HCT116$^{\Delta gRNA}$ cells. However, incubation with MS-275 did not display significant differences in cyclin D1 protein levels between both cell systems.

5.2.1.2 HDAC1 and 2 control expression of PR130 and p21

Western blot analysis showed that HDAC inhibition by MS-275 treatment strongly increased the expression of p21 (Figure 5.9), which is in line with literature reports (Davie 2003). Next, it was investigated which HDACs exactly control the expression of the cell cycle regulator. Therefore, HCT116^{wt} cells were treated with different class I HDACi (Figure 5.10 A).

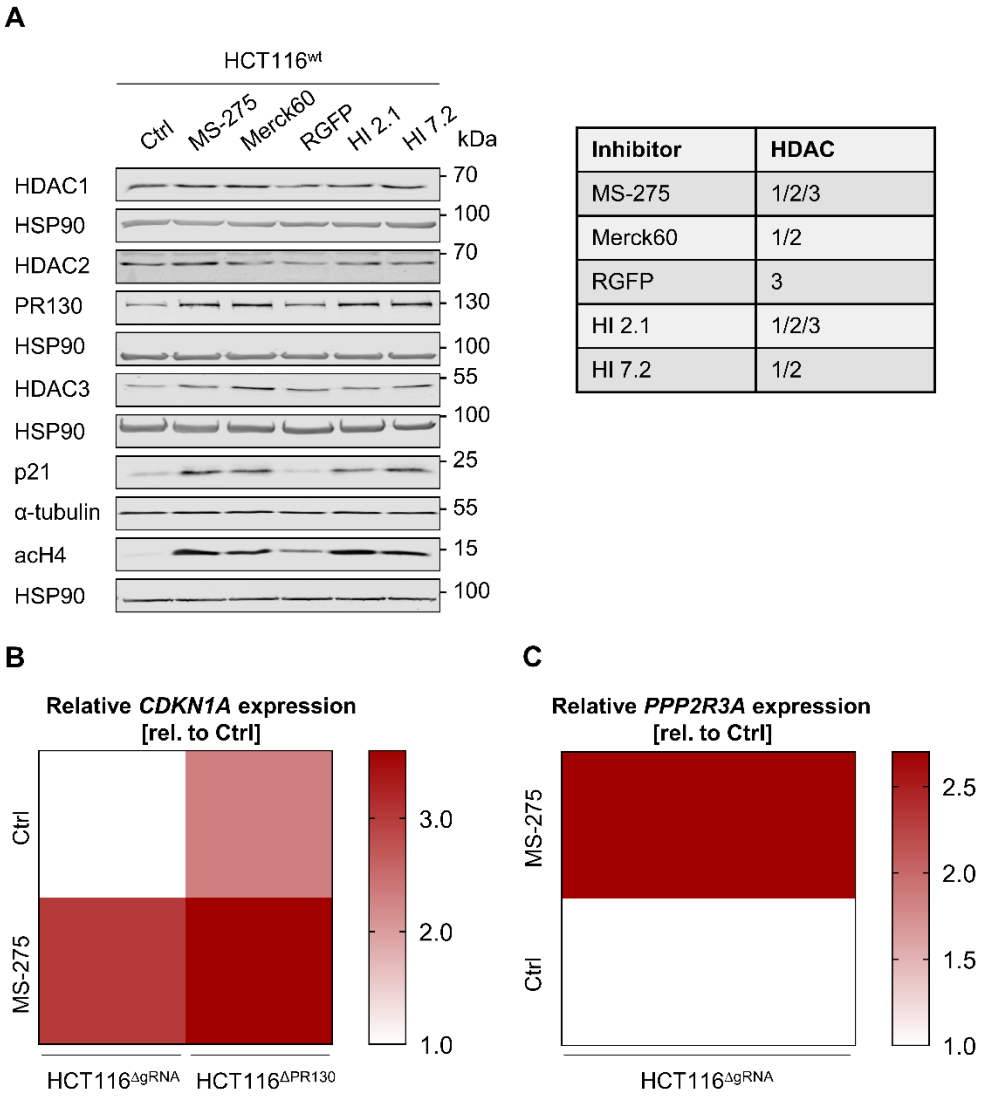

Figure 5.10: HDAC1 and 2 control the expression of PR130 and p21. A HCT116^{wt} cells were treated with 5 µM of different class I HDACi (see table on the right side) for 24 h. These HDACi inhibit different combinations of HDAC1, HDAC2 and HDAC3. **B** and **C** HCT116$^{\Delta gRNA}$ and HCT116$^{\Delta PR130}$ were treated with 5 µM MS-275 for 24 h. RNA sequencing analysis was carried out using the NextSeq500 system (n=3). **B** shows the relative p21 expression (encoded by the *CDKN1A* gene) normalized to untreated HCT116$^{\Delta gRNA}$ cells. **C** displays the relative PR130 expression (encoded by the *PPP2R3A* gene) normalized to untreated HCT116$^{\Delta gRNA}$ cells.

Interestingly, HDAC1 and HDAC2, which also control the expression of the PP2A regulatory subunit PR130 (Göder et al. 2018) were found to regulate p21 expression, since all tested HDACi, except for HDAC3-specific RGFP, induced the cell cycle regulators' expression (Figure 5.10 A).

Next, the PR130-dependent *CDKN1A* expression of untreated and MS-275-treated cells was investigated, since cells lacking the regulatory subunit showed higher levels of the cell cycle regulator on protein level (Figure 5.8 and Figure 5.9). Therefore, HCT116$^{\Delta gRNA}$ and HCT116$^{\Delta PR130}$ cells were treated with MS-275 and submitted to RNA sequencing analysis (Figure 5.10 B). Untreated HCT116$^{\Delta PR130}$ cells already showed 2.3-fold higher *CDKN1A* levels compared to wild-type cells. This points to a transcriptional control of the cell cycle regulator by the PP2A-PR130 complex, which will be analyzed in more detail in chapter 5.3. MS-275 treatment increased the expression of p21 in both cell lines. In case of HCT116$^{\Delta gRNA}$ cells the expression was increased 3.0-fold, in case of HCT116$^{\Delta PR130}$ cells 1.3-fold. RNA sequencing analysis further validated MS-275-induced *PPP2R3A* expression in HCT116$^{\Delta gRNA}$ cells (Figure 5.10 C). In conclusion, expression of PR130 and p21 is controlled by HDAC1/2.

5.2.1.3 Class I HDACs maintain expression of cell cycle regulators

Due to the significant differences in the two cell cycle regulators p21 and cyclin D1 in the global proteome screen (Figure 5.8), a RNA sequencing analysis should clarify whether other cell cycle regulators are also regulated by replication stress, HDACi and PR130. HCT116$^{\Delta gRNA}$ and HCT116$^{\Delta PR130}$ cells were incubated with HU ± MS-275 for 24 h and RNAs were analyzed using the NextSeq500 system (Figure 5.11).

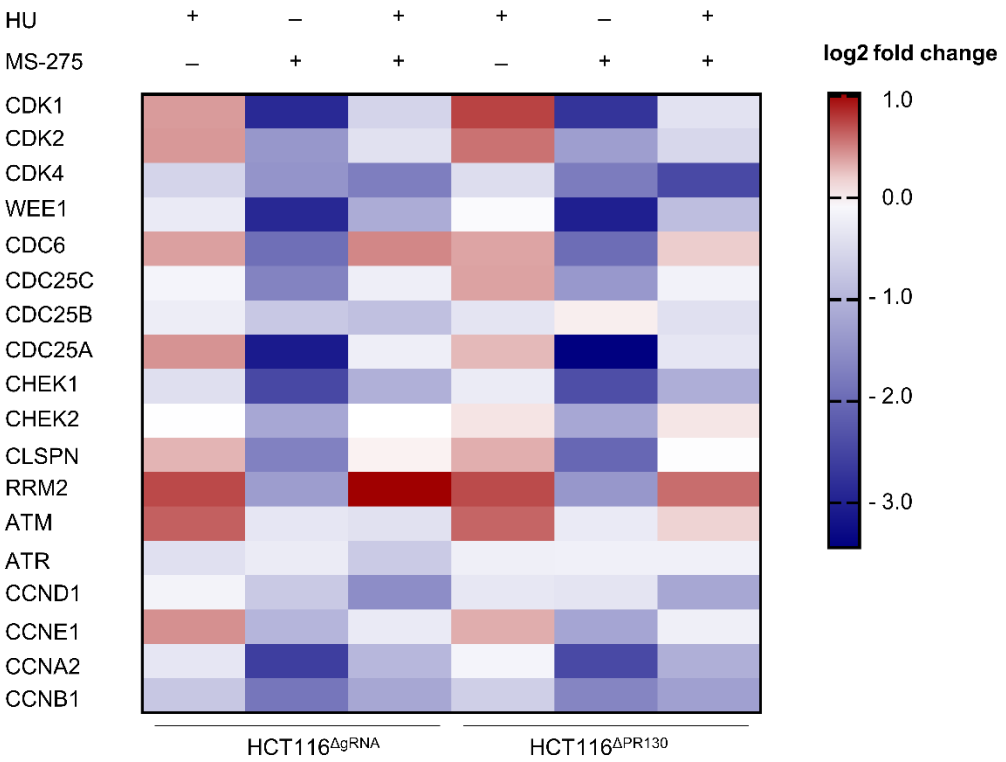

Figure 5.11: Heatmap of cell cycle regulators. HCT116$^{\Delta gRNA}$ and HCT116$^{\Delta PR130}$ cells were treated with 1 mM HU ± 5 µM MS-275 for 24 h. RNA sequencing analysis (n=3) was carried out using the NextSeq500 system. Heatmap shows log2 fold changes (red: upregulated, blue: downregulated).

Whereas HU treatment only had a moderate effect on the expression of various cell cycle regulators, MS-275 treatment decreased the expression of multiple target genes in both cell lines. The combinatorial treatment slightly decreased the expression of some of the investigated genes; however, the changes were not as strong as for MS-275 single-treatments. The PR130 status of the cells did not have a strong impact on the gene expression of the analyzed cell cycle regulators (Supplementary Figure 8.11), except for *CDKN1A*, which had already been shown (Figure 5.10 B).

A gene set enrichment analysis of MS-275-treated HCT116$^{\Delta gRNA}$ and HCT116$^{\Delta PR130}$ cells showed that class I HDACi decreased the expression of genes which are important for

G1/S transition and during S phase (Figure 5.12), underlining the reduced S phase fraction in MS-275-treated cells (Figure 5.1 B).

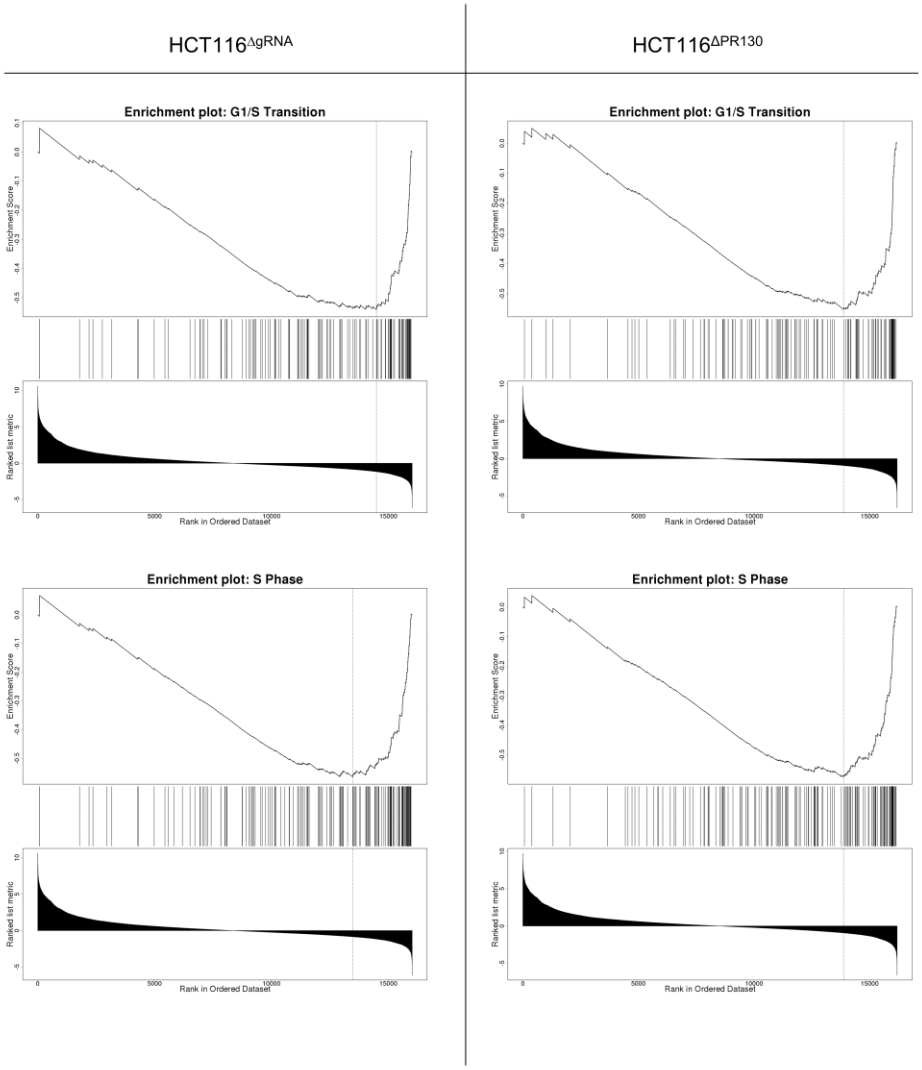

Figure 5.12: Class I HDACi downregulate genes important for G1/S transition and S phase. HCT116$^{\Delta gRNA}$ and HCT116$^{\Delta PR130}$ cells were treated with 5 µM MS-275 for 24 h. Gene set enrichment analysis plots were created using WebGestalt.

5.2.2 Gene set enrichment analysis revealed further PP2A-PR130-dependent pathways

Since MS-275 treatment increased the expression of the regulatory subunit PR130 (Figure 5.10 C), the RNA sequencing analysis of HCT116$^{\Delta gRNA}$ and HCT116$^{\Delta PR130}$ cells treated with HU + MS-275 was also performed to determine which genes and pathways are further regulated in a PR130-dependent manner upon replication stress (Figure 5.13).

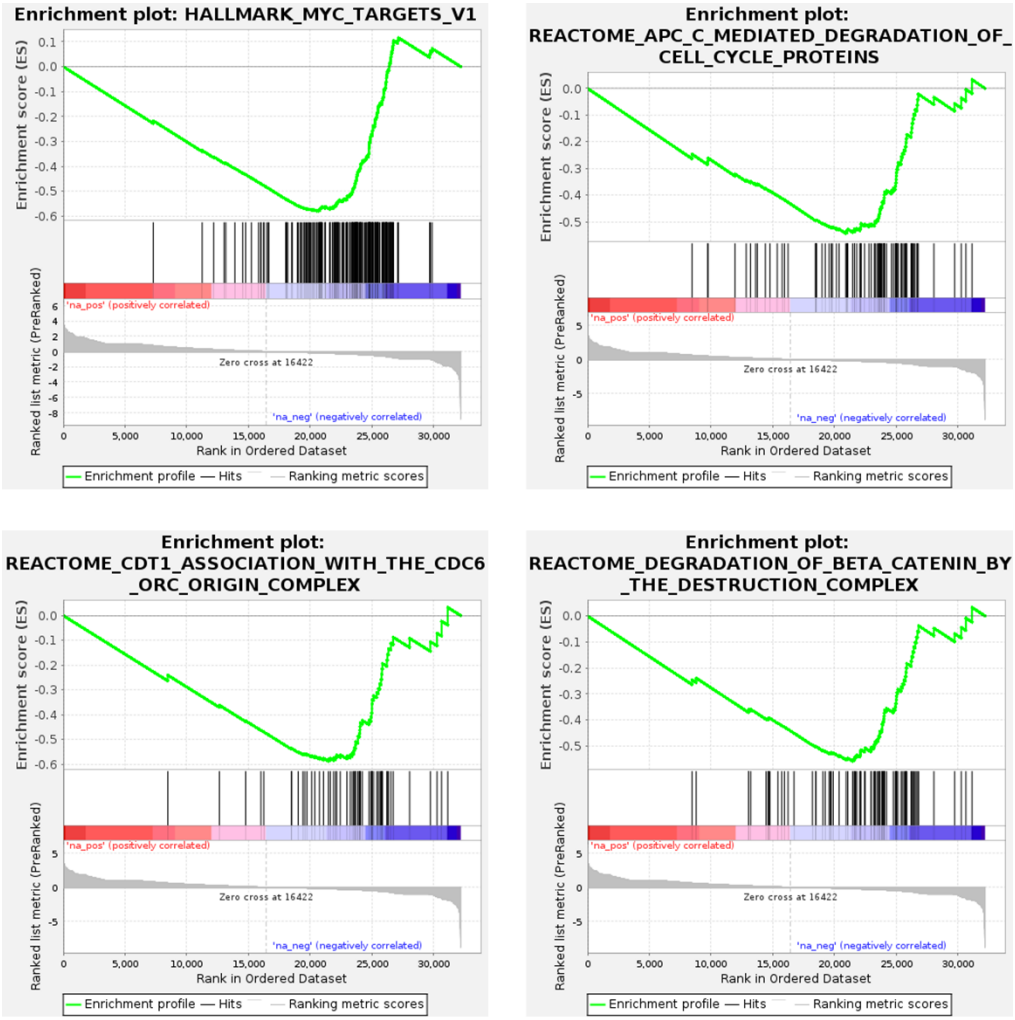

Figure 5.13: Cellular pathways regulated by PR130 upon replication stress. HCT116$^{\Delta gRNA}$ and HCT116$^{\Delta PR130}$ were treated with 1 mM HU ± 5 µM MS-275 for 24 h. Gene set enrichment analysis was kindly performed by [redacted].

Especially *MYC targets* genes, *Cdc6/ORC-related* and genes responsible for *APC-mediated degradation of cell cycle proteins and β-catenin* were downregulated in PR130-deficient cells compared to control cells.

5.3 PR130-dependent control of CHK1 phosphorylation by the p21-CDK2-WEE1 signalling axis

5.3.1 PR130 regulates p21 on protein and mRNA levels through ATM and p53

Proteome (Figure 5.8) and RNA sequencing (Figure 5.10) analysis revealed that the cell cycle regulator p21 is significantly upregulated on protein and mRNA levels in HCT116$^{\Delta PR130}$ cells compared to HCT116$^{\Delta gRNA}$ cells. Western blot analysis of p21 supported this finding (Figure 5.9). These differences in p21 levels suggest a transcriptional control of the cell cycle regulator by the PP2A-PR130 complex. As the protein kinase ATM is a known target of the PP2A-PR130 complex (Göder et al. 2018) and an upstream regulator of the tumor transcription factor p53 (Smith et al. 2020), ATM inhibition and p53 knockdown and their influence on p21 levels were further investigated.

Therefore, HCT116$^{\Delta gRNA}$ and HCT116$^{\Delta PR130}$ cells were treated with 3 µM KU-60019 (ATMi) for 1 h and afterwards with 1 mM HU for 24 h (Figure 5.14).

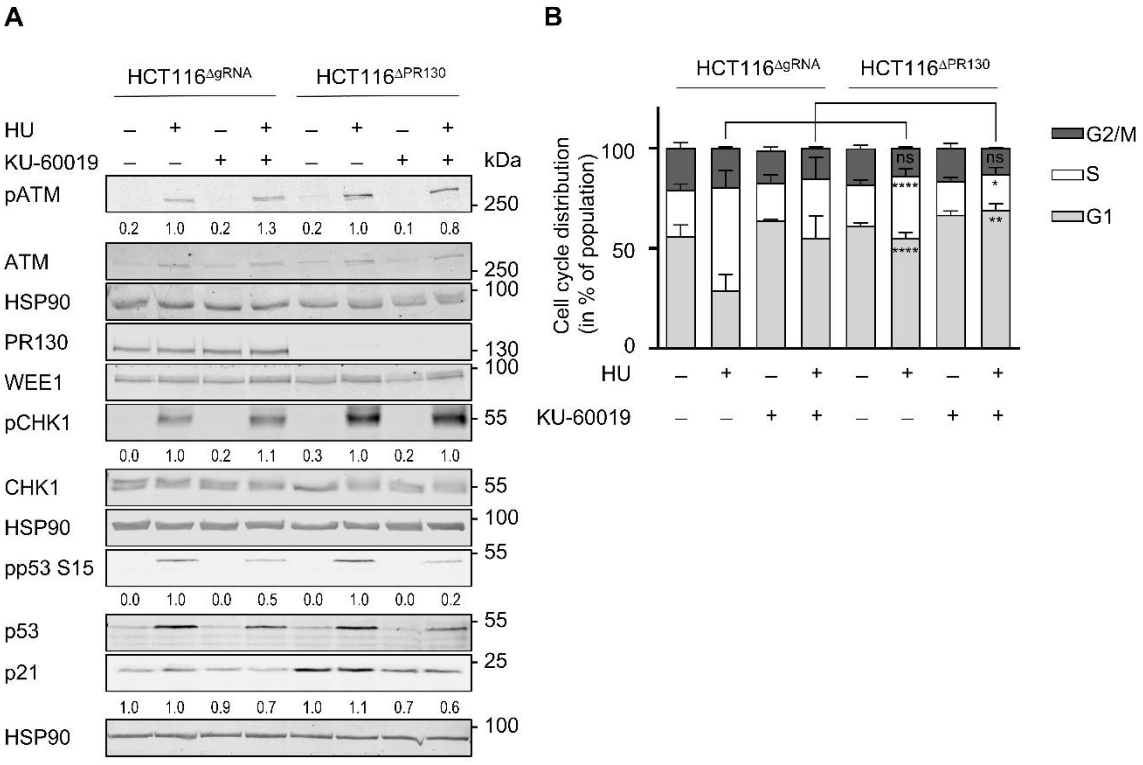

Figure 5.14: ATM controls expression of p21. A HCT116$^{\Delta gRNA}$ and HCT116$^{\Delta PR130}$ cells were treated with 1 mM HU ± 3 µM KU-60019 (1 h pre-treatment) for 24 h. Indicated proteins were analyzed by immunoblot. Numbers indicate densitometric values of the immunoblot signals relative to those of lysates from HU-treated (pATM, pCHK1, pp53 S15) or untreated (p21) cells normalized to the respective loading control. **B** Cell cycle distribution of HU ± KU-60019-treated cells was measured on the flow cytometer. SubG1 fractions were excluded. Data show mean ±

SD (n=3). Statistical analysis was performed using Two-way ANOVA and Tukey's Multiple Comparison Test (*p<0.05, **p<0.01, ****p<0.0001, ns=not significant).

It was observed that HU treatment increased phosphorylation of ATM at S1981 in both cell lines. Combinatorial treatment with the ATMi had no significant influence on phosphorylation of ATM and CHK1. However, the combinatorial treatment decreased levels of p53, phosphorylated p53 (S15) and p21, especially in case of PR130-deficient cells (Figure 5.14 A). Looking at the cell cycle distribution, higher amounts of HCT116$^{\Delta PR130}$ cells arrested in G1 phase upon replication stress compared to HCT116$^{\Delta gRNA}$ cells. Upon combinatorial treatment the difference of cells in G1 phase between both cell systems became less pronounced (Figure 5.14 B). Next, p53 knockdown and its influence on p21 levels (Figure 5.15 A) was analyzed since p53 is a known upstream regulator of p21.

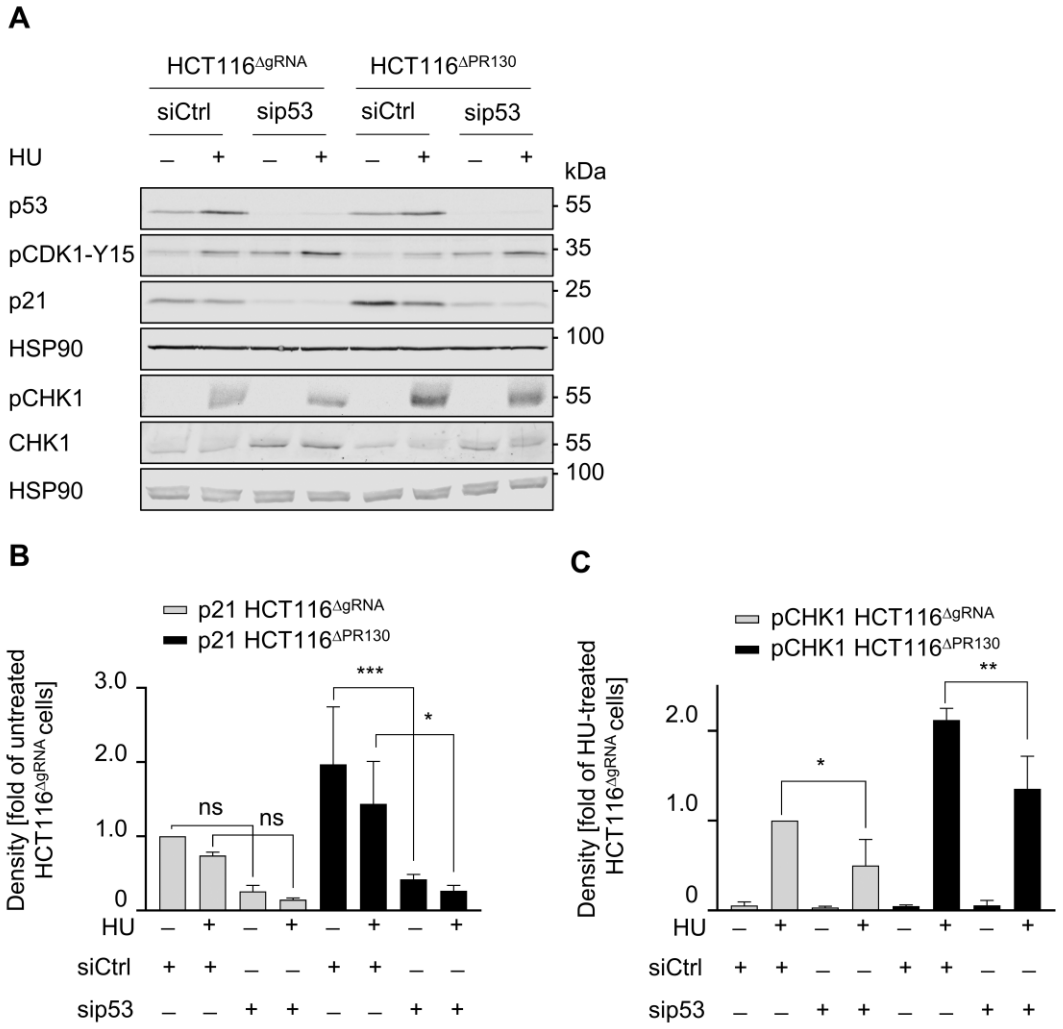

Figure 5.15: p53 controls the expression of p21. A HCT116$^{\Delta gRNA}$ and HCT116$^{\Delta PR130}$ cells were transfected with 30 pmol siRNA against p53 or control siRNA (siCtrl) for 24 h. Thereafter, cells were incubated with 1 mM HU for 24 h. Proteins were detected by immunoblot. HSP90 served as loading control. **B** Densitometric analysis of p21 levels in HCT116$^{\Delta gRNA}$ and HCT116$^{\Delta PR130}$ cells

relative to untreated HCT116$^{\Delta gRNA}$ cells. Data are presented as mean ± SD (n=3). Statistical analysis was carried out using One-way ANOVA and Tukey's Multiple Comparison Test (*p<0.05; ***p<0.001). **C** Densitometric analysis of pCHK1 levels relative to untreated wild-type cells. Statistical analysis was performed as stated in **B** (*p<0.05; **p<0.01; mean ± SD; n=3).

Knockdown of p53 reduced p21 levels to a minimum in both cell lines (Figure 5.15 B). In HCT116$^{\Delta PR130}$ cells, this effect was significant, whereas in HCT116$^{\Delta gRNA}$ cells only a trend was visible. Furthermore, a reduction in CHK1 phosphorylation upon HU treatment and p53 knockdown compared to HU single treatment was observed (Figure 5.15 C). In HCT116$^{\Delta gRNA}$ cells, pCHK1 signals decreased by 50%, whereas HCT116$^{\Delta PR130}$ cells showed 33% less protein induction after p53 knockdown. Moreover, phosphorylation of the cell cycle regulating protein CDK1 at tyrosine 15 (pCDK1-Y15) correlated negatively with p53 and p21 levels (Figure 5.15 A). HCT116$^{p53-/-}$ cells were also tested for p21 and pCHK1 levels (Supplementary Figure 8.4) and showed similar results as p53 knockdown experiments.

5.3.2 p21 is essential for efficient CHK1 phosphorylation upon replication stress

Due to the differences in p21 levels in both cell systems, the impact of p21-knockdown for cell cycle distribution and checkpoint kinase activation were analyzed. Therefore, HCT116$^{\Delta gRNA}$ and HCT116$^{\Delta PR130}$ cells were transfected with siRNA against p21 or control siRNA for 24 h and were afterwards treated with 1 mM HU for another 24 h (Figure 5.16).

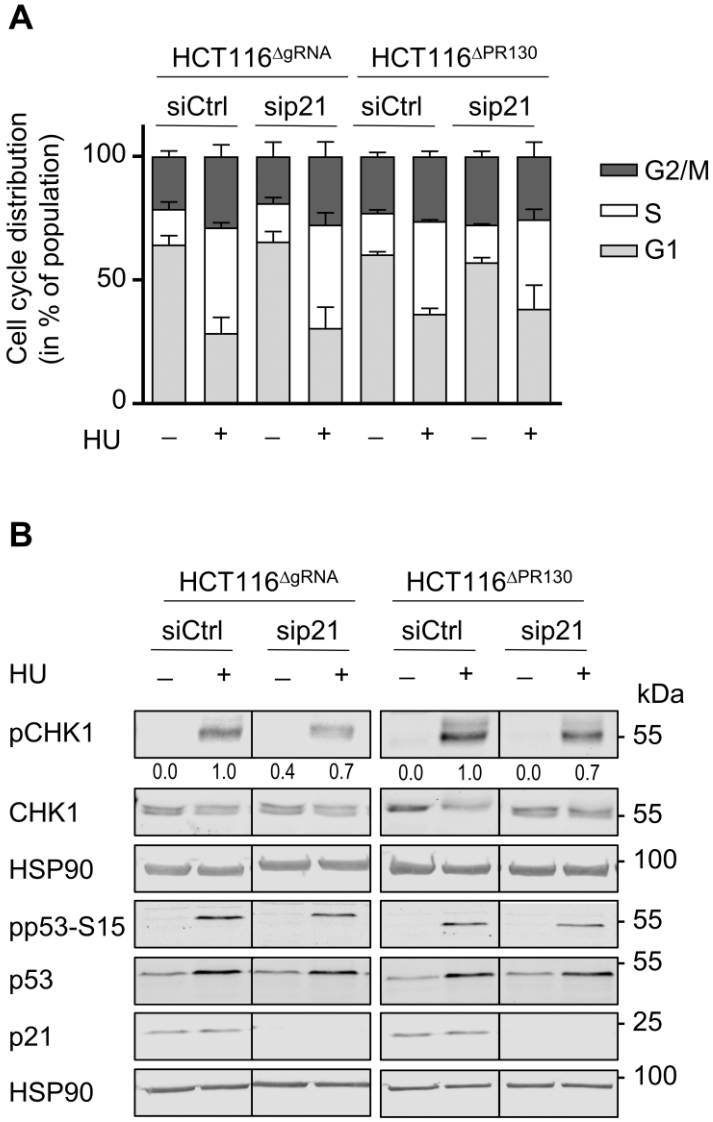

Figure 5.16: p21 is essential for phosphorylation of CHK1 upon replication stress. **A** HCT116$^{\Delta gRNA}$ and HCT116$^{\Delta PR130}$ cells were transfected with 30 pmol siRNA against p21 or siCtrl (24 h). Cells were then treated with 1 mM HU for 24 h. Cell cycle distribution of PI-stained cells was analyzed on the flow cytometer (n=3). **B** Cells were handled as stated in **A** (n=3). Indicated proteins were detected using the Odyssey Infrared Imaging System. Densitometrical analysis was carried out with Image Studio Lite. Signals were normalized to HU-treated HCT116$^{\Delta gRNA}$ or HCT116$^{\Delta PR130}$ cells transfected with siCtrl. All shown proteins are located on the same membrane, but it was cut for better comparability.

While there was no difference in the cell cycle distribution upon HU treatment with or without p21 (Figure 5.16 A), the checkpoint kinase activation showed a different picture (Figure 5.16 B). Knockdown of p21 reduced phosphorylation of CHK1 upon HU treatment around 30% in both cell lines. Similarly treated HCT116$^{p21-/-}$ cells compared to HCT116^{wt} cells gave a congruent result (Supplementary Figure 8.5). This shows that p21 is essential for phosphorylation of CHK1 upon replication stress.

5.3.3 CDK2 is essential for CHK1 phosphorylation upon replication stress

p21 can suppress the catalytic activities of the cyclin-dependent kinases CDK1 and CDK2, which promote CHK1 phosphorylation upon DNA damage (Xu et al. 2012). The focus was placed on CDK2, since it is highly active in a complex with cyclin E in early S-phase (Bačević et al. 2017). HCT116$^{\Delta gRNA}$ and HCT116$^{\Delta PR130}$ cells were treated with HU ± CDK2i for 24 h and the cell cycle progression and CHK1 phosphorylation were analyzed (Figure 5.17).

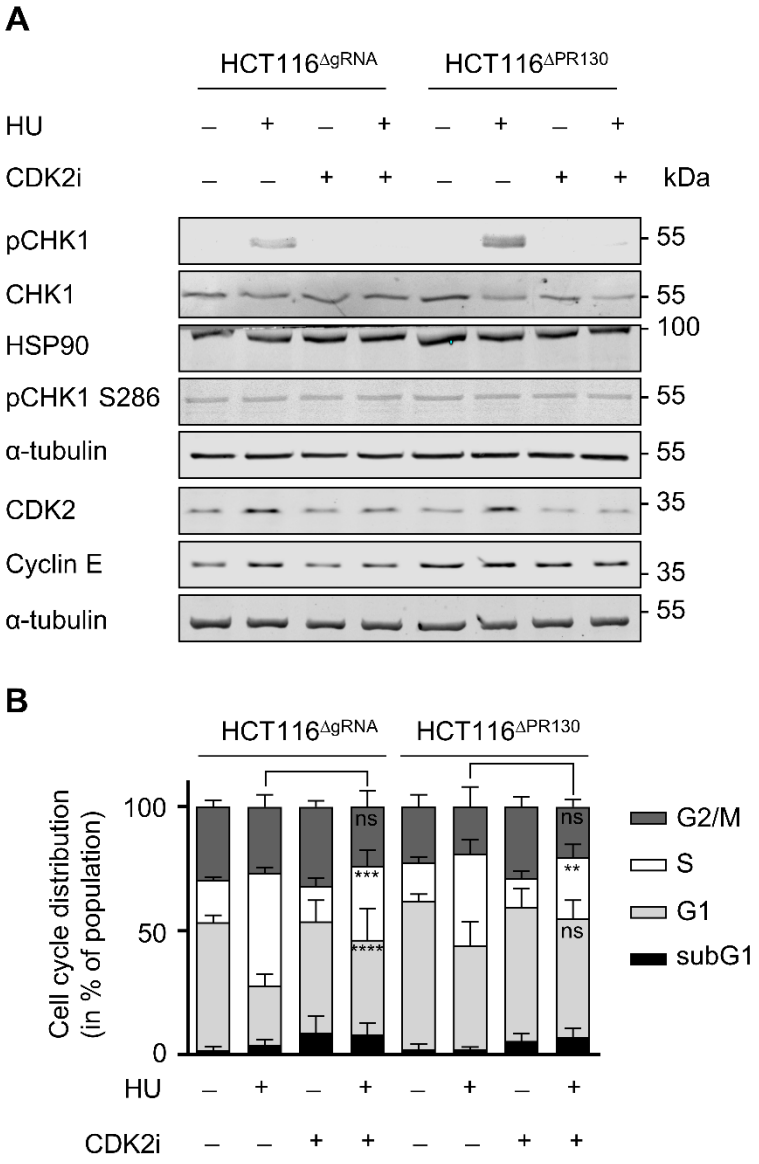

Figure 5.17: CDK2 is essential for CHK1 phosphorylation upon replication stress. **A** HCT116$^{\Delta gRNA}$ and HCT116$^{\Delta PR130}$ cells were treated with 1 mM HU ± 5 µM CDK2i for 24 h. Proteins were analyzed by immunoblot with HSP90 and α-tubulin as loading controls. **B** Cells were treated as stated in **A**. Cell cycle analysis of PI-stained cells was carried out on the BD FACS Canto II system (n=5)**.** Statistical analysis was performed using Two-way ANOVA and Tukey's Multiple Comparison Test (**p<0.01, ***p<0.001, ****p<0.0001, ns=not significant).

While HU treatment increased, the combinatorial treatment completely abrogated phosphorylation of CHK1 (Figure 5.17 A). The combinatorial treatment arrested significantly more HCT116$^{\Delta gRNA}$ cells in G1 phase, while there was no difference in case of HCT116$^{\Delta PR130}$ cells (Figure 5.17 B).

The close interaction between p21, CDK2 and PR130 as shown above begs the question whether these proteins interact in a complex. To test this hypothesis, immunoprecipitation experiments were carried out (Figure 5.18).

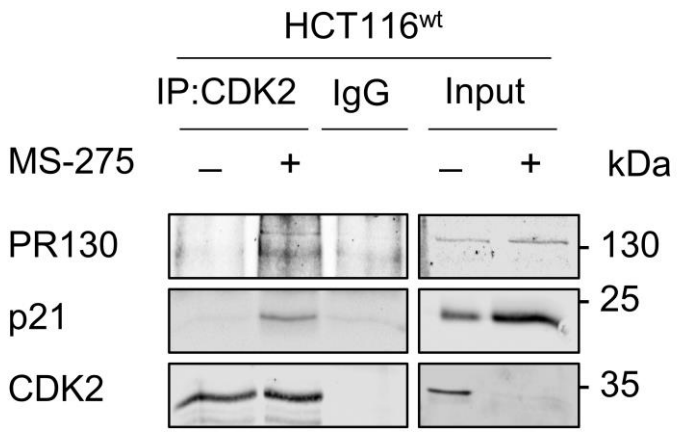

Figure 5.18: CDK2, p21 and PR130 form a complex upon class I HDACi treatment. HCT116^{wt} cells were treated with 5 µM MS-275 for 24 h. Immunoprecipitation (IP) was performed using CDK2 antibody or mouse IgG. PR130, p21 and CDK2 were detected by immunoblot. Input represents 4% of the lysate used for the IP (n=3).

Immunoprecipitation experiments showed that p21 binds CDK2 in MS-275-treated cells. Moreover, this complex of p21 and CDK2 contains the PP2A B-type subunit PR130 (Figure 5.18).

5.3.4 pp21-S130 and pWEE1-T190 are targets of the PP2A-PR130 complex

Since p21 suppresses CDK2 activity, which primes CHK1 for phosphorylation upon replication stress, it was still not clear why HCT116$^{\Delta PR130}$ cells with high p21 levels showed a stronger phosphorylation of CHK1 compared to wild-type cells. Here, a phosphoproteome analysis, which was carried out to identify potential targets of the PP2A-PR130 complex, gave detailed insights. For the analysis, cells were cultured for two weeks in light, medium and heavy SILAC media (Figure 5.19 A) for isotopic labeling and were afterwards treated with 1 mM HU for 24 h. Since HCT116$^{\Delta gRNA}$ and HCT116$^{\Delta PR130}$ cells showed significant differences in CHK1 phosphorylation upon

replication stress, the phosphorylation status was examined prior to the analysis to ensure that the labeling did not directly affect checkpoint kinase signaling.

A

SILAC	Cells	Treatment
Light	HCT116$^{\Delta gRNA}$	-
Medium	HCT116$^{\Delta gRNA}$	1 mM HU (24 h)
Heavy	HCT116$^{\Delta PR130}$	1 mM HU (24 h)

B

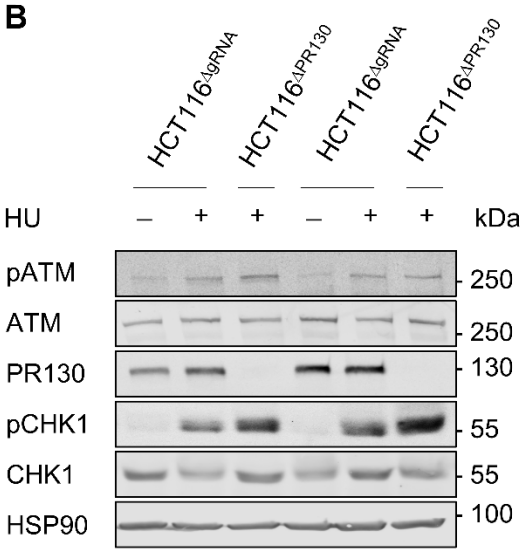

C

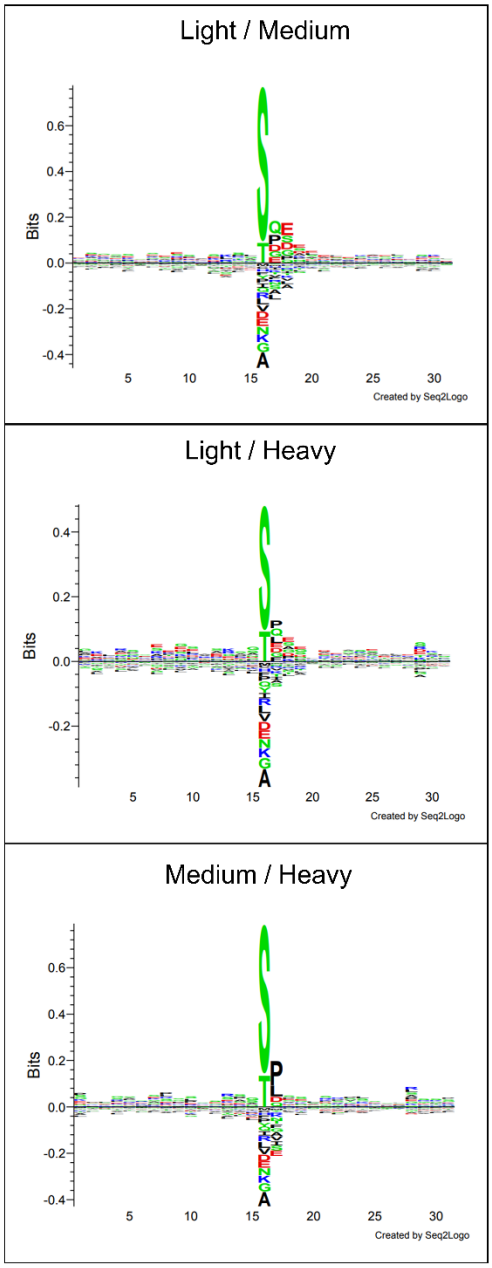

D

Gene	Sequence	Phospho site
CDKN1A	SGEQAEGS(1)PGG PGDSQGR	S130
WEE1	LRLFDTPHT(1)PK	T190

Figure 5.19: pp21-S130 and pWEE1-T190 are novel targets of the PP2A-PR130 complex. **A** HCT116$^{\Delta gRNA}$ and HCT116$^{\Delta PR130}$ cells were cultured in light, medium and heavy SILAC medium for 2 weeks. Cells were then treated with 1 mM HU for 24 h. **B** Prior to the mass spectrometry-based phosphoproteome analysis, cells were validated for CHK1 phosphorylation. **C** Sequence logo analysis of compared conditions was carried out using upregulated phosphorylated sites with ± 15-residue flaking sequences. **D** Gene sequences and detected phosphosites of p21 (encoded by the *CDKN1A* gene) and WEE1 (encoded by the *WEE1* gene).

Both HCT116$^{\Delta gRNA}$ and HCT116$^{\Delta PR130}$ cells displayed no differences in CHK1 phosphorylation whether they were cultured in SILAC media or not (Figure 5.19 B). The comparison between the conditions “medium” and “heavy” was the most interesting to look at, as it compares both cell systems upon replication stress. The analysis revealed that the S/T-directed PP2A-PR130 complex favors interaction partners having proline or leucine near serine or threonine (Figure 5.19 C). The two phospho-proteins, pp21-S130 and pWEE1-T190, which exhibit this kind of structure, were consequently identified as novel targets of the PP2A-PR130 complex (Figure 5.19 D). Phosphorylation of WEE1 at T190 has been shown to inactivate the kinase activity (Pagliuca et al. 2011). The results from the phosphoproteome analysis were validated by immunoblot. Both cell systems were treated with 1 mM HU and investigated in respect to phosphorylation of p21 at S130 (Figure 5.20 A) and phosphorylation of CDK1 (Figure 5.20 B), which indicates WEE1 activity.

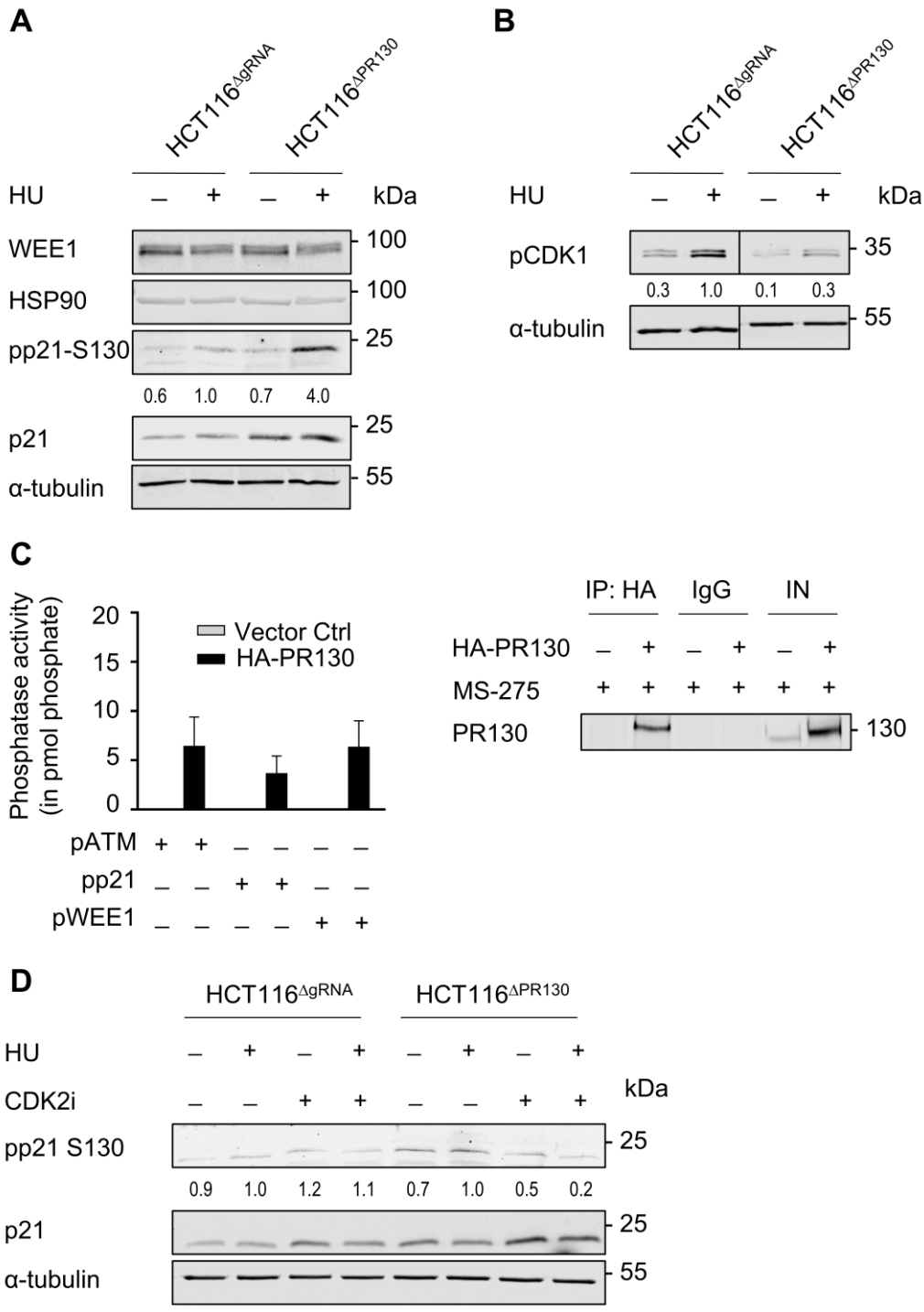

Figure 5.20: Validation of pp21-S130 and pWEE1-T190 as targets of the PP2A-PR130 complex. A HCT116$^{\Delta gRNA}$ and HCT116$^{\Delta PR130}$ cells were treated with 1 mM HU for 24 h. WEE1, pp21-S130 and p21 were detected by immunoblot. HSP90 and α-tubulin served as loading controls. **B** Cells were treated as stated in **A**. pCDK1 levels were analyzed by immunoblot. All shown proteins are located on the same membrane which was cut for better comparability. Numbers indicate densitometric analysis of pp21 (**A**) and pCDK1 (**B**) signals (normalized to HU-treated HCT116$^{\Delta gRNA}$ cells) relative to α-tubulin. **C** HCT116^{wt} cells were transfected with HA-tagged PR130 or a vector control (Ctrl). Afterwards, cells were treated with 5 µM MS-275 (24 h) to increase the amount of PR130. The phosphatase activity of PR130-complexes against pp21-

S130 an pWEE1-T190 peptides was measured using the malachite green assay. The pATM-S1981 peptide served as positive control (mean ± SEM; pATM, pp21: n=4; pWEE1: n=3). The representative immunoblot displays the precipitated HA-PR130 complex (IP=immunoprecipitation; IN=input). **D** HCT116$^{\Delta gRNA}$ and HCT116$^{\Delta PR130}$ cells were treated with 1 mM HU ± 5 µM CDK2i for 24 h. pp21-S130 and p21 were analyzed by immunoblot with α-tubulin as loading control. Numbers indicate densitometric values of the immunoblot signals relative to untreated cells normalized to α-tubulin.

HCT116$^{\Delta PR130}$ cells showed 4.0-fold higher levels of pp21-S130 upon replication stress compared to similar treated wild-type cells (Figure 5.20 A). Moreover, the cells showed 70% less phosphorylation of CDK1 upon replication stress compared to HCT116$^{\Delta gRNA}$ cells, indicating that PR130 controls WEE1 activity. Further, the activity of HA-tagged PR130 against pp21-S130 and pWEE1-T190 phospho-peptides was tested (Figure 5.20 C). pATM-S1981 served as positive control as shown previously in (Göder et al. 2018). PR130 was able to dephosphorylate both tested phospho-peptides. Taken together, the PP2A-PR130 complex controls dephosphorylation of p21 and WEE1 at specific serine/threonine phosphorylation sites.

Moreover, HU-treated HCT116$^{\Delta PR130}$ cells showed 80% less phosphorylation of p21 at S130 upon combinatorial treatment with CDK2i (Figure 5.20 D). HCT116$^{\Delta gRNA}$ cells did not show significant changes in phosphorylation of p21 upon HU ± CDK2i treatment. HCT116$^{\Delta PR130}$ cells also had higher cyclin E levels compared to wild-type cells (Supplementary Figure 8.7). This indicates that CDK2 is more active in PR130-deficient cells and phosphorylates p21 at S130.

5.3.5 WEE1 controls phosphorylation of CHK1 via cyclin-dependent kinase CDK2

In the following, HCT116$^{\Delta gRNA}$ and HCT116$^{\Delta PR130}$ cells were analyzed regarding their responsiveness to WEE1 inhibition. Therefore, both cell systems were treated with HU ± the WEE1i MK-1775 (Figure 5.21).

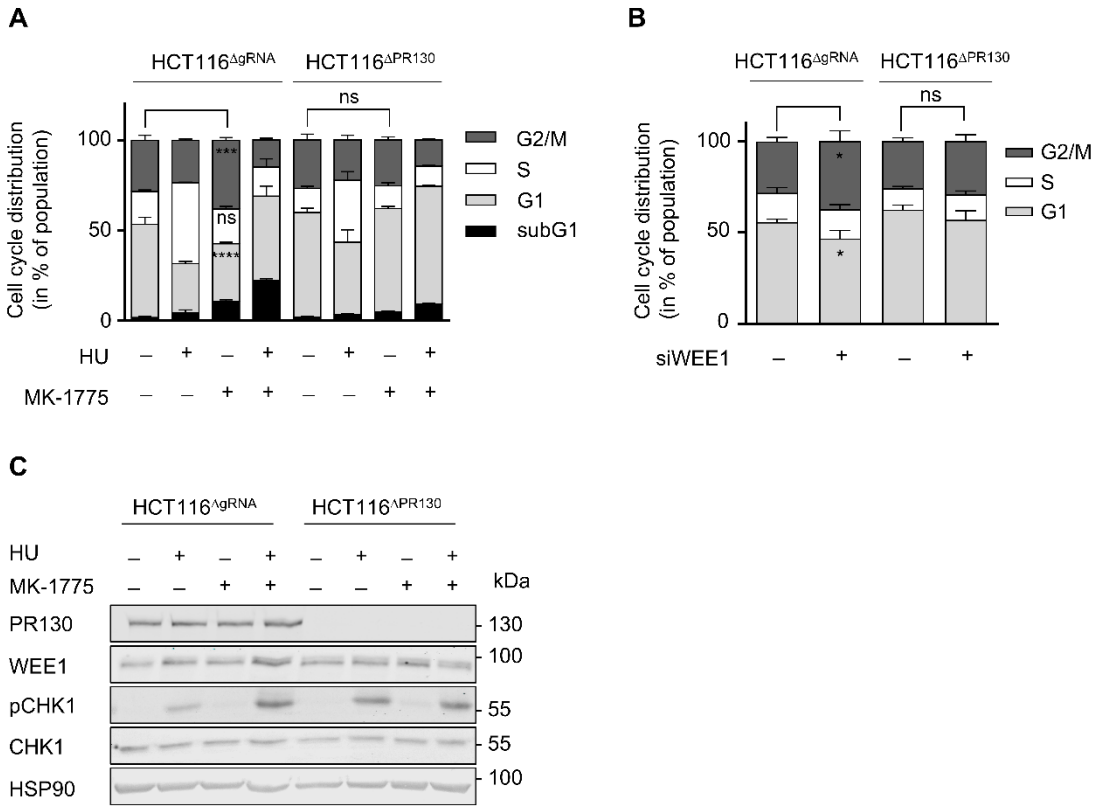

Figure 5.21: HCT116$^{\Delta PR130}$ cells are independent of WEE1. A HCT116$^{\Delta gRNA}$ and HCT116$^{\Delta PR130}$ cells were treated with 1 mM HU ± 500 nM MK-1775 for 24 h. Cell cycle distribution was analyzed by flow cytometry (mean ± SD; n=3). Statistical analysis was performed using Two-way ANOVA and Tukey's Multiple Comparison Test (***p<0.001, ****p<0.0001, ns=not significant). **B** Cells were transfected with 30 pmol siRNA against WEE1 (+) or siCtrl (-). Cell cycle distribution was analyzed, and statistical analysis was carried out as described in **A** (mean ± SD; n=3; *p<0.05, ns=not significant). **C** HCT116$^{\Delta gRNA}$ and HCT116$^{\Delta PR130}$ cells were treated with 1 mM HU for 24 h and afterwards with 500 nM MK-1775 for 1 h. Indicated proteins (HSP90=loading control) were analyzed by the Odyssey Imaging system.

While HCT116$^{\Delta gRNA}$ cells arrested significantly more in G2/M phase upon single treatment with the WEE1 inhibitor, it had no impact on the cell cycle distribution of HCT116$^{\Delta PR130}$ cells (Figure 5.21 A). Knockdown of WEE1 using siRNA gave a similar result (Figure 5.21 B). Interestingly, the combinatorial treatment of HU ± MK-1775 increased phosphorylation of CHK1 in case of PR130-proficient cells. PR130-deficient cells, however, did not show an increase upon HU ± MK-1775 incubation compared to HU only treatment (Figure 5.21 C).

To better visualize the connection between WEE1, CDK2 and phosphorylation of CHK1, all treatment combinations were combined on one immunoblot (Figure 5.22 A).

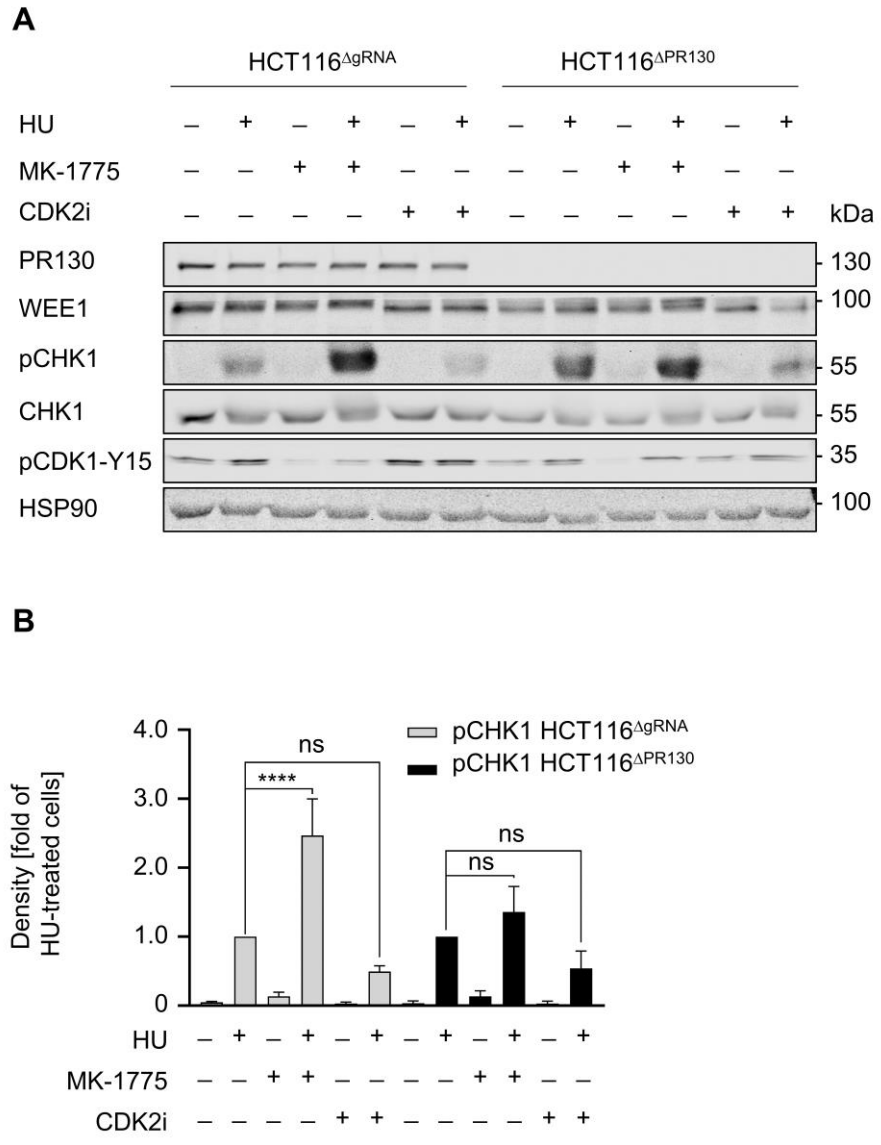

Figure 5.22: Phosphorylation of CHK1 is regulated by WEE1 and CDK2 activity. A HCT116$^{\Delta gRNA}$ and HCT116$^{\Delta PR130}$ cells were treated with 1 mM HU for 24 h and afterwards with 500 nM MK-1775 or 5 µM CDK2i for 1 h. Indicated proteins were detected by immunoblot. **B** Densitometric analysis of pCHK1 levels upon HU ± MK-1175/CDK2i treatment in HCT116$^{\Delta gRNA}$

and HCT116$^{\Delta PR130}$ cells relative to untreated cells. Data are presented as mean ± SD (n=3). Statistical analysis was carried out using One-way ANOVA and Tukey's Multiple Comparison Test (****p<0.0001, ns=not significant).

Combinatorial treatment of HU and the WEE1i MK-1775 increased phosphorylation of CHK1 in case of HU-treated HCT116$^{\Delta gRNA}$ cells, whereas HCT116$^{\Delta PR130}$ cells displayed no significant difference. WEE1 inhibition further decreased phosphorylation of CDK1 at Y15. Combinatorial treatment of HU and the CDK2i reduced phosphorylation of HU-treated HCT116$^{\Delta gRNA}$ and HCT116$^{\Delta PR130}$ cells, however the effect was not significant and only a trend was visible (Figure 5.22 B). To test whether these effects are cancer cell line-specific, non-cancerous fibroblasts (VH10tert) were tested as well and showed similar results (Supplementary Figure 8.8). In summary, WEE1 controls phosphorylation of CHK1 via cyclin-dependent kinase CDK2, a process that is mediated by PR130.

5.4 Regulation of HR and NHEJ by class I HDAC and PR130

As already shown in the global proteome screen, the RIF1 protein was enriched in HCT116$^{\Delta gRNA}$ cells upon all treatment conditions (Figure 5.8 A-D). RIF1 is essential for the DNA repair mechanism NHEJ, as described in chapter 1.3.2 (Bayley et al. 2022). Therefore, the two major DNA repair mechanisms HR and NHEJ were investigated in connection to the PR130 status of the cells. First, HCT116$^{\Delta gRNA}$ and HCT116$^{\Delta PR130}$ cells were incubated with MS-275 to increase the amount of PR130 and DNA repair-related gene expression was analyzed by RNA sequencing analysis (Figure 5.23).

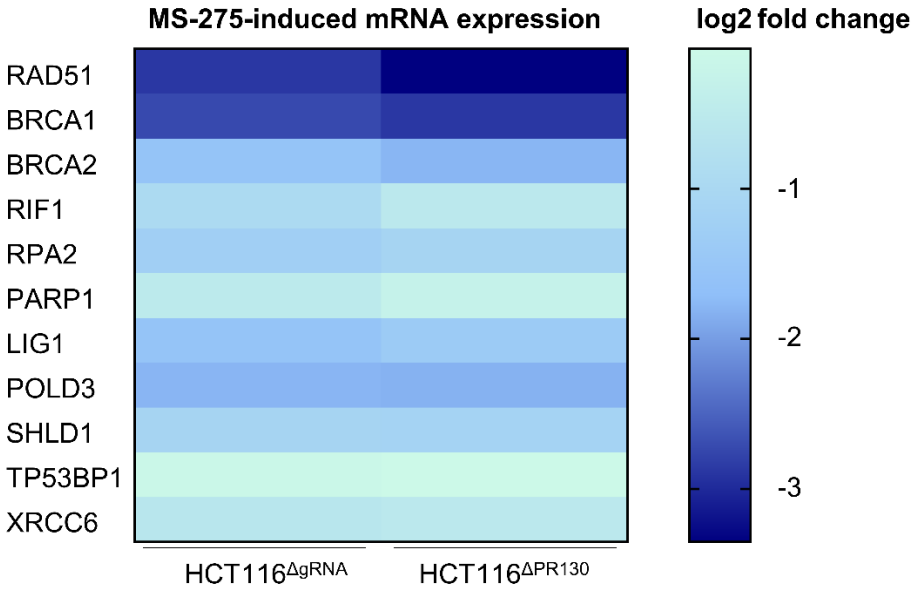

Figure 5.23: Class I HDACs regulate the expression of DNA repair proteins. HCT116$^{\Delta gRNA}$ and HCT116$^{\Delta PR130}$ cells were treated with 5 µM MS-275 for 24 h. RNA sequencing analysis (n=3) was carried out using the NextSeq500 system. Heatmap shows log2 fold changes of genes involved in DNA repair.

Both cell lines showed a decreased expression of RAD51 and BRCA1 upon HDACi. All other tested DNA repair proteins were not significantly affected. There was also no significant difference between the two cell lines regarding the mRNA expression of the tested DNA repair proteins (data not shown).

To analyze whether the MS-275-dependent mRNA decrease of the two essential HR proteins RAD51 and BRCA1 (Prakash et al. 2015) subsequently increases NHEJ, a reporter assay was carried out (in cooperation with [redacted]). HCT116^{wt} cells were transfected with a plasmid expressing GFP upon NHEJ or HR. Cells were then treated with MS-275 for 24 h and analyzed by flow cytometry (Figure 5.24).

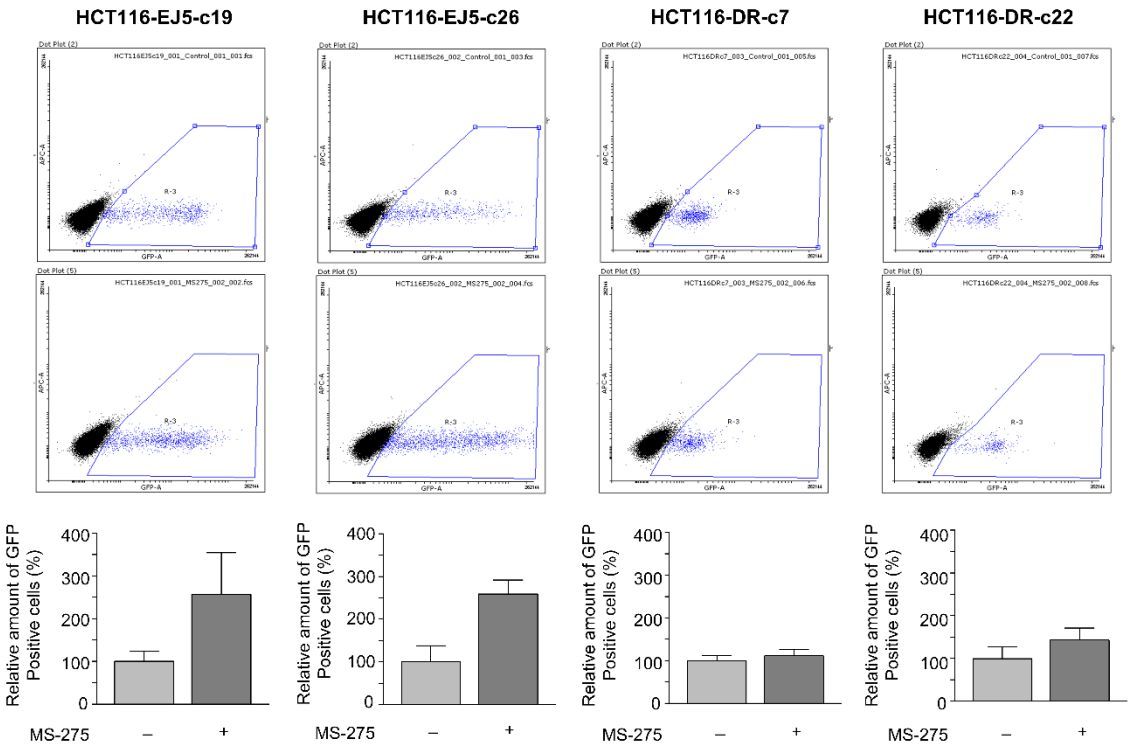

Figure 5.24: Class I HDACi increase NHEJ. HCT116^{wt} cells with a reporter plasmid expressing GFP upon repair by NHEJ or HR were treated with 1.5 µM MS-275 (24 h) and then transfected with the endonuclease I-Sce1. Shown is the percentage of GFP-positive cells, with untreated cells set to 100% (n=3). The reporter assay was kindly performed by [redacted].

The reporter assay revealed that MS-275 treatment stimulated NHEJ-dependent repair of a GFP substrate (Figure 5.24). Cells which carried the HR-GFP plasmid were not affected by HDACi treatment. Taken together, the experiment showed that class I HDACi treatment causes NHEJ as preferred repair mechanism.

In the following, the role of PR130 in the two DNA repair mechanisms HR and NHEJ was analyzed. HCT116$^{\Delta gRNA}$ and HCT116$^{\Delta PR130}$ cells were treated with 1 mM HU and the RAD51 inhibitor RI-1 (30 µM) for 24 h (Figure 5.25). RAD51 is an essential HR protein and its inhibition should cause disruption of HR (Budke et al. 2012).

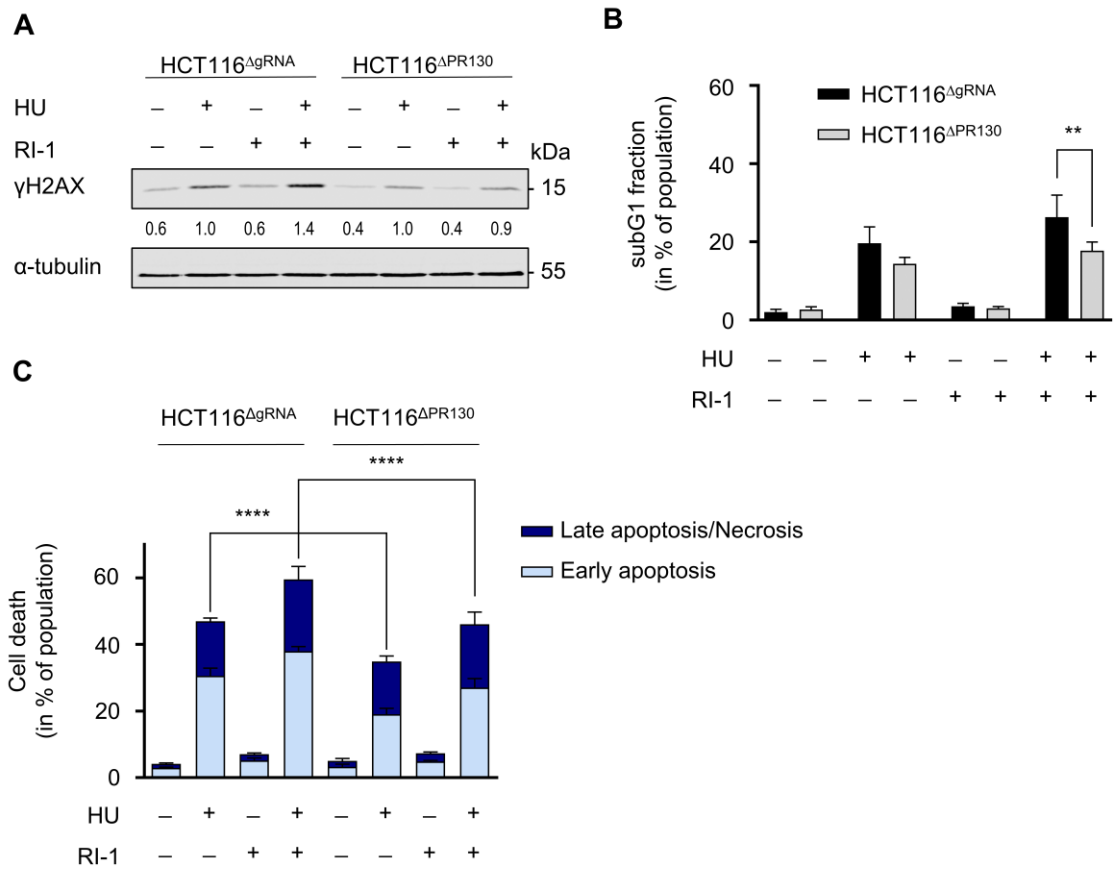

Figure 5.25: PR130 and its involvement in HR. A HCT116$^{\Delta gRNA}$ and HCT116$^{\Delta PR130}$ cells were treated with 1 mM HU ± 30 µM RI-1 for 24 h. γH2AX levels were detected by immunoblot with α-tubulin as loading control. **B** Graph shows subG1 fractions of HCT116$^{\Delta gRNA}$ and HCT116$^{\Delta PR130}$ cells, which were treated with 1 mM HU ± 30 µM RI-1 for 48 h. Statistical analysis: One-Way ANOVA and Tukey's Multiple Comparison Test (**p<0.01). **C** Cells were treated for 48 h and stained with annexin V/PI for cell death analysis. Statistical analysis was done using Two-way ANOVA and Tukey's Multiple Comparison Test (****p<0.0001; n=3).

The combinatorial treatment showed a 1.4-fold increase of the DSB marker γH2AX in case of HCT116$^{\Delta gRNA}$ cells compared to single treatment with HU. However, there was no significant difference in case of HCT116$^{\Delta PR130}$ cells (Figure 5.25 A). Moreover, PR130-proficient cells displayed higher levels of cell death compared to PR130-deficient cells after 48 h of HU ± RI-1 treatment measured by subG1 fractions (Figure 5.25 B) and annexin V/PI-stained cells (Figure 5.25 C).

Next, HCT116$^{\Delta gRNA}$ and HCT116$^{\Delta PR130}$ cells were analyzed via immunofluorescence and stained for γH2AX foci to analyze the induction of DNA damage (Figure 5.26). Both cell lines were incubated with HU ± MS-275 for 24 h.

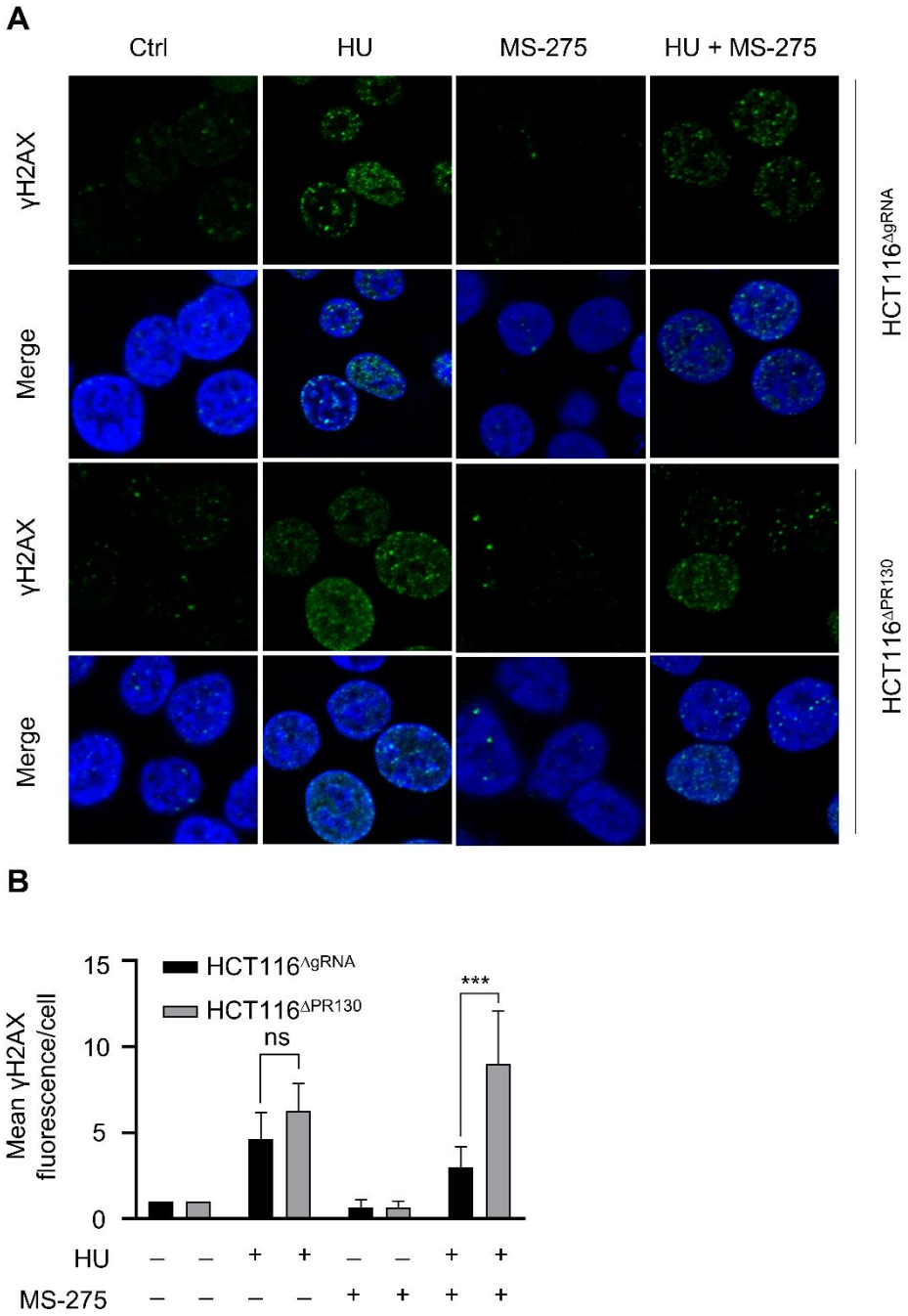

Figure 5.26: γH2AX foci formation upon HU and MS-275 treatment in cells with different PR130 status. A HCT116$^{\Delta gRNA}$ and HCT116$^{\Delta PR130}$ cells were treated with 1 mM HU ± 5 µM MS-275 for 24 h (γH2AX (green); TO-PRO-3 (blue); n=3; >150 cells). Representative images are shown. **B** Mean γH2AX fluorescence of all three performed experiments (mean ± SD; relative to untreated cells). Statistical analysis was performed using One-way ANOVA and Tukey's Multiple Comparison Test (***p<0.001, ns=not significant).

HU treatment increased the γH2AX signal in HCT116$^{\Delta gRNA}$ and HCT116$^{\Delta PR130}$ cells, whereas the combinatorial treatment did not increase it further (Figure 5.26 B; not significant; not shown for better clarity of the graph). However, HCT116$^{\Delta PR130}$ cells displayed a significant higher level of γH2AX upon the combinatorial treatment compared

to wild-type cells (HCT116$^{\Delta PR130}$: 9-fold compared to untreated cells; HCT116$^{\Delta gRNA}$: 3-fold compared to untreated cells).

HCT116$^{\Delta gRNA}$ and HCT116$^{\Delta PR130}$ cells were furthermore treated with HU ± MS-275 for 24 h and analyzed for chromosomal aberrations (Figure 5.27).

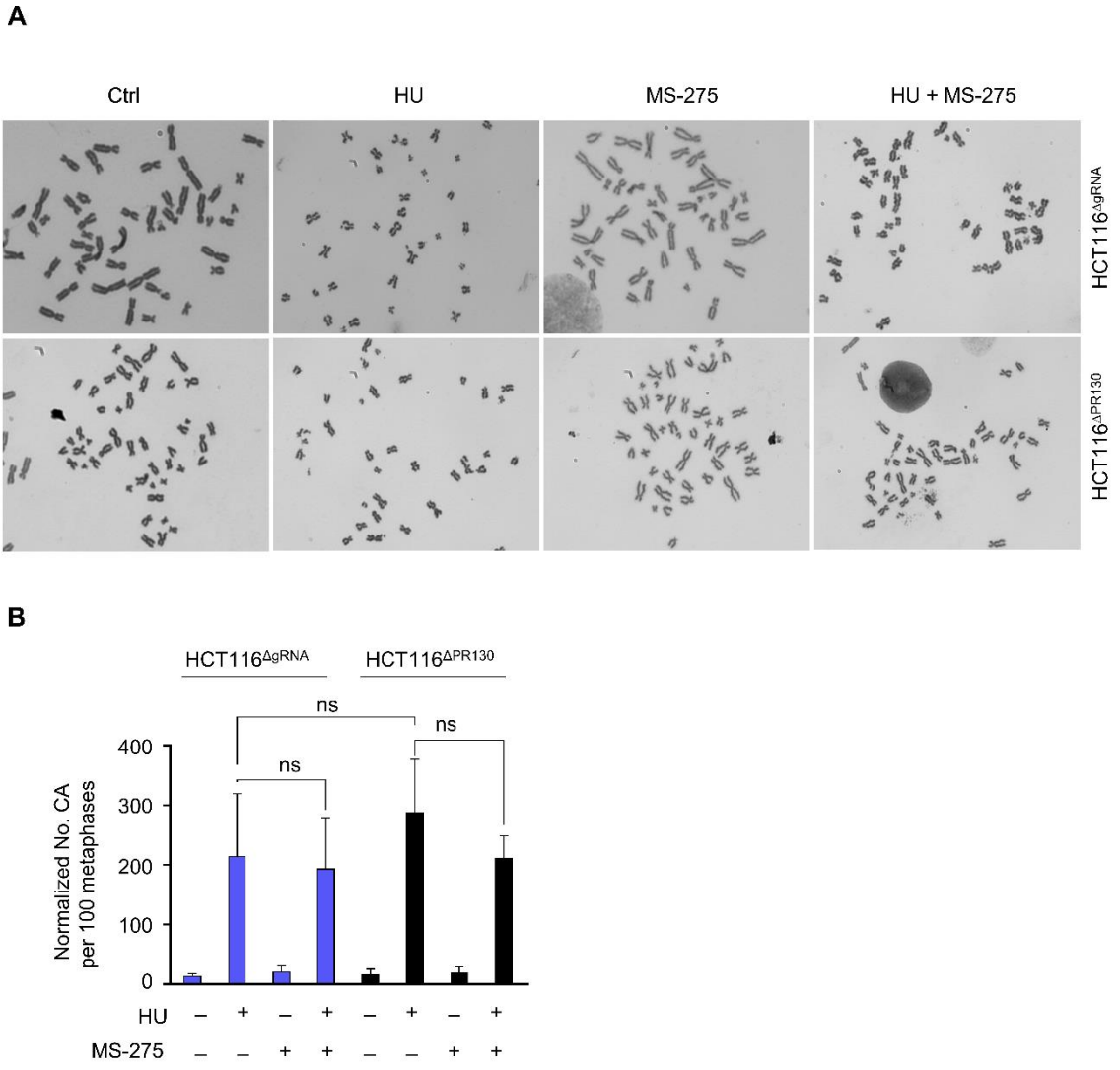

Figure 5.27: Chromosomal aberrations upon HU and MS-275 treatment in cells with different PR130 status. HCT116$^{\Delta gRNA}$ and HCT116$^{\Delta PR130}$ cells were treated with 1 mM HU ± 2 µM MS-275 for 24 h. Medium was changed and after 8 h, colcemide (1:200) was added overnight. On the next day (~ 15 h of incubation) chromosomal aberration assay was performed by [redacted]. **A** Representative image of chromosomes upon HU ± MS-275 treatment. **B** Normalized number of chromosomal aberrations per 100 metaphases. Statistical analysis was carried out using One-way ANOVA and Tukey's Multiple Comparison Test (ns=not significant).

Interestingly, there was no difference between both cell systems and also none between only HU treatment and the combinatorial treatment with the HDACi.

Even though no difference in RIF1 protein could be detected between HCT116$^{\Delta gRNA}$ and HCT116$^{\Delta PR130}$ cells in the mRNA screen (Figure 5.23), the protein was nevertheless analyzed in more detail due to the differences in the proteome screen (Figure 5.8) and its important role in DNA repair (Chapman et al. 2013). Both cell lines were therefore treated with 1 mM HU ± 5 µM MS-275 for 24 h and RIF1 foci formation was investigated (Figure 5.28).

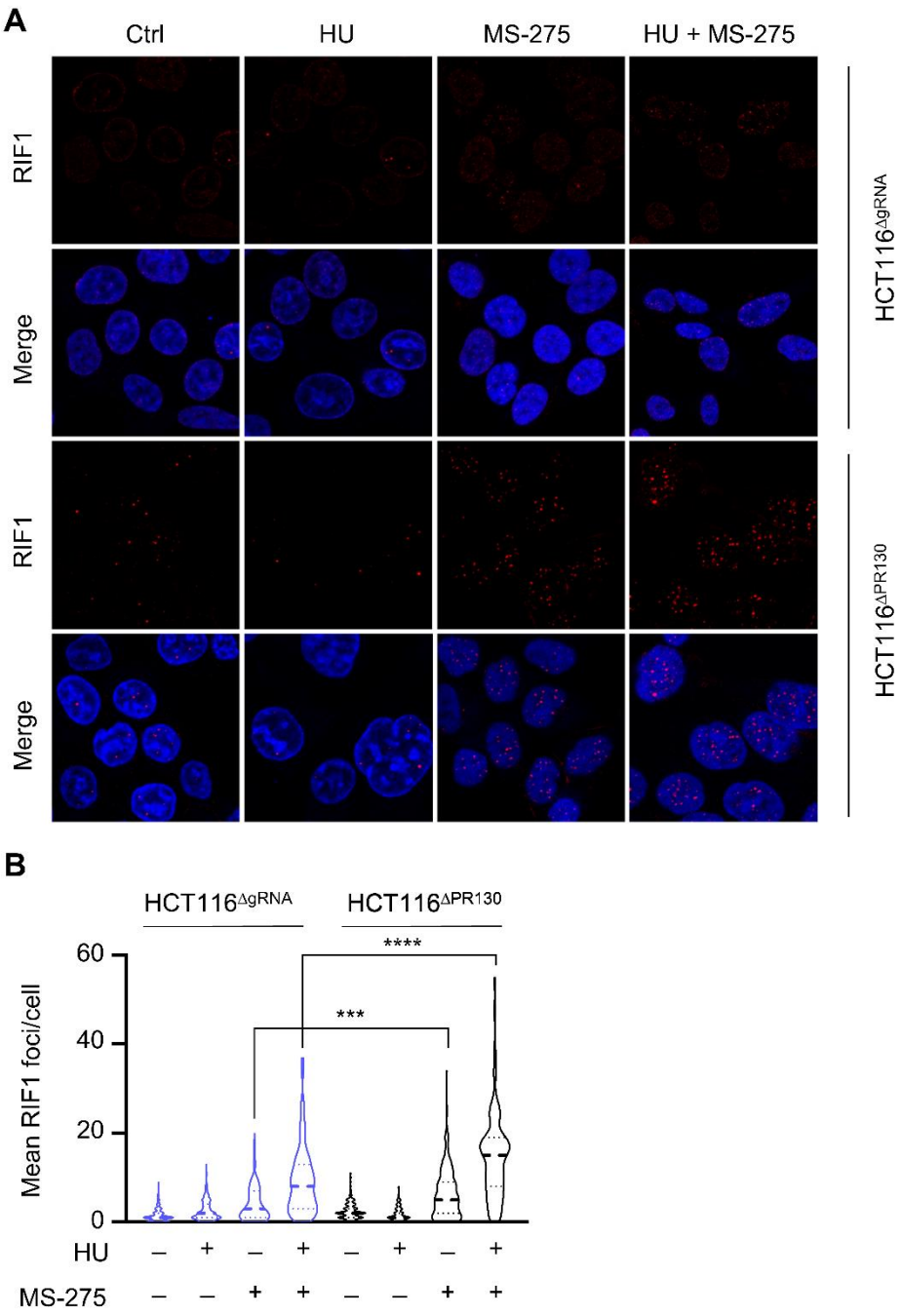

Figure 5.28: RIF1 foci formation upon HU and MS-275 treatment in cells with different PR130 status. A HCT116$^{\Delta gRNA}$ and HCT116$^{\Delta PR130}$ cells were treated with 1 mM HU ± 5 µM MS-275 for 24 h. For immunofluorescence (n=3), cells were fixed and stained with RIF1 primary antibody. Cy3 (red) was used as secondary antibody and TO-PRO-3 (blue) as nuclear staining.

Representative images are shown. **B** Quantitative analysis of RIF1 foci/cell was done using ImageJ/FIJI. At least 150 cells were analyzed for each treatment. Graph shows one experiment presented as violin plot. Statistical analysis was performed using One-way ANOVA and Tukey's Multiple Comparison Test (***p<0.001, ****p<0.0001).

It was observed that PR130-deficient cells had significantly higher levels of RIF1 foci compared to control cells, especially when treated with the HDACi MS-275.

6 Discussion

Phosphorylation and dephosphorylation are important post-translational modifications, which regulate the activity of proteins and thereby control a variety of cellular pathways. Mutations or defects in these regulatory mechanisms can promote cancer development as they directly influence processes like cell proliferation, differentiation, and apoptosis (Ardito et al. 2017).

This thesis focuses on the serine/threonine phosphatase PP2A, which dephosphorylates about 30–50% of such residues in many cell types. Various cancers show mutations in the phosphatase or an increased expression of PP2A inhibitors leading to inactivation of this essential cellular key player (Nader et al. 2019, Janssens and Goris 2001, Kauko and Westermarck 2018, Peng et al. 2015). PP2A was found to dephosphorylate ATM in human lymphoblastoid cells and ATM as well as ATR in *Xenopus* egg extracts (Petersen et al. 2006, Goodarzi et al. 2004). Previous studies from our laboratory showed that the PP2A regulatory B-type subunit PR130 in particular controls ATM phosphorylation upon replication stress. Moreover, the epigenetic modifiers HDAC1 and HDAC2 were identified as regulators of PR130 expression (Göder et al. 2018).

While treatment with the replication stress inducer HU resulted in increased CHK1 phosphorylation, the combinatorial treatment with the HDACi MS-275 decreased CHK1 phosphorylation (Figure 5.1 A). The exact mechanism by which HDACs and PR130 control CHK1 phosphorylation has not been clarified yet.

The aim of this work was the characterization of the role of PR130 in the DNA damage response upon replication stress in more detail. How does it control cell cycle progression, checkpoint kinase signaling, and DNA repair mechanisms? To date, not many functions and targets of PR130 are known, thus the expression and phosphorylation of proteins regulated by the regulatory B-type subunit should be investigated. Moreover, new molecular pathways in which PR130 is involved should be unraveled. For this purpose, global (phospho-)proteome, as well as RNA sequencing experiments were performed. Gene set enrichment analyses were carried out to cluster genes according to their involvement in specific pathways.

6.1 PR130 regulates proliferative and cell-cycle-related pathways

PP2A is involved in the regulation of various pathways, such as apoptosis, autophagy, cell proliferation, and DNA repair (Dzulko et al. 2020). Active PP2A complexes consist of a structural, regulatory, and catalytical subunit, whereby the regulatory subunit defines the substate specificity and the subcellular localization of the holoenzyme (Dzulko et al. 2020). Some subunits are better known and studied than others. The B-type subunit PR130, however, belongs to the less studied subunits. It is yet unknown how many proteins are controlled by PR130 in resting and stressed cells, and how many interaction partners the regulatory subunit has. Therefore, a global proteome screen and RNA sequencing analysis should give insight into the network of PR130-dependent protein regulation.

The proteome screen revealed that many proteins were differentially regulated in HCT116$^{\Delta PR130}$ cells compared to HCT116$^{\Delta gRNA}$ cells (Figure 5.8). However, a STRING analysis using the most upregulated proteins in both cell systems did not show a clear pattern of proteins which belong to a certain pathway (Supplementary Figure 8.3). This emphasizes the versatile role of the phosphatase subunit. Nevertheless, untreated PR130-deficient cells displayed higher levels of p21 (encoded by the *CDKN1A* gene) and cyclin D1 (encoded by the *CCND1* gene) compared to wild-type cells, indicating a PR130-dependent cell cycle regulation function (Figure 5.8). This result was validated by immunoblot analysis (Figure 5.9). Moreover, HCT116$^{\Delta gRNA}$ cells showed higher levels of RIF1 protein upon all tested treatment conditions compared to HCT116$^{\Delta PR130}$ cells (Figure 5.8) suggesting a PR130-dependent control of DNA repair pathway choice between HR and NHEJ. In the following chapters 6.2 and 6.5 the relevance of p21 and RIF1 for cells with different PR130 background will be analyzed in more detail.

Furthermore, an RNA sequencing analysis was carried out to identify PR130-dependent gene expression. HCT116$^{\Delta gRNA}$ and HCT116$^{\Delta PR130}$ cells were therefore treated with MS-275 to increase the amount of PR130 and HU to induce replication stress. The most interesting pathways differentially regulated in both cell systems showed up upon the combinatorial treatment. Especially MYC targets, Cdc6/ORC-related genes, or genes responsible for APC-mediated degradation of cell cycle proteins and β-catenin were downregulated in PR130-deficient cells compared to control cells upon HU + MS-275 treatment (Figure 5.13).

MYC and PP2A can regulate each other: on one hand, MYC regulates the transcription of the PP2A inhibitors SET and CIP2A (Pippa and Odero 2020). On the other hand, the PP2A-B56α complex dephosphorylates MYC at S62, causing proteasomal degradation of the transcription factor (Pippa and Odero 2020). Creyghton et al. found that PR130

acts indirectly as an activator of the Wnt signaling pathway, as it binds to the Wnt-antagonist NKD (Creyghton et al. 2006). This is in line with the results from the RNA sequencing analysis, since PR130-deficient cells showed a downregulation of MYC target genes (Figure 5.13 and Supplementary Table 1), whose expression is controlled by Wnt signaling (Zhang and Wang 2020). Loss of PR130 was also reported to result in MYC overexpression and increased MYC function in HEK cells (Sablina et al. 2010), which is contradictory to the aforementioned result. However, in this study the authors used small hairpin RNA (shRNA) inhibiting both PR130 and its splice variant PR72. Since PR72 was found to inhibit Wnt signaling (Creyghton et al. 2005), this could explain the contrasting result. It further illustrates the opposing effects of PR72 and PR130 and clarifies that both variants are needed to efficiently control MYC activity.

Furthermore, HCT116$^{\Delta PR130}$ cells showed lower enrichment of β-catenin degradation pathways (Figure 5.13). β-Catenin facilitates the transcription of several genes important for cell proliferation, differentiation, survival, and migration and is part of the Wnt signaling pathway (Liu et al. 2022). The β-catenin destruction complex regulates β-catenin levels in the absence of exogenous Wnt signals (Kimelman and Xu 2006). The lower Wnt signaling activity is underlined by the lower enrichment in β-catenin degradation pathways in PR130-deficient cells, since activation of Wnt signaling leads to higher levels of β-catenin, resulting in stronger activation of degradation by the proteasome. This is in line with lower levels of β-catenin and TCF7, a transcriptional regulator of Wnt/β-catenin signaling (Tang et al. 2008), in HCT116$^{\Delta PR130}$ cells (Supplementary Table 4).

The RNA sequencing analysis also revealed less APC-mediated degradation of cell cycle regulators and a downregulation of Cdc6/ORC-related genes in PR130-deficient cells compared to wild-type cells (Figure 5.13). The gene list, however, showed that HCT116$^{\Delta PR130}$ cells had less CDK2, cyclin B1, and cyclin A2, as well as Cdc6 and Chromatin licensing and DNA replication factor 1 (CDT1) compared to wild-type cells

Supplementary Table 2 and Supplementary Table 3). Downregulation of these mRNAs can be explained by the different cell cycle distribution of HCT116$^{\Delta gRNA}$ and HCT116$^{\Delta PR130}$ cells upon HU + MS-275 treatment (Figure 5.1 B).

Taken together, it was shown that the PP2A-PR130 complex is involved in various pathways including cell cycle regulation, cell proliferation, and DNA repair.

6.2 PR130-dependent regulation of p21 levels controls cell cycle

One key task of this thesis was to determine the molecular mechanisms that are decisive for the different cell cycle distribution of cells lacking PR130 compared to wild-type cells.

HCT116$^{\Delta PR130}$ cells arrested earlier at the G1/S boundary upon HU treatment compared to similar treated HCT116$^{\Delta gRNA}$ cells, which arrested in S phase (Figure 5.1). Incubation with HU ± nocodazole has ruled out the possibility that PR130-deficient cells traversed through G2/M phase and were stalled in the subsequent G1 phase, since the combinatorial treatment arrested fewer cells in G2/M phase than nocodazole only treatment (Figure 5.6).

It was found that HCT116$^{\Delta PR130}$ cells showed higher levels of the cell cycle regulator p21 on protein and mRNA levels compared to wild-type HCT116$^{\Delta gRNA}$ cells. While in the proteome analysis (Figure 5.8) the higher levels could only be seen in the untreated state, an immunoblot analysis (Figure 5.9) displayed higher levels of the cell cycle regulator also upon HU ± MS-275 treated cells. The discrepancy in the assays could be explained by the fact that the proteome screen only showed top hits of the analysis. The differences in the p21 levels of the HU ± MS-275-treated HCT116$^{\Delta gRNA}$ and HCT116$^{\Delta PR130}$ cells could be not as significant as for the untreated state.

p21 expression was especially increased upon treatment with the HDACi MS-275 in both cell lines on protein (Figure 5.9) and mRNA levels (Figure 5.10 B) compared to untreated cells. Moreover, the class I HDACi did not only increase the expression of p21, but also of the PP2A B-type subunit PR130 as seen in RNA sequencing experiments (Figure 5.10 C), which is in line with the corresponding immunoblot analysis (Figure 5.10 A).

To unravel the reason of higher levels of p21 in PR130-deficient cells, the ATM-CHK2-p53 axis was analyzed in more detail, since it is known to regulate the expression of the cell cycle protein (Abuetabh et al. 2022). PR130 regulates ATM phosphorylation at S1981 (Göder et al. 2018), therefore a regulation of p21 expression through the ATM-CHK2-p53 pathway appeared obvious. Indeed, incubation with an ATMi reduced levels of pp53-S15, p53 and p21, especially in case of HCT116$^{\Delta PR130}$ cells (Figure 5.14 A).

RNAi-based elimination of p53 confirmed that p21 expression depends on the tumor-suppressive transcription factor (Figure 5.15 A and B). Especially in PR130-deficient cells, p21 levels significantly decreased upon p53-knockdown. Nevertheless, there is also a p53-independent pathway regulating p21 expression, since HCT116$^{p53-/-}$ cells treated with MS-275 displayed high levels of the cell cycle regulator (Supplementary Figure 8.4 A). In this case, p21 expression could be regulated via other transcription

factors such as SP1 and SP3 as described in the literature (Gartel et al. 2001, Hsieh et al. 2014).

Another explanation for higher p21 levels in HCT116$^{\Delta PR130}$ cells could be cyclin E, since such cells showed higher levels of the cyclin compared to HCT116$^{\Delta gRNA}$ cells (Supplementary Figure 8.7). Hughes et al. found that inhibition of CDK2 phosphorylation leads to cyclin E degradation and is important for the maintenance of genomic stability. Therefore, cyclin E overexpression triggers p53-dependent induction of p21 (Hughes et al. 2013).

Depending on its cellular localization, p21 carries out different functions. Nuclear p21 is commonly known to carry out tumor-suppressive activities as it binds to CDKs and inhibits cell cycle progression upon DNA damage (Abbas and Dutta 2009). The role of p21 as a cell cycle inhibitor with anti-proliferative characteristics (Shamloo and Usluer 2019) can be seen in flow cytometry analysis as high p21 levels in MS-275 treated cells arrested cells in G1 phase (Figure 5.1 A). Immunoprecipitation experiments, moreover, revealed that p21 binds to CDK2 when treated with the class I HDACi MS-275 (Figure 5.18). CDK2 is necessary for G1/S phase (Bačević et al. 2017); consequently, cancer cells cannot enter the cell cycle efficiently (Figure 5.1 B). In the cytoplasm, p21 has anti-apoptotic effects as it can bind to pro-caspase 3 and inhibits Fas-mediated apoptosis (Suzuki et al. 1999). It has also been found to associate with apoptosis signal-regulating kinase 1 (Zhan et al. 2007). Many tumor types exhibit high levels of p21 correlating with chemoresistance and enhanced survival of the cancer cells (Jung et al. 1995, Sarbia et al. 1998, Ferrandina et al. 2000, Baretton et al. 1999, Korkolopoulou et al. 1998). HCT116$^{\Delta PR130}$ cells with high levels of p21 were more robust against HU treatment compared to wild-type cells (Figure 5.25 C), which is therefore in line with the anti-apoptotic effects of p21. In the future, the cellular localization of p21 should be analyzed in more detail in order to understand how this influences the function of the protein.

All in all, the results displayed that PR130 controls p21 on transcriptional level via the ATM-CHK2-p53 axis. Moreover, p21 regulates the cell cycle by binding to CDK2.

6.3 pp21-S130 and pWEE1-T190 are direct targets of the PP2A-PR130 complex

Another key task of this thesis was the identification of novel targets of the PP2A-PR130 complex. Using a phosphoproteome analysis, the two phospho-proteins pp21-S130 and pWEE1-T190 were identified as targets. A sequence logo analysis showed that the S/T-directed phosphatase complex prefers targets with P/L next to S/T when cells were treated with HU (Figure 5.19 C); accordingly, pp21-S130 and pWEE1-T190, exhibited this kind of structure (Figure 5.19 D). An immunoblot analysis validated pp21-S130 as a target of PR130 as HCT116$^{\Delta PR130}$ cells displayed higher levels of pp21-S130 upon HU treatment compared to wild-type cells (Figure 5.20 A). The presence of pWEE1-T190 could not be shown directly as there was no commercially available antibody for this specific phosphorylation site. However, it was indirectly validated as a target of the PP2A-PR130 complex by testing the phosphorylation of CDK1, which is a target of the WEE1 kinase. pWEE1-T190 is described as an inactive form of the kinase (Pagliuca et al. 2011). HCT116$^{\Delta PR130}$ cells showed less phosphorylation of CDK1 indicating less WEE1 activity (Figure 5.20 B). For further validation, the phosphatase activity of immunoprecipitated HA-tagged PR130 was tested against a pp21-S130 and pWEE1-T190 peptide. To increase the amount of the regulatory B-type subunit, cells were additionally treated with MS-275. pATM-S1981 served as positive control as Göder et al. could already validate this phospho-protein as a target of the PP2A-PR130 complex (Göder et al. 2018). Immunoprecipitated PR130 dephosphorylated both tested phospho-peptides, which confirmed the aforementioned finding once more (Figure 5.20 C). However, the phosphatase activity against pWEE1-T190 was stronger than for pp21-S130.

In the literature, pp21-S130 is also described as a target of the PP2A complex. Gao et al. tested the small molecule PP2A inhibitor LB-100 in bladder carcinoma and found that PP2A dephosphorylates p21 at S130 causing its stabilization. Consequently, treatment with LB-100 led to a reduction of total p21 levels and induction of apoptosis (Gao et al. 2022). Moreover, they found that LB100 abrogated the G1/S cell cycle checkpoint due to p21 degradation. Interestingly, our cell systems cells devoid of PR130 show p21 stabilization as they have higher levels of the cell cycle regulator (Figure 5.9) and an increased G1 phase upon replication stress (Figure 5.1 B) compared to wild-type cells.

Phosphorylation of p21 at S130 and its either stabilization or destabilization are the subject of intense debate: in addition to the aforementioned instability of pp21-S130 by Gao et. al, it was shown that the CDK1/cyclin B1 complex phosphorylates p21 at S130 reducing the cell cycle regulator's stability and binding affinity for the CDK-cyclin complex

(Kreis et al. 2016). It was also described that CDK2/cyclin E complexes phosphorylate p21 at S130. However, this phosphorylation depends on the Cy2-binding domain and results in destabilization of the p21 protein. The CDK- and Cy1-binding domains, in contrast, support stabilization of the cell cycle regulator (Zhu et al. 2005). In another study it was shown that cyclin D1 stabilizes p21 through binding to the Cy2 domain, which interrupts interaction with the proteasome and its degradation (Coleman et al. 2003). Moreover, it has been reported that cyclin E binds to a greater extent to the Cy1- than to the Cy2-binding domain. Therefore, Zhu et. al suggest that excess cyclin E causes recruitment of CDK2, phosphorylation of p21 at S130 and its degradation. Upon excess p21 the authors propose direct inhibition of CDK2, leading to p21 stabilization (Zhu et al. 2005). Kim et al. further describe that stress signals activate JNK and p38 MAPK signaling initiated by TGF-β1, which causes G1 arrest by stabilization of p21 and inhibition of CDK2/Cyclin E complexes (Kim et al. 2002). They showed that p38α and JNK1 phosphorylate p21 at S130 in vitro and in vivo. Mutation of serine to alanine led to proteasomal degradation of p21. In another study, it was published that cyclin K/CDK6 phosphorylates p21 at S130, however this did not affect the stability or subcellular localization of p21, but impedes its binding to CDK2 (Järviluoma et al. 2006). Bisteau et al. showed that p21 was more efficiently phosphorylated at S130 when bound to CDK4-cyclin D complexes (Bisteau et al. 2013). Moreover, pp21-S130 seems to be important for activation of CDK4 (Coulonval et al. 2022, Bisteau et al. 2013). S130A mutation of p21 prevented activating CDK4 phosphorylation, and inhibition of CDK4/6 and CDK2 impaired the phosphorylation of both p21 and p21-bound CDK4. S130 phosphorylation was abundant in general and CDK4-bound p21 during G1 phase, indicating that it does not rapidly lead to p21 degradation at this stage, possibly because SCF^{SKP2} E3 ubiquitin ligase levels are kept low in G1 phase (Bisteau et al. 2013).

In this thesis, CDK2 was shown to phosphorylate p21 at S130 (Figure 5.17 A). $HCT116^{\Delta PR130}$ cells incubated with HU ± CDK2i displayed reduced pp21-S130 levels compared to HU-treated ones. This indicates that CDK2 is responsible for phosphorylation of p21 at S130 in PR130-deficient cells. In case of $HCT116^{\Delta gRNA}$ cells there was no difference which could be explained due to pp21-S130 being a target of the PP2A-PR130 complex and already being dephosphorylated upon HU treatment. Moreover, one study showed that phosphorylation of p21 at S130 disables the interaction between CDKs and p21 (Kreis et al. 2016), which can consequently promote phosphorylation of WEE1 by CDKs. This is in line with the increased pWEE1-T190 levels in $HCT116^{\Delta PR130}$ cells (Figure 5.19 D).

In summary it was shown that pp21-S130 and pWEE-T190 were targets of the PP2A-PR130 complex. Phosphorylation at S130 might increase the stability of p21 in our cell

system, which need to be verified by additional experiments; phosphorylation at T190 decreased the activity of the WEE1 kinase. Moreover, as CDKs phosphorylate WEE1 at T190, the increased phosphorylation is consistent with the phosphorylation of p21 at S130.

6.4 WEE1, p21 and CDK2 orchestrate CHK1 phosphorylation upon replication stress

Another key task was to determine the molecular mechanisms that regulate PR130-dependent CHK1 phosphorylation and its control by HDACi. It was found that HU-treated HCT116$^{\Delta PR130}$ cells have higher levels of phosphorylated CHK1 compared to HCT116$^{\Delta gRNA}$ cells (Figure 5.1 A). This result could be reproduced using other replicative stress inducers (ara-C, siRRM2) and cell systems (short-term colorectal cancer HROC24 cells) (Figure 5.2, Figure 5.3, Figure 5.4). Since HCT116$^{\Delta gRNA}$ and HCT116$^{\Delta PR130}$ cells showed the same activation of ATR (Göder et al. 2018), which is in general the direct activator of CHK1 phosphorylation upon replication stress (Smith et al. 2010), the differences in CHK1 phosphorylation in HCT116$^{\Delta gRNA}$ and HCT116$^{\Delta PR130}$ cells needed to be explained by another mechanism.

Upon replication stress, ATR inhibits cyclin E ubiquitinylation and degradation (Lim and Kaldis 2013). Cyclin E is required for stabilization of Cdc6, which is an essential regulator of DNA replication (Borlado and Méndez 2008). Cyclin E accumulates at stalled replication forks, prevents initiation of replication, and stabilized Cdc6 activates CHK1 (Lim and Kaldis 2013). This ensures that all DNA is replicated before cells enter into mitosis (Clay-Farrace et al. 2003). Elevated cyclin E levels also reduce the activity of CDK2-cyclin A complexes, which causes a slowed S phase progression (Lim and Kaldis 2013). Paradoxically, overexpressed cyclin E levels accelerate S phase entry but show a slower progression throughout the replication phase (Lu et al. 2009). In this thesis, 2-fold higher levels of cyclin E were observed in HCT116$^{\Delta PR130}$ cells compared to control cells. Therefore, the earlier cell cycle arrest (Figure 5.1 B) and the stronger phosphorylation of CHK1 (Figure 5.1 A) are in line with the aforementioned characteristics of elevated cyclin E levels.

p21 was also found to be important for efficient CHK1 phosphorylation as p21-depleted (Figure 5.16 B) or -deficient (Supplementary Figure 8.5) cells showed less phosphorylation of the checkpoint kinase upon replication stress compared to wild-type cells. Moreover, MS-275-induced induction of p21 (Supplementary Figure 8.4) could explain why CHK1 phosphorylation is decreased upon HU + MS-275 treatment in HCT116$^{\Delta gRNA}$ and HCT116$^{\Delta PR130}$ cells (Figure 5.1 A), since p21 bound to CDK2 upon MS-

275 treatment in immunoprecipitation experiments (Figure 5.18). The decrease in CHK1 phosphorylation upon the combinatorial treatment could also be explained by a reduction in total CHK1 mRNA levels as seen in the RNA sequencing analysis of HCT116$^{\Delta gRNA}$ and HCT116$^{\Delta PR130}$ cells (Supplementary Figure 8.9 and Supplementary Figure 8.10). This creates a link between the control of gene expression and response to DNA replication stress.

Furthermore, HU-treated PR130-deficient cells displayed a reduced activity of the WEE1 kinase measured by phosphorylation of its target CDK1 (Figure 5.20 B). WEE1 phosphorylates CDK1 and CDK2 and regulates their activity and cell cycle progression upon DNA damage (Di Ghelli Luserna Rorà et al. 2020). In this thesis, the focus was on CDK2, since it is highly active in a complex with cyclin E in early S phase (Fagundes and Teixeira 2021). Using a CDK2 inhibitor, it was found that CDK2 is essential for CHK1 phosphorylation upon replication stress. After 24 h, the HU-induced phosphorylation was already reduced to a minimum (Figure 5.17 A). However, treatment with HU + CDK2i increased cells in G1 phase for both cell lines compared to an S phase arrest upon HU single treatment (Figure 5.17 B). In order to rule out that the reduction in CHK1 phosphorylation was due to these changes in cell cycle distribution, the experiment was repeated with a short-term treatment (Figure 5.22 A). This time, the cell cycle distribution of HU ± CDK2i-treated cells did not change (Supplementary Figure 8.6), whereas levels of CHK1 were slightly reduced (Figure 5.22 B). At the same time, treatment of HU-treated cells with the WEE1i MK-1775 increased phosphorylation of CHK1 significantly in case of HCT116$^{\Delta gRNA}$ cells (Figure 5.22). pCDK1 levels were reduced accordingly, validating that the WEE1 inhibitor worked efficiently. In case of HCT116$^{\Delta PR130}$ cells, pCHK1 and pCDK1 levels did not change significantly. Again, only a trend toward slightly increased levels was seen in case of pCHK1. This could be explained by the fact that PR130-deficient cells already have lower WEE1 activity due to the inhibitory phosphorylation at T190 (see chapter 6.3). Therefore, such cells did not respond as strongly as HCT116$^{\Delta gRNA}$ cells to the WEE1 inhibitor. The experiment was further carried out in non-cancerous VH10tert cells to show that the CDK2/WEE1 regulated mechanism of CHK1 phosphorylation is cell line- and disease-independent (Supplementary Figure 8.8).

Furthermore, the increase in CHK1 phosphorylation upon HU + MK-1775 treatment (Figure 5.22 C) was accompanied by an earlier G1/S phase arrest of HCT116$^{\Delta gRNA}$ and HCT116$^{\Delta PR130}$ cells (Figure 5.21 A). HU-treated PR130-deficient cells, which showed the inhibitory phosphorylation of WEE1, also arrested earlier at the G1/S boundary than HCT116$^{\Delta gRNA}$ cells (Figure 5.1 B). This shows that CHK1 controls the cell cycle arrest and that high pCHK1 levels in HCT116$^{\Delta PR130}$ cells are the reason for their earlier G1/S phase arrest upon replication stress. Furthermore, the higher activity of CDKs caused by

the inhibitory phosphorylation of WEE1 causes more origin firing, which shortens nucleotide pools. Accordingly, the replication fork speed reduces, leading to more stalled forks and an increased binding of MUS81 endonuclease complexes (Beck et al. 2012). Beck et al. showed an increased uptake of EdU upon WEE1i with MK-1775, which shows that WEE1 inhibition stimulates DNA replication. However, this increase in DNA replication depends on higher activity of CDK1 and CDK2 (Beck et al. 2012). Since HU-treated HCT116$^{\Delta PR130}$ cells arrested earlier at the G1/S boundary compared to wild-type cells (Figure 5.1 B), this is in line with findings from the literature. By looking at the cell cycle distribution of HCT116$^{\Delta gRNA}$ and HCT116$^{\Delta PR130}$ cells treated with the WEE1 inhibitor (Figure 5.22 A) or siWEE1 (Figure 5.22 B), it can further be seen that PR130-deficient cells do not respond to WEE1 inhibition as similarly treated wild-type cells, which can again be explained by the inhibitory phosphorylation at T190.

Moreover, the question was raised why HCT116$^{\Delta PR130}$ cells with high levels of p21 paradoxically did not show reduced pCHK1 levels upon replication stress. This could be explained by the fact that phosphorylation of p21 at S130 reduces the binding affinity to CDK-cyclin complexes (Kreis et al. 2016). Therefore, CDK2 is more active in PR130-deficient cells with high levels of pp21-S130. To better understand the role of pp21-S130 for phosphorylation of CHK1, HCT116$^{p21-/-}$ cells were transfected with different pp21-S130 plasmids. Unfortunately, there was no significant difference in pCHK1 levels between all tested plasmids. However, the phospho-mimetic S130D mutant displayed less inhibitory pCDK1 levels (Supplementary Figure 8.13 A) and a slight trend toward more cells in G1 phase (Supplementary Figure 8.13 B) compared to the non-phosphorylatable S130A mutant. Since the result was not that clear, the experiment should be repeated. Beyond that it should also be carried out in cells devoid of PR130 and p21 to guarantee that the PP2A-PR130 complex cannot dephosphorylate the pp21-S130 constructs.

Further, a cell line deficient for PR130 and p21 was created using CRISPR-Cas9 to better characterize the importance of the cell cycle regulator in PR130-deficient cells (Supplementary Figure 8.12 A-C). One clone (#2) deficient for both proteins was analyzed for CHK1 phosphorylation upon replication stress compared to HCT116$^{\Delta PR130}$ cells. HCT116$^{\Delta PR130\Delta p21}$ cells showed less phosphorylation of CHK1 than HCT116$^{\Delta PR130}$ cells (Supplementary Figure 8.12 D), which indicates once more that p21 is important for CHK1 phosphorylation. Moreover, the double-knockout cells displayed a slowed cell cycle, since HCT116$^{\Delta PR130\Delta p21}$ cells arrested in G1/S phase upon HU treatment compared to PR130-deficient cells, which arrested in S phase (Supplementary Figure 8.12 E). This highlights the important function of p21 for cell cycle regulation. Low p21 levels are needed to stabilize CDK4/CDK6-cyclin D complexes stimulating their activity ((Sherr and

Roberts 1999). Paradoxically, HCT116$^{\Delta PR130\Delta p21}$ cells also showed less pCDK1, indicating higher CDK activity, which should cause more phosphorylation of CHK1. Since this is not the case, it cannot be excluded that HCT116$^{\Delta PR130\Delta p21}$ cells only displayed less pCHK1 due to lower levels of CDKs in general. This newly generated cell system needs to be further analyzed in more detail in the future.

To sum up, it was found that there is a close network of p21, CDK2 and WEE1 in the DNA damage response. These proteins orchestrate CHK1 phosphorylation upon replication stress in a PR130-dependent manner.

6.5 HDACi promote NHEJ and RIF1 foci formation in PR130-deficient cells

Another key task of this thesis was to analyze how PR130 modulates the DNA repair pathway choice. A proteome screen revealed higher RIF1 levels in HCT116$^{\Delta gRNA}$ cells compared to HCT116$^{\Delta PR130}$ cells upon all tested treatment conditions (Figure 5.8). The RIF1 protein, together with 53BP1, was identified to be required for DNA repair pathway choice between NHEJ and HR. HR only takes place during S or G2/M phase, since it needs an identical sister chromatid as a template for repair (Helleday et al. 2007). NHEJ happens throughout all cell cycle phases, but is favored in G1 phase upon HR, since no sister chromatid is available (Daley and Sung 2013). Interestingly, HCT116$^{\Delta PR130}$ cells displayed more and larger RIF1 foci upon MS-275 treatment compared to HCT116$^{\Delta gRNA}$ cells (Figure 5.28), which is contrasting to the proteome screen (Figure 5.8). However, the amount of protein alone does not reflect its functionality. Therefore, the RIF1 foci formation is more likely to indicate which repair mechanism is favored. PR130-deficient cells showed more RIF1 foci, suggesting that these cells rather use NHEJ as a favored repair mechanism compared to wild-type cells. A reporter assay confirmed MS-275-induced NHEJ (Figure 5.24). Moreover, the mRNA expression of HR proteins such as RAD51 and BRCA1 was downregulated in HCT116$^{\Delta gRNA}$ and HCT116$^{\Delta PR130}$ cells upon class I HDACi (Figure 5.23). Treatment with the RAD51 inhibitor RI-1 and HU showed that more HCT116$^{\Delta gRNA}$ cells undergo apoptosis when RAD51 is inhibited in comparison to similar treated HCT116$^{\Delta PR130}$ cells (Figure 5.25 B, C). PR130-deficient cells also showed less γH2AX than wild-type cells (Figure 5.25 A), indicating that these cells do not strongly rely on HR as repair mechanism. Keeping in mind that NHEJ is a more error-prone DNA-repair mechanism and occurs during each cell cycle phase, the preference of this mechanism in dPR130 cells could have clinical implications with higher mutational rates and higher resistance to genotoxic stress due to faster strand repair (Brandsma and Gent 2012).

RIF1 locates to the damaged sites via ATM-dependent phosphorylation of 53BP1 (Gupta et al. 2014). RIF1 has 14 potential SQ/TQ ATM phosphorylation sites (Wang et al. 2018), whereas 53BP1 has 28 (Gupta et al. 2014). Since ATM phosphorylation is maintained in HCT116$^{\Delta PR130}$ cells upon HU + MS-275 treatment compared to wild-type cells (Göder et al. 2018), this could explain why such cells have more RIF1 foci than wild-type cells (Figure 5.28). It would also be interesting to see if inhibition of ATM reduces RIF1 foci formation. It was further tested how additional ATM inhibition of HU + MS-275-treated cells affects their fate (Supplementary Figure 8.14) since higher ATM activity plays an important role for the DNA damage repair in PR130-deficient cells. Cell death increased significantly, suggesting pro-survival functions of ATM and NHEJ in PR130-deficient cells. RNAi based experiments with siRNA against RIF1 and 53BP1 could support this finding.

The phosphoproteome analysis further revealed various phosphorylation sites of 53BP1 and RIF1, indicating that both proteins could also be novel targets of the PP2A-PR130 complex (Supplementary Table 5). Moreover, the CDK1 kinase is described to be required for the maintenance of RIF1 phosphorylation (Robertson et al. 2023). Therefore, high RIF1 phosphorylation is in line with less WEE1 and higher CDK activity in HCT116$^{\Delta PR130}$ cells compared to wild-type cells (see chapter 6.4). However, not all phosphorylation sites showed the preferred target structure with S/T next to P/L. Future experiments using an in vitro dephosphorylation assay could show if the PP2A-PR130 directly dephosphorylates 53BP1 and RIF1 at these specific phosphorylation sites.

HCT116$^{\Delta gRNA}$ and HCT116$^{\Delta PR130}$ cells were also analyzed for chromosomal aberrations. Interestingly, there was no difference between both cell systems or HU only and the combinatorial treatment with MS-275 (Figure 5.27). This speaks in favor of HU ± MS-275 treatment, as the combinatorial treatment does not additionally lead to a mutation of the cells; rather the treatment increased apoptosis in both cell lines (Göder et al. 2018).

In summary, the results showed that PR130-deficient cells favor NHEJ as repair mechanism and NHEJ is induced upon class I HDACi treatment.

7 Literature

Abbas, Tarek; Dutta, Anindya (2009): p21 in cancer: intricate networks and multiple activities. In: *Nature reviews. Cancer* 9 (6), S. 400–414. DOI: 10.1038/nrc2657.

Abuetabh, Yasser; Wu, H. Helena; Chai, Chengsen; Al Yousef, Habib; Persad, Sujata; Sergi, Consolato M.; Leng, Roger (2022): DNA damage response revisited: the p53 family and its regulators provide endless cancer therapy opportunities. In: *Experimental & molecular medicine* 54 (10), S. 1658–1669. DOI: 10.1038/s12276-022-00863-4.

Ackerson, Stephanie M.; Romney, Carlan; Schuck, P. Logan; Stewart, Jason A. (2021): To Join or Not to Join: Decision Points Along the Pathway to Double-Strand Break Repair vs. Chromosome End Protection. In: *Frontiers in cell and developmental biology* 9, S. 708763. DOI: 10.3389/fcell.2021.708763.

Aleem, Eiman; Arceci, Robert J. (2015): Targeting cell cycle regulators in hematologic malignancies. In: *Frontiers in cell and developmental biology* 3, S. 16. DOI: 10.3389/fcell.2015.00016.

Ardito, Fatima; Giuliani, Michele; Perrone, Donatella; Troiano, Giuseppe; Lo Muzio, Lorenzo (2017): The crucial role of protein phosphorylation in cell signaling and its use as targeted therapy (Review). In: *International Journal of Molecular Medicine* 40 (2), S. 271–280. DOI: 10.3892/ijmm.2017.3036.

Arnold, Hugh K.; Sears, Rosalie C. (2006): Protein phosphatase 2A regulatory subunit B56alpha associates with c-myc and negatively regulates c-myc accumulation. In: *Molecular and cellular biology* 26 (7), S. 2832–2844. DOI: 10.1128/MCB.26.7.2832-2844.2006.

Asfaha, Yodita; Skerhut, Alexander Jan; Alves-Avelar, Leandro A.; Horstick-Muche, Nadine; Lungerich, Beate; Klinken, Stefan et al. (2021): Synthesis of thiazolyl-based hydroxamic acids as histone deacetylase inhibitors. In: *Arkivoc* 2020 (7), S. 228–241. DOI: 10.24820/ark.5550190.p011.279.

Asghar, Uzma; Witkiewicz, Agnieszka K.; Turner, Nicholas C.; Knudsen, Erik S. (2015): The history and future of targeting cyclin-dependent kinases in cancer therapy. In: *Nature reviews. Drug discovery* 14 (2), S. 130–146. DOI: 10.1038/nrd4504.

Bačević, Katarina; Lossaint, Gérald; Achour, Thiziri Nait; Georget, Virginie; Fisher, Daniel; Dulić, Vjekoslav (2017): Cdk2 strengthens the intra-S checkpoint and counteracts cell cycle exit induced by DNA damage. In: *Scientific reports* 7 (1), S. 13429. DOI: 10.1038/s41598-017-12868-5.

Bakkenist, Christopher J.; Kastan, Michael B. (2003): DNA damage activates ATM through intermolecular autophosphorylation and dimer dissociation. In: *Nature* 421 (6922), S. 499–506. DOI: 10.1038/nature01368.

Baretton, G. B.; Klenk, U.; Diebold, J.; Schmeller, N.; Löhrs, U. (1999): Proliferation- and apoptosis-associated factors in advanced prostatic carcinomas before and after androgen deprivation therapy: prognostic significance of p21/WAF1/CIP1 expression. In: *British journal of cancer* 80 (3-4), S. 546–555. DOI: 10.1038/sj.bjc.6690390.

Bayley, Rachel; Borel, Valerie; Moss, Rhiannon J.; Sweatman, Ellie; Ruis, Philip; Ormrod, Alice et al. (2022): H3K4 methylation by SETD1A/BOD1L facilitates RIF1-dependent NHEJ. In: *Molecular cell* 82 (10), 1924-1939.e10. DOI: 10.1016/j.molcel.2022.03.030.

Beck, Halfdan; Nähse-Kumpf, Viola; Larsen, Marie Sofie Yoo; O'Hanlon, Karen A.; Patzke, Sebastian; Holmberg, Christian et al. (2012): Cyclin-dependent kinase suppression by WEE1 kinase protects the genome through control of replication initiation and nucleotide consumption. In: *Molecular and cellular biology* 32 (20), S. 4226–4236. DOI: 10.1128/MCB.00412-12.

Bertoli, Cosetta; Skotheim, Jan M.; Bruin, Robertus A. M. de (2013): Control of cell cycle transcription during G1 and S phases. In: *Nature reviews. Molecular cell biology* 14 (8), S. 518–528. DOI: 10.1038/nrm3629.

Bisteau, Xavier; Paternot, Sabine; Colleoni, Bianca; Ecker, Karin; Coulonval, Katia; Groote, Philippe de et al. (2013): CDK4 T172 phosphorylation is central in a CDK7-dependent bidirectional CDK4/CDK2 interplay mediated by p21 phosphorylation at the restriction point. In: *PLoS genetics* 9 (5), e1003546. DOI: 10.1371/journal.pgen.1003546.

Blackford, Andrew N.; Jackson, Stephen P. (2017): ATM, ATR, and DNA-PK: The Trinity at the Heart of the DNA Damage Response. In: *Molecular cell* 66 (6), S. 801–817. DOI: 10.1016/j.molcel.2017.05.015.

Borlado, Luis R.; Méndez, Juan (2008): CDC6: from DNA replication to cell cycle checkpoints and oncogenesis. In: *Carcinogenesis* 29 (2), S. 237–243. DOI: 10.1093/carcin/bgm268.

Brandsma, Inger; Gent, Dik C. (2012): Pathway choice in DNA double strand break repair: observations of a balancing act. In: *Genome integrity* 3 (1), S. 9. DOI: 10.1186/2041-9414-3-9.

Budke, Brian; Logan, Hillary L.; Kalin, Jay H.; Zelivianskaia, Anna S.; Cameron McGuire, William; Miller, Luke L. et al. (2012): RI-1: a chemical inhibitor of RAD51 that disrupts homologous recombination in human cells. In: *Nucleic acids research* 40 (15), S. 7347–7357. DOI: 10.1093/nar/gks353.

Buonomo, Sara B. C.; Wu, Yipin; Ferguson, David; Lange, Titia de (2009): Mammalian Rif1 contributes to replication stress survival and homology-directed repair. In: *The Journal of Cell Biology* 187 (3), S. 385–398. DOI: 10.1083/jcb.200902039.

Camilo, Vânia; Jerónimo, Carmen (2020): Chapter 17 - Present and future perspectives for targeting histone modifications in therapy. In: Pedro Castelo-Branco und Carmen Jeronimo (Hg.): Histone Modifications in Therapy : Translational Epigenetics, Bd. 20: Academic Press, S. 415–457. Online verfügbar unter https://www.sciencedirect.com/science/article/pii/B9780128164228000180.

Chang, Howard H. Y.; Pannunzio, Nicholas R.; Adachi, Noritaka; Lieber, Michael R. (2017): Non-homologous DNA end joining and alternative pathways to double-strand break repair. In: *Nature reviews. Molecular cell biology* 18 (8), S. 495–506. DOI: 10.1038/nrm.2017.48.

Chapman, J. Ross; Barral, Patricia; Vannier, Jean-Baptiste; Borel, Valérie; Steger, Martin; Tomas-Loba, Antonia et al. (2013): RIF1 is essential for 53BP1-dependent nonhomologous end joining and suppression of DNA double-strand break resection. In: *Molecular cell* 49 (5), S. 858–871. DOI: 10.1016/j.molcel.2013.01.002.

Chapman, J. Ross; Taylor, Martin R. G.; Boulton, Simon J. (2012): Playing the end game: DNA double-strand break repair pathway choice. In: *Molecular cell* 47 (4), S. 497–510. DOI: 10.1016/j.molcel.2012.07.029.

Chatterjee, Nimrat; Walker, Graham C. (2017): Mechanisms of DNA damage, repair, and mutagenesis. In: *Environmental and molecular mutagenesis* 58 (5), S. 235–263. DOI: 10.1002/em.22087.

Chen, Huijuan; Xu, Jing; Wang, Peixiao; Shu, Qingming; Huang, Lihong; Guo, Jing et al. (2019a): Protein phosphatase 2 regulatory subunit B"Alpha silencing inhibits tumor cell proliferation in liver cancer. In: *Cancer medicine* 8 (18), S. 7741–7753. DOI: 10.1002/cam4.2620.

Chen, Jian; Shu, Shu; Chen, Yanting; Liu, Zhuo; Yu, Linjie; Yang, Lixuan et al. (2019b): AIM2 deletion promotes neuroplasticity and spatial memory of mice. In: *Brain research bulletin* 152, S. 85–94. DOI: 10.1016/j.brainresbull.2019.07.011.

Chen, Xuefeng; Niu, Hengyao; Chung, Woo-Hyun; Zhu, Zhu; Papusha, Alma; Shim, Eun Yong et al. (2011): Cell cycle regulation of DNA double-strand break end resection by Cdk1-dependent Dna2 phosphorylation. In: *Nature structural & molecular biology* 18 (9), S. 1015–1019. DOI: 10.1038/nsmb.2105.

Cho, Uhn Soo; Morrone, Seamus; Sablina, Anna A.; Arroyo, Jason D.; Hahn, William C.; Xu, Wenqing (2007): Structural basis of PP2A inhibition by small t antigen. In: *PLoS biology* 5 (8), e202. DOI: 10.1371/journal.pbio.0050202.

Christmann, Markus; Tomicic, Maja T.; Roos, Wynand P.; Kaina, Bernd (2003): Mechanisms of human DNA repair: an update. In: *Toxicology* 193 (1-2), S. 3–34. DOI: 10.1016/s0300-483x(03)00287-7.

Clark, Andrew R.; Ohlmeyer, Michael (2019): Protein phosphatase 2A as a therapeutic target in inflammation and neurodegeneration. In: *Pharmacology & therapeutics* 201, S. 181–201. DOI: 10.1016/j.pharmthera.2019.05.016.

Clay-Farrace, Lorena; Pelizon, Cristina; Santamaria, David; Pines, Jonathon; Laskey, Ronald A. (2003): Human replication protein Cdc6 prevents mitosis through a checkpoint mechanism that implicates Chk1. In: *The EMBO journal* 22 (3), S. 704–712. DOI: 10.1093/emboj/cdg046.

Cortez, D.; Guntuku, S.; Qin, J.; Elledge, S. J. (2001): ATR and ATRIP: partners in checkpoint signaling. In: *Science (New York, N.Y.)* 294 (5547), S. 1713–1716. DOI: 10.1126/science.1065521.

Coulonval, Katia; Vercruysse, Vincent; Paternot, Sabine; Pita, Jaime M.; Corman, Robert; Raspé, Eric; Roger, Pierre P. (2022): Monoclonal antibodies to activated CDK4: use to investigate normal and cancerous cell cycle regulation and involvement of phosphorylations of p21 and p27. In: *Cell cycle (Georgetown, Tex.)* 21 (1), S. 12–32. DOI: 10.1080/15384101.2021.1984663.

Creyghton, Menno P.; Roël, Giulietta; Eichhorn, Pieter J. A.; Hijmans, E. Marielle; Maurer, Irma; Destrée, Olivier; Bernards, René (2005): PR72, a novel regulator of Wnt signaling required for Naked cuticle function. In: *Genes & development* 19 (3), S. 376–386. DOI: 10.1101/gad.328905.

Creyghton, Menno P.; Roël, Giulietta; Eichhorn, Pieter J. A.; Vredeveld, Liesbeth C.; Destrée, Olivier; Bernards, René (2006): PR130 is a modulator of the Wnt-signaling cascade that counters repression of the antagonist Naked cuticle. In: *Proceedings of the National Academy of Sciences of the United States of America* 103 (14), S. 5397–5402. DOI: 10.1073/pnas.0507237103.

Daley, James M.; Sung, Patrick (2013): RIF1 in DNA break repair pathway choice. In: *Molecular cell* 49 (5), S. 840–841. DOI: 10.1016/j.molcel.2013.02.019.

D'Arcy, Mark S. (2019): Cell death: a review of the major forms of apoptosis, necrosis and autophagy. In: *Cell biology international* 43 (6), S. 582–592. DOI: 10.1002/cbin.11137.

David, Laure; Fernandez-Vidal, Anne; Bertoli, Sarah; Grgurevic, Srdana; Lepage, Benoît; Deshaies, Dominique et al. (2016): CHK1 as a therapeutic target to bypass chemoresistance in AML. In: *Science signaling* 9 (445), ra90. DOI: 10.1126/scisignal.aac9704.

Davie, James R. (2003): Inhibition of histone deacetylase activity by butyrate. In: *The Journal of nutrition* 133 (7 Suppl), 2485S-2493S. DOI: 10.1093/jn/133.7.2485S.

Di Ghelli Luserna Rorà, Andrea; Cerchione, Claudio; Martinelli, Giovanni; Simonetti, Giorgia (2020): A WEE1 family business: regulation of mitosis, cancer progression, and therapeutic target. In: *Journal of hematology & oncology* 13 (1), S. 126. DOI: 10.1186/s13045-020-00959-2.

Dzulko, Melanie; Pons, Miriam; Henke, Andreas; Schneider, Günter; Krämer, Oliver H. (2020): The PP2A subunit PR130 is a key regulator of cell development and oncogenic transformation. In: *Biochimica et biophysica acta. Reviews on cancer* 1874 (2), S. 188453. DOI: 10.1016/j.bbcan.2020.188453.

Elbæk, Camilla R.; Petrosius, Valdemaras; Sørensen, Claus S. (2020): WEE1 kinase limits CDK activities to safeguard DNA replication and mitotic entry. In: *Mutation research* 819-820, S. 111694. DOI: 10.1016/j.mrfmmm.2020.111694.

Elmore, Susan (2007): Apoptosis: a review of programmed cell death. In: *Toxicologic pathology* 35 (4), S. 495–516. DOI: 10.1080/01926230701320337.

El-Rayes, Samir; M S, Gomaa; A, Abouelmagd; Fathalla, Walid; Ali, Ibrahim A. I. (2019): Synthesis and antiproliferative assay of triazolyl-2,2-dimethyl-3-phenylpropanoates as potential HDAC inhibitors. In: *RSC advances* 9 (24), S. 13896–13907. DOI: 10.1039/c9ra01277j.

Escribano-Díaz, Cristina; Orthwein, Alexandre; Fradet-Turcotte, Amélie; Xing, Mengtan; Young, Jordan T. F.; Tkáč, Ján et al. (2013): A cell cycle-dependent regulatory circuit composed of 53BP1-RIF1 and BRCA1-CtIP controls DNA repair pathway choice. In: *Molecular cell* 49 (5), S. 872–883. DOI: 10.1016/j.molcel.2013.01.001.

Fagundes, Rafaela; Teixeira, Leonardo K. (2021): Cyclin E/CDK2: DNA Replication, Replication Stress and Genomic Instability. In: *Frontiers in cell and developmental biology* 9, S. 774845. DOI: 10.3389/fcell.2021.774845.

Fane, Mitchell; Weeraratna, Ashani T. (2020): How the ageing microenvironment influences tumour progression. In: *Nature reviews. Cancer* 20 (2), S. 89–106. DOI: 10.1038/s41568-019-0222-9.

Farrington, Caroline C.; Yuan, Eric; Mazhar, Sahar; Izadmehr, Sudeh; Hurst, Lauren; Allen-Petersen, Brittany L. et al. (2020): Protein phosphatase 2A activation as a therapeutic strategy for managing MYC-driven cancers. In: *The Journal of biological chemistry* 295 (3), S. 757–770. DOI: 10.1074/jbc.RA119.011443.

Fedak, Elizabeth A.; Adler, Frederick R.; Abegglen, Lisa M.; Schiffman, Joshua D. (2021): ATM and ATR Activation Through Crosstalk Between DNA Damage Response Pathways. In: *Bulletin of mathematical biology* 83 (4), S. 38. DOI: 10.1007/s11538-021-00868-6.

Ferrandina, G.; Stoler, A.; Fagotti, A.; Fanfani, F.; Sacco, R.; Pasqua, A. de et al. (2000): p21WAF1/CIP1 protein expression in primary ovarian cancer. In: *International journal of oncology* 17 (6), S. 1231–1235. DOI: 10.3892/ijo.17.6.1231.

Ferrell, James E.; Pomerening, Joseph R.; Kim, Sun Young; Trunnell, Nikki B.; Xiong, Wen; Huang, Chi-Ying Frederick; Machleder, Eric M. (2009): Simple, realistic models of complex biological processes: positive feedback and bistability in a cell fate switch and a cell cycle oscillator. In: *FEBS letters* 583 (24), S. 3999–4005. DOI: 10.1016/j.febslet.2009.10.068.

Fujiki, Hirota; Sueoka, Eisaburo; Watanabe, Tatsuro; Suganuma, Masami (2018): The concept of the okadaic acid class of tumor promoters is revived in endogenous protein inhibitors of protein phosphatase 2A, SET and CIP2A, in human cancers. In: *Journal of cancer research and clinical oncology* 144 (12), S. 2339–2349. DOI: 10.1007/s00432-018-2765-7.

Gao, Song; Shan, Liping; Zhang, Mo; Wang, Yan; Zhan, Xi; Yin, Yalei et al. (2022): Inhibition of PP2A by LB100 sensitizes bladder cancer cells to chemotherapy by inducing p21 degradation. In: *Cellular oncology (Dordrecht)* 45 (6), S. 1203–1215. DOI: 10.1007/s13402-022-00710-8.

García-Osta, Ana; Dong, Jinya; Moreno-Aliaga, María Jesús; Ramirez, Maria Javier (2022): p27, The Cell Cycle and Alzheimer´s Disease. In: *International journal of molecular sciences* 23 (3). DOI: 10.3390/ijms23031211.

Gartel, A. L.; Ye, X.; Goufman, E.; Shianov, P.; Hay, N.; Najmabadi, F.; Tyner, A. L. (2001): Myc represses the p21(WAF1/CIP1) promoter and interacts with Sp1/Sp3. In: *Proceedings of the National Academy of Sciences of the United States of America* 98 (8), S. 4510–4515. DOI: 10.1073/pnas.081074898.

Gasser, Stephan; Raulet, David (2006): The DNA damage response, immunity and cancer. In: *Seminars in cancer biology* 16 (5), S. 344–347. DOI: 10.1016/j.semcancer.2006.07.004.

Glozak, M. A.; Seto, E. (2007): Histone deacetylases and cancer. In: *Oncogene* 26 (37), S. 5420–5432. DOI: 10.1038/sj.onc.1210610.

Göder, Anja; Emmerich, Claudia; Nikolova, Teodora; Kiweler, Nicole; Schreiber, Maria; Kühl, Toni et al. (2018): HDAC1 and HDAC2 integrate checkpoint kinase phosphorylation and cell fate through the phosphatase-2A subunit PR130. In: *Nature communications* 9 (1), S. 764. DOI: 10.1038/s41467-018-03096-0.

Goodarzi, Aaron A.; Jonnalagadda, Jyoti C.; Douglas, Pauline; Young, David; Ye, Ruiqiong; Moorhead, Greg B. G. et al. (2004): Autophosphorylation of ataxia-telangiectasia mutated is regulated by protein phosphatase 2A. In: *The EMBO journal* 23 (22), S. 4451–4461. DOI: 10.1038/sj.emboj.7600455.

Goodwin, Jonathan F.; Knudsen, Karen E. (2014): Beyond DNA repair: DNA-PK function in cancer. In: *Cancer discovery* 4 (10), S. 1126–1139. DOI: 10.1158/2159-8290.CD-14-0358.

Guo, Sun-Wei (2012): The Epigenetics of Endometriosis. In: Trygve O. Tollefsbol (Hg.): Epigenetics in human disease. Amsterdam: Elsevier, S. 443–469.

Gupta, Arun; Hunt, Clayton R.; Chakraborty, Sharmistha; Pandita, Raj K.; Yordy, John; Ramnarain, Deepti B. et al. (2014): Role of 53BP1 in the regulation of DNA double-strand break repair pathway choice. In: *Radiation research* 181 (1), S. 1–8. DOI: 10.1667/RR13572.1.

Haanen, C.; Vermes, I. (1995): Apoptosis and inflammation. In: *Mediators of inflammation* 4 (1), S. 5–15. DOI: 10.1155/S0962935195000020.

Hanahan, D.; Weinberg, R. A. (2000): The hallmarks of cancer. In: *Cell* 100 (1), S. 57–70. DOI: 10.1016/s0092-8674(00)81683-9.

Hanahan, Douglas (2022): Hallmarks of Cancer: New Dimensions. In: *Cancer discovery* 12 (1), S. 31–46. DOI: 10.1158/2159-8290.CD-21-1059.

Hanahan, Douglas; Weinberg, Robert A. (2011): Hallmarks of cancer: the next generation. In: *Cell* 144 (5), S. 646–674. DOI: 10.1016/j.cell.2011.02.013.

Harbour, J. W.; Dean, D. C. (2000): The Rb/E2F pathway: expanding roles and emerging paradigms. In: *Genes & development* 14 (19), S. 2393–2409. DOI: 10.1101/gad.813200.

Helleday, Thomas; Lo, Justin; van Gent, Dik C.; Engelward, Bevin P. (2007): DNA double-strand break repair: from mechanistic understanding to cancer treatment. In: *DNA repair* 6 (7), S. 923–935. DOI: 10.1016/j.dnarep.2007.02.006.

Hendrix, P.; Mayer-Jackel, R. E.; Cron, P.; Goris, J.; Hofsteenge, J.; Merlevede, W.; Hemmings, B. A. (1993): Structure and expression of a 72-kDa regulatory subunit of protein phosphatase 2A. Evidence for different size forms produced by alternative splicing. In: *The Journal of biological chemistry* 268 (20), S. 15267–15276.

Ho, Terence C. S.; Chan, Alex H. Y.; Ganesan, A. (2020): Thirty Years of HDAC Inhibitors: 2020 Insight and Hindsight. In: *Journal of medicinal chemistry* 63 (21), S. 12460–12484. DOI: 10.1021/acs.jmedchem.0c00830.

Ho, Winson S.; Sizdahkhani, Saman; Hao, Shuyu; Song, Hua; Seldomridge, Ashlee; Tandle, Anita et al. (2018): LB-100, a novel Protein Phosphatase 2A (PP2A) inhibitor, sensitizes malignant meningioma cells to the therapeutic effects of radiation. In: *Cancer letters* 415, S. 217–226. DOI: 10.1016/j.canlet.2017.11.035.

Hong, Christopher S.; Ho, Winson; Zhang, Chao; Yang, Chunzhang; Elder, J. Bradley; Zhuang, Zhengping (2015): LB100, a small molecule inhibitor of PP2A with potent chemo- and radio-sensitizing potential. In: *Cancer biology & therapy* 16 (6), S. 821–833. DOI: 10.1080/15384047.2015.1040961.

Hsieh, Ya-Ju; Hwu, Luen; Chen, Yi-Chieh; Ke, Chien-Chih; Chen, Fu-Du; Wang, Hsin-Ell et al. (2014): P21-driven multifusion gene system for evaluating the efficacy of histone deacetylase inhibitors by in vivo molecular imaging and for transcription targeting therapy of cancer mediated by histone deacetylase inhibitor. In: *Journal of nuclear medicine : official publication, Society of Nuclear Medicine* 55 (4), S. 678–685. DOI: 10.2967/jnumed.113.126573.

Huertas, Pablo; Cortés-Ledesma, Felipe; Sartori, Alessandro A.; Aguilera, Andrés; Jackson, Stephen P. (2008): CDK targets Sae2 to control DNA-end resection and homologous recombination. In: *Nature* 455 (7213), S. 689–692. DOI: 10.1038/nature07215.

Hughes, Bridget T.; Sidorova, Julia; Swanger, Jherek; Monnat, Raymond J.; Clurman, Bruce E. (2013): Essential role for Cdk2 inhibitory phosphorylation during replication stress revealed by a human Cdk2 knockin mutation. In: *Proceedings of*

the National Academy of Sciences of the United States of America 110 (22), S. 8954–8959. DOI: 10.1073/pnas.1302927110.

Isobe, Shin-Ya; Hiraga, Shin-Ichiro; Nagao, Koji; Sasanuma, Hiroyuki; Donaldson, Anne D.; Obuse, Chikashi (2021): Protein phosphatase 1 acts as a RIF1 effector to suppress DSB resection prior to Shieldin action. In: *Cell reports* 36 (2), S. 109383. DOI: 10.1016/j.celrep.2021.109383.

Isobe, Shin-Ya; Nagao, Koji; Nozaki, Naohito; Kimura, Hiroshi; Obuse, Chikashi (2017): Inhibition of RIF1 by SCAI Allows BRCA1-Mediated Repair. In: *Cell reports* 20 (2), S. 297–307. DOI: 10.1016/j.celrep.2017.06.056.

Ito, Akihiro; Kawaguchi, Yoshiharu; Lai, Chun-Hsiang; Kovacs, Jeffrey J.; Higashimoto, Yuichiro; Appella, Ettore; Yao, Tso-Pang (2002): MDM2-HDAC1-mediated deacetylation of p53 is required for its degradation. In: *The EMBO journal* 21 (22), S. 6236–6245. DOI: 10.1093/emboj/cdf616.

Jackson, Maria; Marks, Leah; May, Gerhard H. W.; Wilson, Joanna B. (2018): The genetic basis of disease. In: *Essays in biochemistry* 62 (5), S. 643–723. DOI: 10.1042/EBC20170053.

Janssens, V.; Goris, J. (2001): Protein phosphatase 2A: a highly regulated family of serine/threonine phosphatases implicated in cell growth and signalling. In: *The Biochemical journal* 353 (Pt 3), S. 417–439. DOI: 10.1042/0264-6021:3530417.

Janssens, Veerle; Derua, Rita; Zwaenepoel, Karen; Waelkens, Etienne; Goris, Jozef (2009): Specific regulation of protein phosphatase 2A PR72/B'' subunits by calpain. In: *Biochemical and biophysical research communications* 386 (4), S. 676–681. DOI: 10.1016/j.bbrc.2009.06.096.

Janssens, Veerle; Zwaenepoel, Karen; Rossé, Carine; Petit, Marleen M. R.; Goris, Jozef; Parker, Peter J. (2016): PP2A binds to the LIM domains of lipoma-preferred partner through its PR130/B″ subunit to regulate cell adhesion and migration. In: *Journal of cell science* 129 (8), S. 1605–1618. DOI: 10.1242/jcs.175778.

Järviluoma, Annika; Child, Emma S.; Sarek, Grzegorz; Sirimongkolkasem, Papinya; Peters, Gordon; Ojala, Päivi M.; Mann, David J. (2006): Phosphorylation of the cyclin-dependent kinase inhibitor p21Cip1 on serine 130 is essential for viral cyclin-mediated bypass of a p21Cip1-imposed G1 arrest. In: *Molecular and cellular biology* 26 (6), S. 2430–2440. DOI: 10.1128/MCB.26.6.2430-2440.2006.

Jirawatnotai, Siwanon; Hu, Yiduo; Michowski, Wojciech; Elias, Joshua E.; Becks, Lisa; Bienvenu, Frederic et al. (2011): A function for cyclin D1 in DNA repair uncovered

by protein interactome analyses in human cancers. In: *Nature* 474 (7350), S. 230–234. DOI: 10.1038/nature10155.

Jung, J. M.; Bruner, J. M.; Ruan, S.; Langford, L. A.; Kyritsis, A. P.; Kobayashi, T. et al. (1995): Increased levels of p21WAF1/Cip1 in human brain tumors. In: *Oncogene* 11 (10), S. 2021–2028.

Kashyap, Dharambir; Garg, Vivek Kumar; Goel, Neelam (2021): Intrinsic and extrinsic pathways of apoptosis: Role in cancer development and prognosis. In: *Advances in protein chemistry and structural biology* 125, S. 73–120. DOI: 10.1016/bs.apcsb.2021.01.003.

Kauko, Otto; Westermarck, Jukka (2018): Non-genomic mechanisms of protein phosphatase 2A (PP2A) regulation in cancer. In: *The international journal of biochemistry & cell biology* 96, S. 157–164. DOI: 10.1016/j.biocel.2018.01.005.

Khan, Mohd Moin; Kalim, Ubaid Ullah; Khan, Meraj H.; Lahesmaa, Riitta (2021): PP2A and Its Inhibitors in Helper T-Cell Differentiation and Autoimmunity. In: *Frontiers in immunology* 12, S. 786857. DOI: 10.3389/fimmu.2021.786857.

Kijas, Amanda W.; Lim, Yi Chieh; Bolderson, Emma; Cerosaletti, Karen; Gatei, Magtouf; Jakob, Burkhard et al. (2015): ATM-dependent phosphorylation of MRE11 controls extent of resection during homology directed repair by signalling through Exonuclease 1. In: *Nucleic acids research* 43 (17), S. 8352–8367. DOI: 10.1093/nar/gkv754.

Kim, Geum-Yi; Mercer, Stephen E.; Ewton, Daina Z.; Yan, Zhongfa; Jin, Kideok; Friedman, Eileen (2002): The stress-activated protein kinases p38 alpha and JNK1 stabilize p21(Cip1) by phosphorylation. In: *The Journal of biological chemistry* 277 (33), S. 29792–29802. DOI: 10.1074/jbc.M201299200.

Kim, Sang Woo; Kim, Hae Jong; Chun, Young Jin; Kim, Mie Young (2010): Ceramide produces apoptosis through induction of p27(kip1) by protein phosphatase 2A-dependent Akt dephosphorylation in PC-3 prostate cancer cells. In: *Journal of toxicology and environmental health. Part A* 73 (21-22), S. 1465–1476. DOI: 10.1080/15287394.2010.511553.

Kimelman, D.; Xu, W. (2006): beta-catenin destruction complex: insights and questions from a structural perspective. In: *Oncogene* 25 (57), S. 7482–7491. DOI: 10.1038/sj.onc.1210055.

Kolupaeva, Victoria; Janssens, Veerle (2013): PP1 and PP2A phosphatases--cooperating partners in modulating retinoblastoma protein activation. In: *The FEBS journal* 280 (2), S. 627–643. DOI: 10.1111/j.1742-4658.2012.08511.x.

Kopytko, Patrycja; Piotrowska, Katarzyna; Janisiak, Joanna; Tarnowski, Maciej (2021): Garcinol-A Natural Histone Acetyltransferase Inhibitor and New Anti-Cancer Epigenetic Drug. In: *International journal of molecular sciences* 22 (6). DOI: 10.3390/ijms22062828.

Korkolopoulou, P.; Kouzelis, K.; Christodoulou, P.; Papanikolaou, A.; Thomas-Tsagli, E. (1998): Expression of retinoblastoma gene product and p21 (WAF1/Cip 1) protein in gliomas: correlations with proliferation markers, p53 expression and survival. In: *Acta neuropathologica* 95 (6), S. 617–624. DOI: 10.1007/s004010050848.

Kreis, Nina-Naomi; Friemel, Alexandra; Zimmer, Brigitte; Roth, Susanne; Rieger, Michael A.; Rolle, Udo et al. (2016): Mitotic p21Cip1/CDKN1A is regulated by cyclin-dependent kinase 1 phosphorylation. In: *Oncotarget* 7 (31), S. 50215–50228. DOI: 10.18632/oncotarget.10330.

Krumm, Andrea; Barckhausen, Christina; Kücük, Pelin; Tomaszowski, Karl-Heinz; Loquai, Carmen; Fahrer, Jörg et al. (2016): Enhanced Histone Deacetylase Activity in Malignant Melanoma Provokes RAD51 and FANCD2-Triggered Drug Resistance. In: *Cancer research* 76 (10), S. 3067–3077. DOI: 10.1158/0008-5472.CAN-15-2680.

Kumagai, A.; Dunphy, W. G. (2000): Claspin, a novel protein required for the activation of Chk1 during a DNA replication checkpoint response in Xenopus egg extracts. In: *Molecular cell* 6 (4), S. 839–849. DOI: 10.1016/s1097-2765(05)00092-4.

Kuo, Yi-Chun; Huang, Kai-Yun; Yang, Chung-Hsiang; Yang, Yu-San; Lee, Wen-Yu; Chiang, Chi-Wu (2008): Regulation of phosphorylation of Thr-308 of Akt, cell proliferation, and survival by the B55alpha regulatory subunit targeting of the protein phosphatase 2A holoenzyme to Akt. In: *The Journal of biological chemistry* 283 (4), S. 1882–1892. DOI: 10.1074/jbc.M709585200.

LeBoeuf, Matthew; Terrell, Anne; Trivedi, Sohum; Sinha, Satrajit; Epstein, Jonathan A.; Olson, Eric N. et al. (2010): Hdac1 and Hdac2 act redundantly to control p63 and p53 functions in epidermal progenitor cells. In: *Developmental cell* 19 (6), S. 807–818. DOI: 10.1016/j.devcel.2010.10.015.

Lee, J.; Li, L.; Gretz, N.; Gebert, J.; Dihlmann, S. (2012): Absent in Melanoma 2 (AIM2) is an important mediator of interferon-dependent and -independent HLA-DRA and

HLA-DRB gene expression in colorectal cancers. In: *Oncogene* 31 (10), S. 1242–1253. DOI: 10.1038/onc.2011.320.

Lee, Ji-Hoon; Paull, Tanya T. (2005): ATM activation by DNA double-strand breaks through the Mre11-Rad50-Nbs1 complex. In: *Science (New York, N.Y.)* 308 (5721), S. 551–554. DOI: 10.1126/science.1108297.

Lee, Jong-Hyuk; Shamanna, Raghavendra A.; Kulikowicz, Tomasz; Borhan Fakouri, Nima; Kim, Edward W.; Christiansen, Louise S. et al. (2021): CDK2 phosphorylation of Werner protein (WRN) contributes to WRN's DNA double-strand break repair pathway choice. In: *Aging cell* 20 (11), e13484. DOI: 10.1111/acel.13484.

Lee, Kenneth K.; Workman, Jerry L. (2007): Histone acetyltransferase complexes: one size doesn't fit all. In: *Nature reviews. Molecular cell biology* 8 (4), S. 284–295. DOI: 10.1038/nrm2145.

Lei, Tiantian; Du, Suya; Peng, Zhe; Chen, Lin (2022): Multifaceted regulation and functions of 53BP1 in NHEJ-mediated DSB repair (Review). In: *International Journal of Molecular Medicine* 50 (1). DOI: 10.3892/ijmm.2022.5145.

Li, Xiaoman; Xu, Hongde; Xu, Chongan; Lin, Meina; Song, Xiaoyu; Yi, Fei et al. (2013): The yin-yang of DNA damage response: roles in tumorigenesis and cellular senescence. In: *International journal of molecular sciences* 14 (2), S. 2431–2448. DOI: 10.3390/ijms14022431.

Lieber, Michael R. (2010): The mechanism of double-strand DNA break repair by the nonhomologous DNA end-joining pathway. In: *Annual review of biochemistry* 79, S. 181–211. DOI: 10.1146/annurev.biochem.052308.093131.

Lim, Shuhui; Kaldis, Philipp (2013): Cdks, cyclins and CKIs: roles beyond cell cycle regulation. In: *Development (Cambridge, England)* 140 (15), S. 3079–3093. DOI: 10.1242/dev.091744.

Liu, Jiaqi; Xiao, Qing; Xiao, Jiani; Niu, Chenxi; Li, Yuanyuan; Zhang, Xiaojun et al. (2022): Wnt/β-catenin signalling: function, biological mechanisms, and therapeutic opportunities. In: *Signal transduction and targeted therapy* 7 (1), S. 3. DOI: 10.1038/s41392-021-00762-6.

Liu, Shizhou; Shiotani, Bunsyo; Lahiri, Mayurika; Maréchal, Alexandre; Tse, Alice; Leung, Charles Chung Yun et al. (2011): ATR autophosphorylation as a molecular switch for checkpoint activation. In: *Molecular cell* 43 (2), S. 192–202. DOI: 10.1016/j.molcel.2011.06.019.

Lu, Xiaoyan; Liu, Jia; Legerski, Randy J. (2009): Cyclin E is stabilized in response to replication fork barriers leading to prolonged S phase arrest. In: *The Journal of biological chemistry* 284 (51), S. 35325–35337. DOI: 10.1074/jbc.M109.035949.

Luo, Yuxiang; Li, Huilin (2020): Structure-Based Inhibitor Discovery of Class I Histone Deacetylases (HDACs). In: *International journal of molecular sciences* 21 (22), S. 8828. DOI: 10.3390/ijms21228828.

Malumbres, Marcos (2014): Cyclin-dependent kinases. In: *Genome biology* 15 (6), S. 122. DOI: 10.1186/gb4184.

Manley, Paul W.; Cowan-Jacob, Sandra W.; Cozens, Robert; Fendrich, Gabriele; Jahnke, Wolfgang; Roesel, Johannes L.; Fabbro, Doriano (2011): Fingolimod (FTY720) Inhibits BCR-ABL Signaling Allosterically by Binding to the Myristate Binding Site. In: *Blood* 118 (21), S. 2746. DOI: 10.1182/blood.V118.21.2746.2746.

Mao, Zhiyong; Bozzella, Michael; Seluanov, Andrei; Gorbunova, Vera (2008): Comparison of nonhomologous end joining and homologous recombination in human cells. In: *DNA repair* 7 (10), S. 1765–1771. DOI: 10.1016/j.dnarep.2008.06.018.

Maréchal, Alexandre; Zou, Lee (2013): DNA damage sensing by the ATM and ATR kinases. In: *Cold Spring Harbor perspectives in biology* 5 (9). DOI: 10.1101/cshperspect.a012716.

Martín, Yusé; Domínguez-Kelly, Raquel; Freire, Raimundo (2011): Novel insights into maintaining genomic integrity: Wee1 regulating Mus81/Eme1. In: *Cell division* 6, S. 21. DOI: 10.1186/1747-1028-6-21.

Martínez-Alonso, Diego; Malumbres, Marcos (2020): Mammalian cell cycle cyclins. In: *Seminars in cell & developmental biology* 107, S. 28–35. DOI: 10.1016/j.semcdb.2020.03.009.

Matos-Rodrigues, Gabriel E.; Grigaravicius, Paulius; Lopez, Bernard S.; Hofmann, Thomas G.; Frappart, Pierre-Olivier; Martins, Rodrigo A. P. (2020): ATRIP protects progenitor cells against DNA damage in vivo. In: *Cell death & disease* 11 (10), S. 923. DOI: 10.1038/s41419-020-03090-9.

Matthews, Helen K.; Bertoli, Cosetta; Bruin, Robertus A. M. de (2022): Cell cycle control in cancer. In: *Nature reviews. Molecular cell biology* 23 (1), S. 74–88. DOI: 10.1038/s41580-021-00404-3.

Mazhar, Sahar; Taylor, Sarah E.; Sangodkar, Jaya; Narla, Goutham (2019): Targeting PP2A in cancer: Combination therapies. In: *Biochimica et biophysica acta. Molecular cell research* 1866 (1), S. 51–63. DOI: 10.1016/j.bbamcr.2018.08.020.

Millán-Zambrano, Gonzalo; Burton, Adam; Bannister, Andrew J.; Schneider, Robert (2022): Histone post-translational modifications - cause and consequence of genome function. In: *Nature reviews. Genetics* 23 (9), S. 563–580. DOI: 10.1038/s41576-022-00468-7.

Miller, Donald M.; Thomas, Shelia D.; Islam, Ashraful; Muench, David; Sedoris, Kara (2012): c-Myc and cancer metabolism. In: *Clinical cancer research : an official journal of the American Association for Cancer Research* 18 (20), S. 5546–5553. DOI: 10.1158/1078-0432.CCR-12-0977.

Miller, Kyle M.; Tjeertes, Jorrit V.; Coates, Julia; Legube, Gaëlle; Polo, Sophie E.; Britton, Sébastien; Jackson, Stephen P. (2010): Human HDAC1 and HDAC2 function in the DNA-damage response to promote DNA nonhomologous end-joining. In: *Nature structural & molecular biology* 17 (9), S. 1144–1151. DOI: 10.1038/nsmb.1899.

Mordes, Daniel A.; Glick, Gloria G.; Zhao, Runxiang; Cortez, David (2008): TopBP1 activates ATR through ATRIP and a PIKK regulatory domain. In: *Genes & development* 22 (11), S. 1478–1489. DOI: 10.1101/gad.1666208.

Morgan, D. O. (1995): Principles of CDK regulation. In: *Nature* 374 (6518), S. 131–134. DOI: 10.1038/374131a0.

Movafagh, Shahrzad; Munson, Amanda (2019): Histone Deacetylase Inhibitors in Cancer Prevention and Therapy. In: Anupam Bishayee und Deepak Bhatia (Hg.): Epigenetics of cancer prevention. London, United Kingdom, San Diego, CA: Academic Press (Translational epigenetics series, volume 8), S. 75–105.

Nader, Cassandra P.; Cidem, Aylin; Verrills, Nicole M.; Ammit, Alaina J. (2019): Protein phosphatase 2A (PP2A): a key phosphatase in the progression of chronic obstructive pulmonary disease (COPD) to lung cancer. In: *Respiratory research* 20 (1), S. 222. DOI: 10.1186/s12931-019-1192-x.

Nam, Robert K.; Benatar, Tania; Amemiya, Yutaka; Wallis, Christopher J. D.; Romero, Joan Miguel; Tsagaris, Melina et al. (2018): MicroRNA-652 induces NED in LNCaP and EMT in PC3 prostate cancer cells. In: *Oncotarget* 9 (27), S. 19159–19176. DOI: 10.18632/oncotarget.24937.

Neviani, Paolo; Perrotti, Danilo (2014): SETting OP449 into the PP2A-activating drug family. In: *Clinical cancer research : an official journal of the American Association for Cancer Research* 20 (8), S. 2026–2028. DOI: 10.1158/1078-0432.CCR-14-0166.

Nguyen, Alexandra; Dzulko, Melanie; Murr, Janine; Yen, Yun; Schneider, Günter; Krämer, Oliver H. (2021): Class 1 Histone Deacetylases and Ataxia-Telangiectasia Mutated Kinase Control the Survival of Murine Pancreatic Cancer Cells upon dNTP Depletion. In: *Cells* 10 (10). DOI: 10.3390/cells10102520.

Nikolova, Teodora; Kiweler, Nicole; Krämer, Oliver H. (2017): Interstrand Crosslink Repair as a Target for HDAC Inhibition. In: *Trends in pharmacological sciences* 38 (9), S. 822–836. DOI: 10.1016/j.tips.2017.05.009.

Ocker, Matthias; Schneider-Stock, Regine (2007): Histone deacetylase inhibitors: signalling towards p21cip1/waf1. In: *The international journal of biochemistry & cell biology* 39 (7-8), S. 1367–1374. DOI: 10.1016/j.biocel.2007.03.001.

Owen, G. I.; Richer, J. K.; Tung, L.; Takimoto, G.; Horwitz, K. B. (1998): Progesterone regulates transcription of the p21(WAF1) cyclin- dependent kinase inhibitor gene through Sp1 and CBP/p300. In: *The Journal of biological chemistry* 273 (17), S. 10696–10701. DOI: 10.1074/jbc.273.17.10696.

Pagliuca, Felicia Walton; Collins, Mark O.; Lichawska, Agata; Zegerman, Philip; Choudhary, Jyoti S.; Pines, Jonathon (2011): Quantitative proteomics reveals the basis for the biochemical specificity of the cell-cycle machinery. In: *Molecular cell* 43 (3), S. 406–417. DOI: 10.1016/j.molcel.2011.05.031.

Paull, Tanya T. (2015): Mechanisms of ATM Activation. In: *Annual review of biochemistry* 84, S. 711–738. DOI: 10.1146/annurev-biochem-060614-034335.

Peng, Bo; Chai, Yurong; Li, Yang; Liu, Xinxin; Zhang, Jianying (2015): CIP2A overexpression induces autoimmune response and enhances JNK signaling pathway in human lung cancer. In: *BMC cancer* 15, S. 895. DOI: 10.1186/s12885-015-1899-0.

Perrotti, Danilo; Neviani, Paolo (2013): Protein phosphatase 2A: a target for anticancer therapy. In: *The Lancet. Oncology* 14 (6), e229-38. DOI: 10.1016/S1470-2045(12)70558-2.

Petersen, Paris; Chou, Danny M.; You, Zhongsheng; Hunter, Tony; Walter, Johannes C.; Walter, Gernot (2006): Protein phosphatase 2A antagonizes ATM and ATR in a

Cdk2- and Cdc7-independent DNA damage checkpoint. In: *Molecular and cellular biology* 26 (5), S. 1997–2011. DOI: 10.1128/MCB.26.5.1997-2011.2006.

Pippa, Raffaella; Odero, Maria D. (2020): The Role of MYC and PP2A in the Initiation and Progression of Myeloid Leukemias. In: *Cells* 9 (3). DOI: 10.3390/cells9030544.

Prakash, Rohit; Zhang, Yu; Feng, Weiran; Jasin, Maria (2015): Homologous recombination and human health: the roles of BRCA1, BRCA2, and associated proteins. In: *Cold Spring Harbor perspectives in biology* 7 (4), a016600. DOI: 10.1101/cshperspect.a016600.

Ranjha, Lepakshi; Howard, Sean M.; Cejka, Petr (2018): Main steps in DNA double-strand break repair: an introduction to homologous recombination and related processes. In: *Chromosoma* 127 (2), S. 187–214. DOI: 10.1007/s00412-017-0658-1.

Repen, Boris; Schneider, Erwin; Alexiev, Ulrike (2012): Optimization of a malachite green assay for detection of ATP hydrolysis by solubilized membrane proteins. In: *Analytical biochemistry* 426 (2), S. 103–105. DOI: 10.1016/j.ab.2012.04.016.

Robertson, Cameron M.; Xue, Yuan; Chowdhury, Shobir; Maringele, Laura (2023): A CDK-Dependent Phosphorylation of a Novel Domain of Rif1 Regulates its Function during Telomere Damage and Other Types of Stress. In: *Molecular and cellular biology* 43 (5), S. 185–199. DOI: 10.1080/10985549.2023.2193768.

Ruff, Sophie E.; Logan, Susan K.; Garabedian, Michael J.; Huang, Tony T. (2020): Roles for MDC1 in cancer development and treatment. In: *DNA repair* 95, S. 102948. DOI: 10.1016/j.dnarep.2020.102948.

Sablina, Anna A.; Hector, Melissa; Colpaert, Nathalie; Hahn, William C. (2010): Identification of PP2A complexes and pathways involved in cell transformation. In: *Cancer research* 70 (24), S. 10474–10484. DOI: 10.1158/0008-5472.CAN-10-2855.

Sanchez, Y.; Wong, C.; Thoma, R. S.; Richman, R.; Wu, Z.; Piwnica-Worms, H.; Elledge, S. J. (1997): Conservation of the Chk1 checkpoint pathway in mammals: linkage of DNA damage to Cdk regulation through Cdc25. In: *Science (New York, N.Y.)* 277 (5331), S. 1497–1501. DOI: 10.1126/science.277.5331.1497.

Sangodkar, Jaya; Farrington, Caroline C.; McClinch, Kimberly; Galsky, Matthew D.; Kastrinsky, David B.; Narla, Goutham (2016): All roads lead to PP2A: exploiting the therapeutic potential of this phosphatase. In: *The FEBS journal* 283 (6), S. 1004–1024. DOI: 10.1111/febs.13573.

Sarbia, M.; Stahl, M.; zur Hausen, A.; Zimmermann, K.; Wang, L.; Fink, U. et al. (1998): Expression of p21WAF1 predicts outcome of esophageal cancer patients treated by surgery alone or by combined therapy modalities. In: *Clinical cancer research : an official journal of the American Association for Cancer Research* 4 (11), S. 2615–2623.

Satyanarayana, Ande; Kaldis, Philipp (2009): A dual role of Cdk2 in DNA damage response. In: *Cell division* 4, S. 9. DOI: 10.1186/1747-1028-4-9.

Schafer, K. A. (1998): The cell cycle: a review. In: *Veterinary pathology* 35 (6), S. 461–478. DOI: 10.1177/030098589803500601.

Schleicher, Emily M.; Dhoonmoon, Ashna; Jackson, Lindsey M.; Khatib, Jude B.; Nicolae, Claudia M.; Moldovan, George-Lucian (2022): The TIP60-ATM axis regulates replication fork stability in BRCA-deficient cells. In: *Oncogenesis* 11 (1), S. 33. DOI: 10.1038/s41389-022-00410-w.

Schneider, Anne; Chatterjee, Snehajyoti; Bousiges, Olivier; Selvi, B. Ruthrotha; Swaminathan, Amrutha; Cassel, Raphaelle et al. (2013): Acetyltransferases (HATs) as targets for neurological therapeutics. In: *Neurotherapeutics : the journal of the American Society for Experimental NeuroTherapeutics* 10 (4), S. 568–588. DOI: 10.1007/s13311-013-0204-7.

Seshacharyulu, Parthasarathy; Pandey, Poomy; Datta, Kaustubh; Batra, Surinder K. (2013): Phosphatase: PP2A structural importance, regulation and its aberrant expression in cancer. In: *Cancer letters* 335 (1), S. 9–18. DOI: 10.1016/j.canlet.2013.02.036.

Shamloo, Bahar; Usluer, Sinem (2019): p21 in Cancer Research. In: *Cancers* 11 (8). DOI: 10.3390/cancers11081178.

Sharma, Sahil; Poetz, Fabian; Bruer, Marius; Ly-Hartig, Thi Bach Nga; Schott, Johanna; Séraphin, Bertrand; Stoecklin, Georg (2016): Acetylation-Dependent Control of Global Poly(A) RNA Degradation by CBP/p300 and HDAC1/2. In: *Molecular cell* 63 (6), S. 927–938. DOI: 10.1016/j.molcel.2016.08.030.

Sherr, C. J.; Roberts, J. M. (1999): CDK inhibitors: positive and negative regulators of G1-phase progression. In: *Genes & development* 13 (12), S. 1501–1512. DOI: 10.1101/gad.13.12.1501.

Sherr, Charles J.; Roberts, James M. (2004): Living with or without cyclins and cyclin-dependent kinases. In: *Genes & development* 18 (22), S. 2699–2711. DOI: 10.1101/gad.1256504.

Shi, Yigong (2002): Mechanisms of caspase activation and inhibition during apoptosis. In: *Molecular cell* 9 (3), S. 459–470. DOI: 10.1016/s1097-2765(02)00482-3.

Silverman, Joshua; Takai, Hiroyuki; Buonomo, Sara B. C.; Eisenhaber, Frank; Lange, Titia de (2004): Human Rif1, ortholog of a yeast telomeric protein, is regulated by ATM and 53BP1 and functions in the S-phase checkpoint. In: *Genes & development* 18 (17), S. 2108–2119. DOI: 10.1101/gad.1216004.

Singh, Puneet; Lim, Bora (2022): Targeting Apoptosis in Cancer. In: *Current oncology reports* 24 (3), S. 273–284. DOI: 10.1007/s11912-022-01199-y.

Singh, Vishakha; Ram, Mahendra; Kumar, Rajesh; Prasad, Raju; Roy, Birendra Kumar; Singh, Kaushal Kumar (2017): Phosphorylation: Implications in Cancer. In: *The protein journal* 36 (1), S. 1–6. DOI: 10.1007/s10930-017-9696-z.

Smith, Hannah L.; Southgate, Harriet; Tweddle, Deborah A.; Curtin, Nicola J. (2020): DNA damage checkpoint kinases in cancer. In: *Expert reviews in molecular medicine* 22, e2. DOI: 10.1017/erm.2020.3.

Smith, Joanne; Tho, Lye Mun; Xu, Naihan; Gillespie, David A. (2010): The ATM-Chk2 and ATR-Chk1 pathways in DNA damage signaling and cancer. In: *Advances in cancer research* 108, S. 73–112. DOI: 10.1016/B978-0-12-380888-2.00003-0.

Smits, Veronique A. J.; Cabrera, Elisa; Freire, Raimundo; Gillespie, David A. (2019): Claspin - checkpoint adaptor and DNA replication factor. In: *The FEBS journal* 286 (3), S. 441–455. DOI: 10.1111/febs.14594.

Soofiyani, Saiedeh Razi; Hejazi, Mohammad Saeid; Baradaran, Behzad (2017): The role of CIP2A in cancer: A review and update. In: *Biomedicine & pharmacotherapy = Biomedecine & pharmacotherapie* 96, S. 626–633. DOI: 10.1016/j.biopha.2017.08.146.

Stiff, Thomas; Walker, Sarah A.; Cerosaletti, Karen; Goodarzi, Aaron A.; Petermann, Eva; Concannon, Pat et al. (2006): ATR-dependent phosphorylation and activation of ATM in response to UV treatment or replication fork stalling. In: *The EMBO journal* 25 (24), S. 5775–5782. DOI: 10.1038/sj.emboj.7601446.

Sun, Yingli; Xu, Ye; Roy, Kanaklata; Price, Brendan D. (2007): DNA damage-induced acetylation of lysine 3016 of ATM activates ATM kinase activity. In: *Molecular and cellular biology* 27 (24), S. 8502–8509. DOI: 10.1128/MCB.01382-07.

Sur, Swastika; Agrawal, Devendra K. (2016): Phosphatases and kinases regulating CDC25 activity in the cell cycle: clinical implications of CDC25 overexpression and

potential treatment strategies. In: *Molecular and cellular biochemistry* 416 (1-2), S. 33–46. DOI: 10.1007/s11010-016-2693-2.

Suski, Jan M.; Braun, Marcin; Strmiska, Vladislav; Sicinski, Piotr (2021): Targeting cell-cycle machinery in cancer. In: *Cancer cell* 39 (6), S. 759–778. DOI: 10.1016/j.ccell.2021.03.010.

Suzuki, A.; Tsutomi, Y.; Miura, M.; Akahane, K. (1999): Caspase 3 inactivation to suppress Fas-mediated apoptosis: identification of binding domain with p21 and ILP and inactivation machinery by p21. In: *Oncogene* 18 (5), S. 1239–1244. DOI: 10.1038/sj.onc.1202409.

Switzer, C. H.; Cheng, R. Y. S.; Vitek, T. M.; Christensen, D. J.; Wink, D. A.; Vitek, M. P. (2011): Targeting SET/I(2)PP2A oncoprotein functions as a multi-pathway strategy for cancer therapy. In: *Oncogene* 30 (22), S. 2504–2513. DOI: 10.1038/onc.2010.622.

Tang, Wei; Dodge, Michael; Gundapaneni, Deepika; Michnoff, Carolyn; Roth, Michael; Lum, Lawrence (2008): A genome-wide RNAi screen for Wnt/beta-catenin pathway components identifies unexpected roles for TCF transcription factors in cancer. In: *Proceedings of the National Academy of Sciences of the United States of America* 105 (28), S. 9697–9702. DOI: 10.1073/pnas.0804709105.

Thomas, Mark P.; Erneux, Christophe; Potter, Barry V. L. (2017): SHIP2: Structure, Function and Inhibition. In: *Chembiochem : a European journal of chemical biology* 18 (3), S. 233–247. DOI: 10.1002/cbic.201600541.

Thompson, Joshua J.; Williams, Christopher S. (2018): Protein Phosphatase 2A in the Regulation of Wnt Signaling, Stem Cells, and Cancer. In: *Genes* 9 (3). DOI: 10.3390/genes9030121.

Thurn, K. Ted; Thomas, Scott; Raha, Paromita; Qureshi, Ian; Munster, Pamela N. (2013): Histone deacetylase regulation of ATM-mediated DNA damage signaling. In: *Molecular cancer therapeutics* 12 (10), S. 2078–2087. DOI: 10.1158/1535-7163.MCT-12-1242.

Townsley, Fiona (1999): PP2A joins the Wnt team. In: *Trends in Cell Biology* 9 (6), S. 214–215. DOI: 10.1016/S0962-8924(99)01589-5.

Uziel, Tamar; Lerenthal, Yaniv; Moyal, Lilach; Andegeko, Yair; Mittelman, Leonid; Shiloh, Yosef (2003): Requirement of the MRN complex for ATM activation by DNA damage. In: *The EMBO journal* 22 (20), S. 5612–5621. DOI: 10.1093/emboj/cdg541.

van Hoof, Christine; Goris, Jozef (2003): Phosphatases in apoptosis: to be or not to be, PP2A is in the heart of the question. In: *Biochimica et biophysica acta* 1640 (2-3), S. 97–104. DOI: 10.1016/s0167-4889(03)00029-6.

Vicente, Carmen; Arriazu, Elena; Martínez-Balsalobre, Elena; Peris, Irene; Marcotegui, Nerea; García-Ramírez, Patricia et al. (2020): A novel FTY720 analogue targets SET-PP2A interaction and inhibits growth of acute myeloid leukemia cells without inducing cardiac toxicity. In: *Cancer letters* 468, S. 1–13. DOI: 10.1016/j.canlet.2019.10.007.

Wang, Jinyu; Zhang, Haitao; Al Shibar, Mohammed; Willard, Belinda; Ray, Alo; Runge, Kurt W. (2018): Rif1 phosphorylation site analysis in telomere length regulation and the response to damaged telomeres. In: *DNA repair* 65, S. 26–33. DOI: 10.1016/j.dnarep.2018.03.001.

Wang, Xiaobin S.; Menolfi, Demis; Wu-Baer, Foon; Fangazio, Marco; Meyer, Stefanie N.; Shao, Zhengping et al. (2021): DNA damage-induced phosphorylation of CtIP at a conserved ATM/ATR site T855 promotes lymphomagenesis in mice. In: *Proceedings of the National Academy of Sciences of the United States of America* 118 (38). DOI: 10.1073/pnas.2105440118.

Wanner, Emma; Thoppil, Harikrishnan; Riabowol, Karl (2020): Senescence and Apoptosis: Architects of Mammalian Development. In: *Frontiers in cell and developmental biology* 8, S. 620089. DOI: 10.3389/fcell.2020.620089.

Wlodarchak, Nathan; Xing, Yongna (2016): PP2A as a master regulator of the cell cycle. In: *Critical reviews in biochemistry and molecular biology* 51 (3), S. 162–184. DOI: 10.3109/10409238.2016.1143913.

Wu, Dianqing; Pan, Weijun (2010): GSK3: a multifaceted kinase in Wnt signaling. In: *Trends in biochemical sciences* 35 (3), S. 161–168. DOI: 10.1016/j.tibs.2009.10.002.

Wu, Donglu; Qiu, Ye; Jiao, Yunshuang; Qiu, Zhidong; Da Liu (2020): Small Molecules Targeting HATs, HDACs, and BRDs in Cancer Therapy. In: *Frontiers in oncology* 10, S. 560487. DOI: 10.3389/fonc.2020.560487.

Xu, N.; Libertini, S.; Black, E. J.; Lao, Y.; Hegarat, N.; Walker, M.; Gillespie, D. A. (2012): Cdk-mediated phosphorylation of Chk1 is required for efficient activation and full checkpoint proficiency in response to DNA damage. In: *Oncogene* 31 (9), S. 1086–1094. DOI: 10.1038/onc.2011.310.

Yamazaki, Satoshi; Ishii, Aii; Kanoh, Yutaka; Oda, Masako; Nishito, Yasumasa; Masai, Hisao (2012): Rif1 regulates the replication timing domains on the human genome. In: *The EMBO journal* 31 (18), S. 3667–3677. DOI: 10.1038/emboj.2012.180.

Yang, Vincent W. (2018): The Cell Cycle. In: Hamid M. Said, Fayez K. Ghishan, Jonathan D. Kaunitz, Juanita L. Merchant und Jack D. Wood (Hg.): Physiology of the gastrointestinal tract. Sixth edition. London: Elsevier/Academic Press, S. 197–219.

Yue, Jingyin; Vendramin, Roberto; Liu, Fan; Lopez, Omar; Valencia, Monica G.; Gomes Dos Santos, Helena et al. (2020): Targeted chemotherapy overcomes drug resistance in melanoma. In: *Genes & development* 34 (9-10), S. 637–649. DOI: 10.1101/gad.333864.119.

Zhan, Jun; Easton, John B.; Huang, Shile; Mishra, Ashutosh; Xiao, Limin; Lacy, Eilyn R. et al. (2007): Negative regulation of ASK1 by p21Cip1 involves a small domain that includes Serine 98 that is phosphorylated by ASK1 in vivo. In: *Molecular and cellular biology* 27 (9), S. 3530–3541. DOI: 10.1128/MCB.00086-06.

Zhang, Wen; Yang, Jun; Liu, Yajuan; Chen, Xi; Yu, Tianxin; Jia, Jianhang; Liu, Chunming (2009): PR55 alpha, a regulatory subunit of PP2A, specifically regulates PP2A-mediated beta-catenin dephosphorylation. In: *The Journal of biological chemistry* 284 (34), S. 22649–22656. DOI: 10.1074/jbc.M109.013698.

Zhang, Ya; Wang, Xin (2020): Targeting the Wnt/β-catenin signaling pathway in cancer. In: *Journal of hematology & oncology* 13 (1), S. 165. DOI: 10.1186/s13045-020-00990-3.

Zhao, H.; Piwnica-Worms, H. (2001): ATR-mediated checkpoint pathways regulate phosphorylation and activation of human Chk1. In: *Molecular and cellular biology* 21 (13), S. 4129–4139. DOI: 10.1128/MCB.21.13.4129-4139.2001.

Zhao, Jianyun; Xie, Chengzhi; Edwards, Holly; Wang, Guan; Taub, Jeffrey W.; Ge, Yubin (2017): Histone deacetylases 1 and 2 cooperate in regulating BRCA1, CHK1, and RAD51 expression in acute myeloid leukemia cells. In: *Oncotarget* 8 (4), S. 6319–6329. DOI: 10.18632/oncotarget.14062.

Zou, Lee; Elledge, Stephen J. (2003): Sensing DNA damage through ATRIP recognition of RPA-ssDNA complexes. In: *Science (New York, N.Y.)* 300 (5625), S. 1542–1548. DOI: 10.1126/science.1083430.

Zuo, Zanwen; Zhou, Zerong; Chang, Yuzhou; Liu, Yan; Shen, Yuping; Li, Qizhang; Zhang, Lei (2024): Ribonucleotide reductase M2 (RRM2): Regulation, function and

targeting strategy in human cancer. In: *Genes & Diseases* 11 (1), S. 218–233. DOI: 10.1016/j.gendis.2022.11.022.

Zwaenepoel, Karen; Goris, Jozef; Erneux, Christophe; Parker, Peter J.; Janssens, Veerle (2010): Protein phosphatase 2A PR130/B''alpha1 subunit binds to the SH2 domain-containing inositol polyphosphate 5-phosphatase 2 and prevents epidermal growth factor (EGF)-induced EGF receptor degradation sustaining EGF-mediated signaling. In: *FASEB journal : official publication of the Federation of American Societies for Experimental Biology* 24 (2), S. 538–547. DOI: 10.1096/fj.09-140228.

Zwaenepoel, Karen; Louis, Justin V.; Goris, Jozef; Janssens, Veerle (2008): Diversity in genomic organisation, developmental regulation and distribution of the murine PR72/B'' subunits of protein phosphatase 2A. In: *BMC genomics* 9, S. 393. DOI: 10.1186/1471-2164-9-393.

8 Supplementary

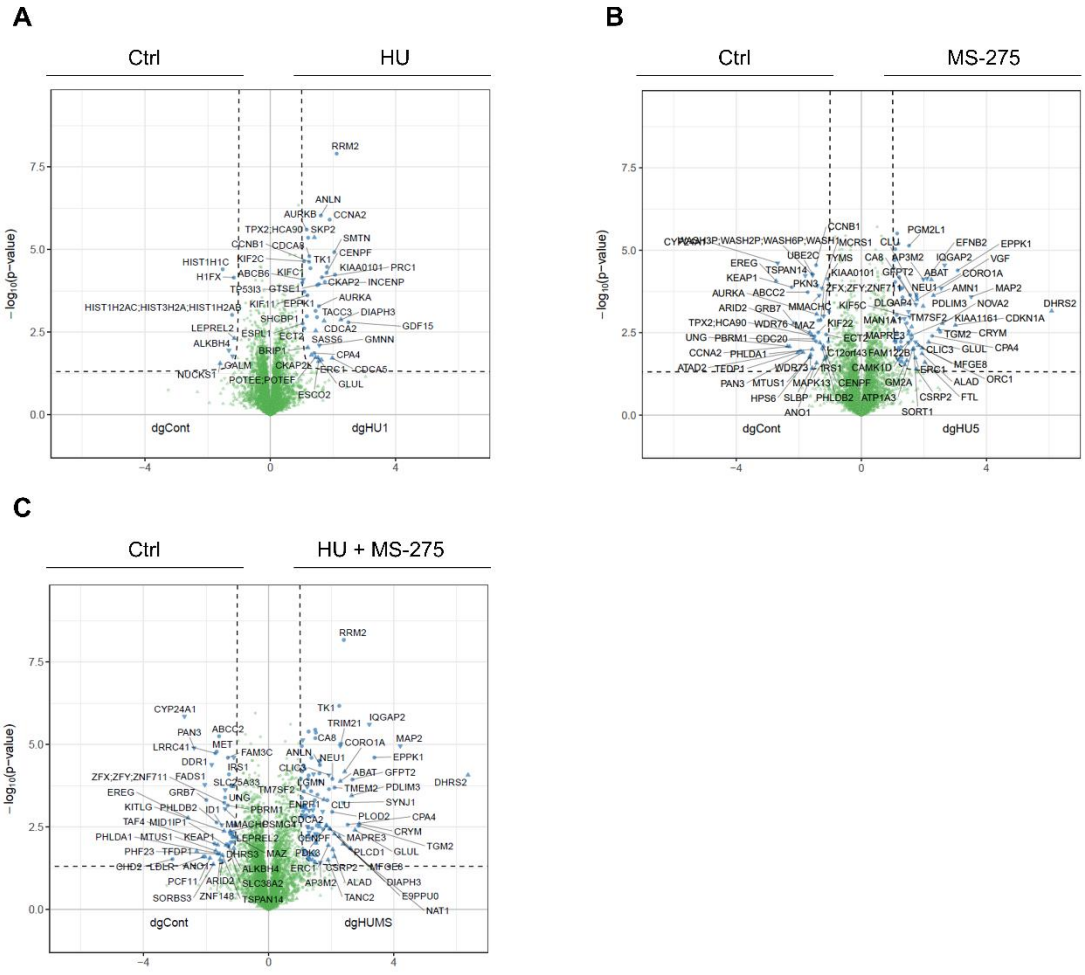

Supplementary Figure 8.1: Volcano blots of HCT116$^{\Delta gRNA}$ cells upon replication stress and HDACi. Cells were treated with 1 mM HU ± 5 µM MS-275 for 24 h. Cell lysates were subjected to mass spectrometry (kindly performed by [redacted]; n=4). **A** Untreated vs. HU; **B** Untreated vs. MS-275; **C** Untreated vs. HU + MS-275.

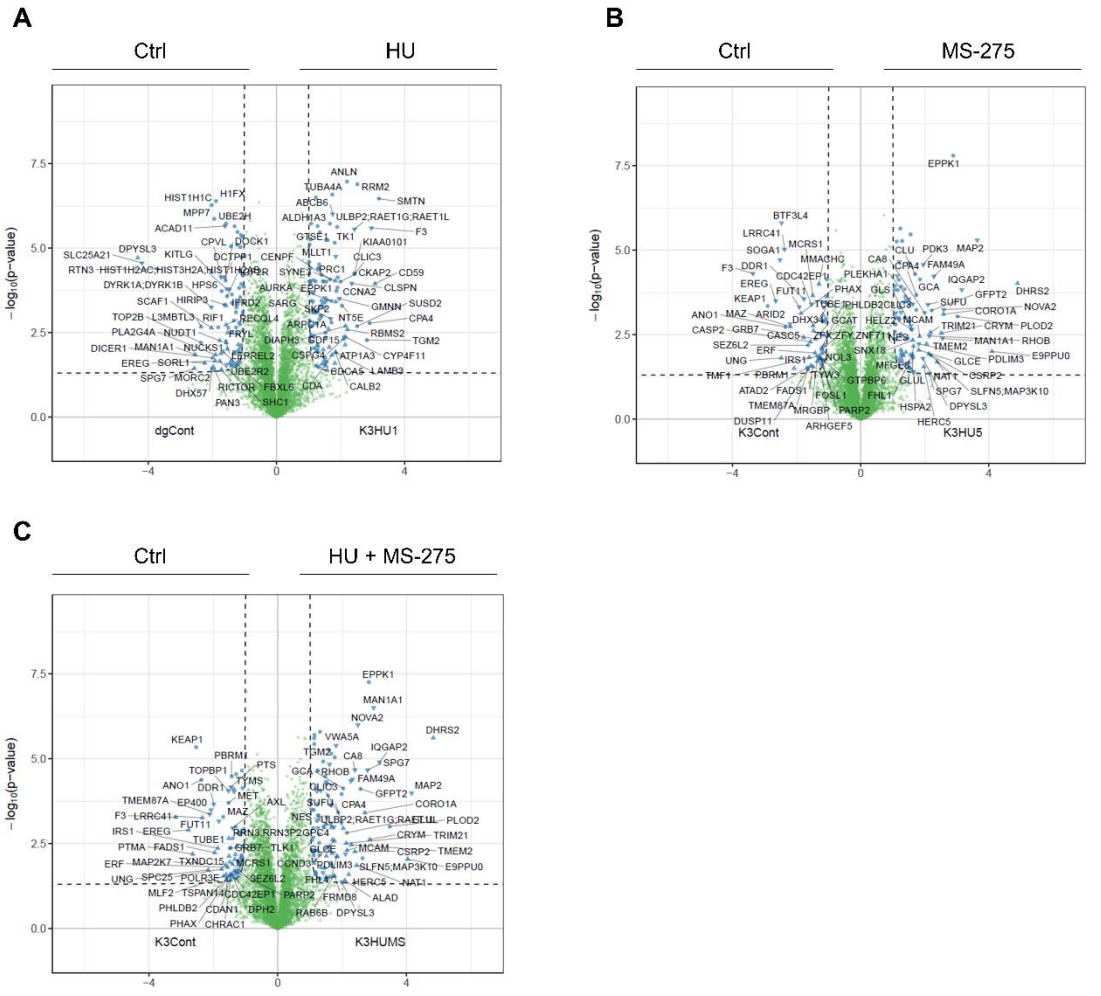

Supplementary Figure 8.2: Volcano blots of HCT116$^{\Delta PR130}$ cells upon replication stress and HDACi. Cells were treated with 1 mM HU ± 5 µM MS-275 for 24 h. Cell lysates were subjected to mass spectrometry (kindly performed by [redacted]; n=4). **A** Untreated vs. HU; **B** Untreated vs. MS-275; **C** Untreated vs. HU + MS-275.

A

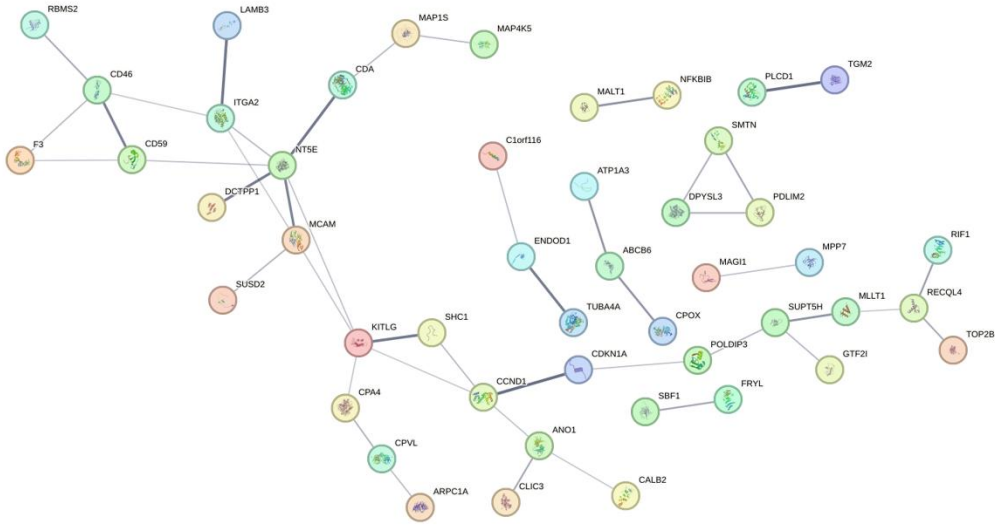
RBMS2
LAMB3
MAP1S
MAP4K5
CD46
CDA
ITGA2
MALT1
NFKBIB
PLCD1
TGM2
F3
CD59
NT5E
C1orf116
SMTN
ATP1A3
DPYSL3
PDLIM2
DCTPP1
MCAM
ENDOD1
ABCB6
MAGI1
MPP7
RIF1
SUSD2
TUBA4A
CPOX
SUPT5H
MLLT1
RECQL4
KITLG
SHC1
POLDIP3
GTF2I
TOP2B
CDKN1A
CCND1
CPA4
SBF1
FRYL
ANO1
CPVL
CLIC3
CALB2
ARPC1A

B

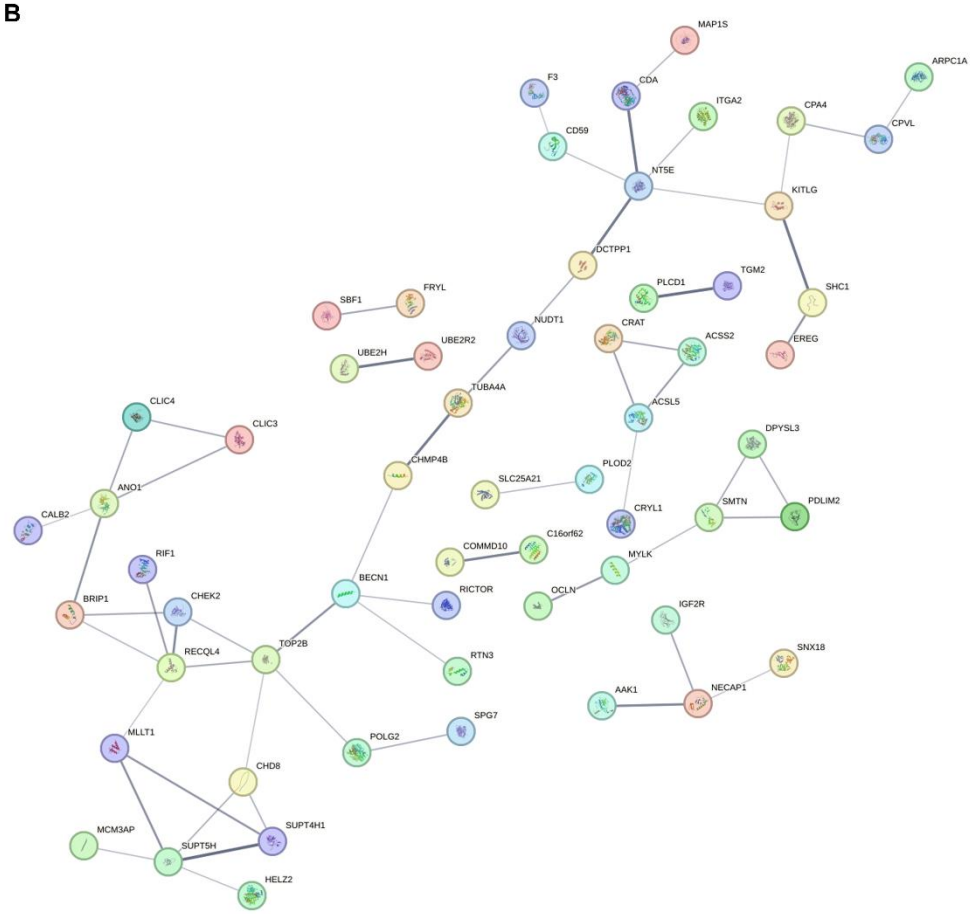
MAP1S
ARPC1A
F3
CDA
ITGA2
CPA4
CPVL
CD59
NT5E
KITLG
DCTPP1
PLCD1
TGM2
SHC1
SBF1
FRYL
NUDT1
CRAT
ACSS2
EREG
UBE2H
UBE2R2
TUBA4A
ACSL5
CLIC4
CLIC3
DPYSL3
CHMP4B
PLOD2
SLC25A21
ANO1
CRYL1
SMTN
PDLIM2
CALB2
COMMD10
C16orf62
MYLK
RIF1
BECN1
OCLN
RICTOR
IGF2R
BRIP1
CHEK2
TOP2B
SNX18
RECQL4
RTN3
AAK1
NECAP1
SPG7
MLLT1
POLG2
CHD8
SUPT4H1
MCM3AP
SUPT5H
HELZ2

C

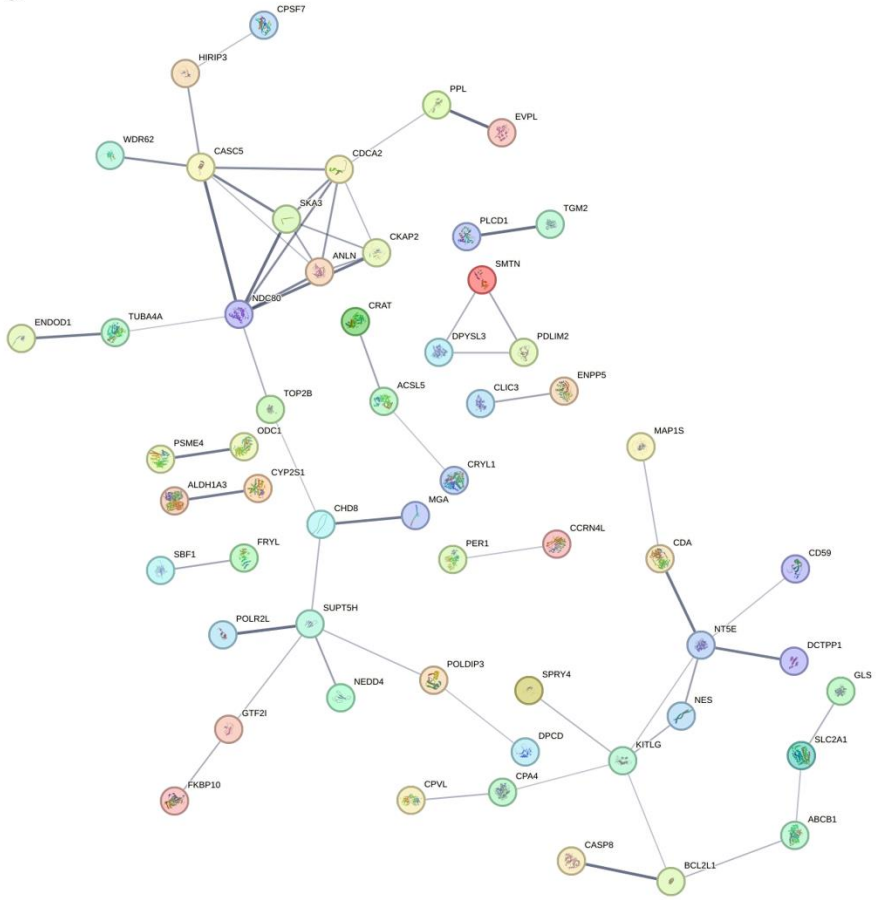
CPSF7
HIRIP3
PPL
EVPL
WDR62
CASC5
CDCA2
SKA3
PLCD1
TGM2
CKAP2
ANLN
SMTN
NDC80
ENDOD1
TUBA4A
CRAT
DPYSL3
PDLIM2
TOP2B
ACSL5
CLIC3
ENPP5
ODC1
MAP1S
PSME4
CRYL1
CYP2S1
ALDH1A3
CHD8
MGA
CCRN4L
PER1
CDA
CD59
SBF1
FRYL
SUPT5H
POLR2L
NT5E
DCTPP1
POLDIP3
SPRY4
GLS
NEDD4
NES
GTF2I
DPCD
KITLG
SLC2A1
FKBP10
CPVL
CPA4
ABCB1
CASP8
BCL2L1

D

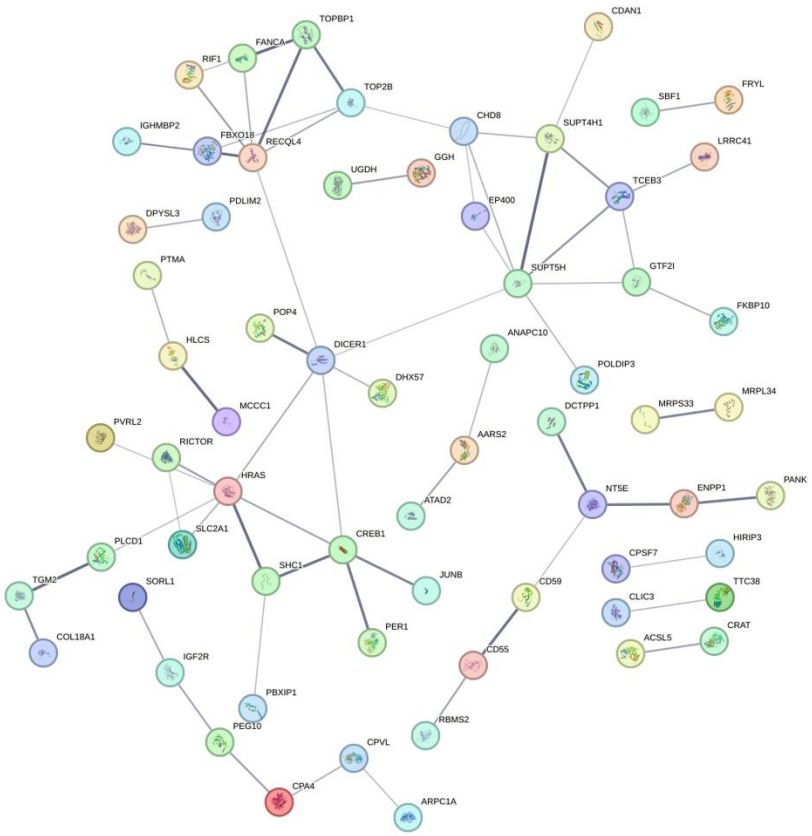

Supplementary Figure 8.3: STRING-analysis of significantly upregulated proteins in HCT116$^{\Delta gRNA}$ and HCT116$^{\Delta PR130}$ cells. Cells were treated with 1 mM HU ± 5 µM MS-275. Upregulated proteins are shown in one figure for both cell lines upon untreated (**A**), HU-treated (**B**), MS-275-treated (**C**), and HU+MS-275-treated (**D**) conditions. Lines display a direct interaction between proteins. Figure was created using https://string-db.org/.

Supplementary Table 1: HALLMARK_MYC_TARGETS_V1.

SYMBOL	RANK IN GENE LIST	RANK METRIC SCORE	RUNNING ES	CORE ENRICHMENT
U2AF1	7288	0.774	-0.2173	No
CTPS1	11246	0.333	-0.3365	No
HSPD1	12180	0.261	-0.3621	No
PRDX4	13017	0.200	-0.3855	No
EXOSC7	13152	0.191	-0.3871	No
EEF1B2	13888	0.137	-0.4082	No
CDC45	14519	0.096	-0.4266	No
CUL1	14762	0.083	-0.4330	No
COPS5	15223	0.057	-0.4466	No
HDAC2	15806	0.025	-0.4645	No
RFC4	15992	0.017	-0.4700	No
TYMS	15995	0.017	-0.4699	No
SNRPA1	16220	0.008	-0.4768	No
NOP56	16238	0.007	-0.4772	No
EIF3D	16463	-0.001	-0.4842	No
NME1	16589	-0.006	-0.4880	No
AIMP2	16633	-0.008	-0.4892	No
SRSF2	18009	-0.026	-0.5319	No
RPS10	18047	-0.028	-0.5327	No
RPL34	18089	-0.030	-0.5335	No
IFRD1	18176	-0.034	-0.5358	No
PSMA1	18492	-0.049	-0.5449	No
XPOT	18533	-0.050	-0.5455	No
RPL6	18954	-0.073	-0.5576	No
ORC2	19018	-0.077	-0.5586	No
PABPC4	19161	-0.086	-0.5618	No
SRSF7	19243	-0.091	-0.5631	No
DUT	19362	-0.097	-0.5655	No
NCBP1	19497	-0.105	-0.5682	No
GNL3	19542	-0.107	-0.5681	No
RPS6	19655	-0.114	-0.5701	No
PSMA6	19723	-0.118	-0.5706	No
UBE2E1	19832	-0.124	-0.5723	No
RPS5	19887	-0.127	-0.5722	No
SSB	19956	-0.131	-0.5725	No
RACK1	20034	-0.136	-0.5731	No
LSM2	20159	-0.142	-0.5750	No
USP1	20228	-0.146	-0.5752	No
CBX3	20312	-0.151	-0.5757	No
MRPL23	20386	-0.155	-0.5759	No
HNRNPD	20509	-0.162	-0.5775	Yes
SRSF1	20545	-0.165	-0.5763	Yes
HNRNPA2B1	20646	-0.170	-0.5771	Yes
NOP16	20665	-0.171	-0.5753	Yes

IMPDH2	20746	-0.176	-0.5754	Yes
RPL14	20774	-0.177	-0.5739	Yes
NCBP2	20783	-0.177	-0.5717	Yes
XPO1	20814	-0.179	-0.5702	Yes
TRA2B	20825	-0.180	-0.5680	Yes
BUB3	20893	-0.184	-0.5676	Yes
RPS3	20906	-0.185	-0.5655	Yes
MYC	20936	-0.187	-0.5638	Yes
ACP1	20967	-0.189	-0.5622	Yes
RPLP0	21185	-0.199	-0.5663	Yes
SSBP1	21196	-0.200	-0.5638	Yes
G3BP1	21214	-0.201	-0.5616	Yes
PPIA	21565	-0.222	-0.5695	Yes
CANX	21591	-0.224	-0.5673	Yes
RPS2	21614	-0.226	-0.5649	Yes
RNPS1	21789	-0.237	-0.5671	Yes
CDC20	21797	-0.237	-0.5640	Yes
FAM120A	21899	-0.244	-0.5639	Yes
HNRNPC	21933	-0.245	-0.5616	Yes
TUFM	21964	-0.247	-0.5591	Yes
HSPE1	22028	-0.251	-0.5577	Yes
PSMD7	22047	-0.251	-0.5548	Yes
CDK2	22117	-0.256	-0.5535	Yes
TXNL4A	22121	-0.257	-0.5500	Yes
PSMA2	22129	-0.258	-0.5467	Yes
POLD2	22200	-0.261	-0.5454	Yes
NAP1L1	22228	-0.263	-0.5426	Yes
RPL18	22267	-0.266	-0.5402	Yes
SYNCRIP	22290	-0.267	-0.5372	Yes
TARDBP	22376	-0.273	-0.5361	Yes
TCP1	22553	-0.284	-0.5378	Yes
EIF4A1	22651	-0.289	-0.5369	Yes
CAD	22660	-0.289	-0.5332	Yes
SF3B3	22737	-0.295	-0.5315	Yes
COX5A	22884	-0.304	-0.5319	Yes
PSMC6	22963	-0.309	-0.5301	Yes
SRPK1	22972	-0.310	-0.5262	Yes
VDAC3	22988	-0.311	-0.5224	Yes
SLC25A3	22989	-0.311	-0.5181	Yes
MCM5	23170	-0.323	-0.5193	Yes
LDHA	23202	-0.325	-0.5159	Yes
MCM6	23206	-0.325	-0.5115	Yes
EIF4E	23314	-0.333	-0.5103	Yes
CSTF2	23367	-0.337	-0.5073	Yes
RAN	23388	-0.339	-0.5033	Yes
CYC1	23398	-0.340	-0.4990	Yes
SRSF3	23417	-0.340	-0.4949	Yes

RRP9	23436	-0.342	-0.4908	Yes
SNRPD3	23492	-0.346	-0.4878	Yes
PCNA	23533	-0.349	-0.4842	Yes
SNRPD2	23567	-0.352	-0.4805	Yes
RUVBL2	23609	-0.355	-0.4769	Yes
CCNA2	23615	-0.356	-0.4722	Yes
PGK1	23617	-0.356	-0.4674	Yes
PSMD14	23662	-0.360	-0.4638	Yes
DEK	23674	-0.361	-0.4593	Yes
SNRPB2	23703	-0.363	-0.4552	Yes
MAD2L1	23742	-0.366	-0.4514	Yes
SF3A1	23749	-0.367	-0.4465	Yes
EIF2S2	23758	-0.368	-0.4418	Yes
MCM4	23781	-0.370	-0.4374	Yes
CCT7	23785	-0.370	-0.4324	Yes
TFDP1	23825	-0.373	-0.4286	Yes
HNRNPU	23833	-0.374	-0.4237	Yes
MRPS18B	23863	-0.376	-0.4194	Yes
HNRNPA3	23944	-0.383	-0.4167	Yes
TRIM28	23977	-0.385	-0.4125	Yes
PSMD3	24007	-0.387	-0.4081	Yes
DDX21	24054	-0.390	-0.4042	Yes
PHB2	24078	-0.393	-0.3995	Yes
DDX18	24079	-0.393	-0.3942	Yes
TOMM70	24085	-0.393	-0.3890	Yes
EIF4G2	24170	-0.400	-0.3861	Yes
SERBP1	24206	-0.404	-0.3817	Yes
CCT4	24231	-0.406	-0.3769	Yes
PRDX3	24362	-0.417	-0.3753	Yes
CCT5	24442	-0.424	-0.3720	Yes
PRPS2	24507	-0.430	-0.3681	Yes
HNRNPR	24560	-0.436	-0.3638	Yes
MCM7	24576	-0.438	-0.3582	Yes
KPNA2	24706	-0.451	-0.3561	Yes
HNRNPA1	24714	-0.451	-0.3502	Yes
PRPF31	24739	-0.455	-0.3447	Yes
STARD7	24744	-0.455	-0.3386	Yes
RPL22	24745	-0.455	-0.3324	Yes
PSMA7	24747	-0.455	-0.3262	Yes
EIF3J	24759	-0.456	-0.3203	Yes
VDAC1	24765	-0.457	-0.3143	Yes
RAD23B	24782	-0.457	-0.3085	Yes
MRPL9	24789	-0.459	-0.3024	Yes
GSPT1	24852	-0.466	-0.2980	Yes
EIF1AX	24854	-0.466	-0.2917	Yes
PPM1G	24870	-0.468	-0.2857	Yes
PHB	24881	-0.470	-0.2796	Yes

LSM7	24904	-0.472	-0.2739	Yes
NDUFAB1	25014	-0.487	-0.2706	Yes
KPNB1	25020	-0.487	-0.2641	Yes
SNRPD1	25022	-0.487	-0.2575	Yes
CCT2	25053	-0.491	-0.2518	Yes
DHX15	25058	-0.492	-0.2452	Yes
RRM1	25060	-0.492	-0.2385	Yes
ETF1	25208	-0.508	-0.2361	Yes
EIF3B	25214	-0.509	-0.2293	Yes
MCM2	25236	-0.512	-0.2230	Yes
PWP1	25242	-0.513	-0.2161	Yes
SMARCC1	25259	-0.515	-0.2096	Yes
CNBP	25334	-0.526	-0.2047	Yes
CLNS1A	25366	-0.530	-0.1985	Yes
HDDC2	25371	-0.530	-0.1914	Yes
XRCC6	25396	-0.533	-0.1848	Yes
SNRPA	25457	-0.545	-0.1793	Yes
CCT3	25469	-0.547	-0.1721	Yes
GOT2	25490	-0.551	-0.1652	Yes
PSMD8	25501	-0.553	-0.1580	Yes
PABPC1	25594	-0.563	-0.1532	Yes
HPRT1	25623	-0.567	-0.1463	Yes
PSMA4	25798	-0.591	-0.1437	Yes
YWHAQ	25818	-0.594	-0.1362	Yes
PSMD1	25838	-0.597	-0.1286	Yes
PCBP1	25897	-0.605	-0.1222	Yes
PA2G4	25936	-0.610	-0.1150	Yes
APEX1	25937	-0.611	-0.1067	Yes
VBP1	25961	-0.613	-0.0990	Yes
C1QBP	25968	-0.613	-0.0908	Yes
RSL1D1	26048	-0.625	-0.0848	Yes
YWHAE	26100	-0.632	-0.0777	Yes
FBL	26101	-0.632	-0.0691	Yes
NHP2	26125	-0.637	-0.0611	Yes
NOLC1	26153	-0.641	-0.0532	Yes
UBA2	26154	-0.642	-0.0444	Yes
SRM	26165	-0.644	-0.0359	Yes
HSP90AB1	26214	-0.654	-0.0285	Yes
EIF2S1	26223	-0.656	-0.0198	Yes
SNRPG	26294	-0.668	-0.0129	Yes
AP3S1	26376	-0.689	-0.0060	Yes
ILF2	26383	-0.691	0.0033	Yes
PTGES3	26394	-0.694	0.0124	Yes
EIF4H	26469	-0.717	0.0199	Yes
SET	26494	-0.721	0.0290	Yes
PSMC4	26521	-0.728	0.0381	Yes
NPM1	26542	-0.734	0.0475	Yes

GLO1	26554	-0.737	0.0573	Yes
UBE2L3	26621	-0.758	0.0656	Yes
CDK4	26641	-0.763	0.0754	Yes
POLE3	26689	-0.781	0.0846	Yes
PSMB3	26706	-0.785	0.0948	Yes
HDGF	26732	-0.793	0.1049	Yes
ODC1	27073	-0.862	0.1060	Yes
ERH	27136	-0.868	0.1159	Yes
RANBP1	29658	-0.996	0.0507	Yes
PSMB2	29713	-1.012	0.0628	Yes
ABCE1	29857	-1.036	0.0725	Yes

Supplementary Table 2: REACTOME: APC-C-MEDIATED DEGRADATION OF CELL CYCLE PROTEINS.

SYMBOL	RANK IN GENE LIST	RANK METRIC SCORE	RUNNING ES	CORE ENRICHMENT
PSME2	8458	0.603	-0.2467	No
ANAPC4	9714	0.468	-0.2727	No
ANAPC16	9758	0.464	-0.2611	No
FBXO5	11938	0.281	-0.3212	No
CCNA1	12841	0.214	-0.3433	No
CDC16	13195	0.188	-0.3490	No
ANAPC5	13607	0.157	-0.3574	No
SKP2	13751	0.146	-0.3578	No
ANAPC1	14398	0.104	-0.3750	No
CUL1	14762	0.083	-0.3840	No
AURKB	15355	0.049	-0.4011	No
CDC14A	15755	0.027	-0.4128	No
CDK1	15944	0.020	-0.4181	No
PSME1	16229	0.007	-0.4267	No
RB1	18447	-0.046	-0.4945	No
PSMB9	18460	-0.047	-0.4936	No
PSMA1	18492	-0.049	-0.4932	No
ANAPC15	18543	-0.050	-0.4933	No
FZR1	18980	-0.075	-0.5048	No
BTRC	19238	-0.091	-0.5103	No
RPS27A	19548	-0.108	-0.5169	No
PSMA6	19723	-0.118	-0.5190	No
UBE2E1	19832	-0.124	-0.5189	No
ANAPC10	20150	-0.141	-0.5248	No
PSMD4	20365	-0.154	-0.5272	No
BUB3	20893	-0.184	-0.5385	Yes
ANAPC7	21002	-0.190	-0.5365	Yes
UBE2D1	21005	-0.190	-0.5313	Yes
PSMD6	21068	-0.194	-0.5278	Yes
UBB	21457	-0.216	-0.5338	Yes

ANAPC2	21612	-0.225	-0.5323	Yes
UBA52	21613	-0.226	-0.5260	Yes
CDC20	21797	-0.237	-0.5251	Yes
PSMD7	22047	-0.251	-0.5258	Yes
CDK2	22117	-0.256	-0.5208	Yes
CDC27	22126	-0.257	-0.5138	Yes
PSMA2	22129	-0.258	-0.5067	Yes
PSMB1	22427	-0.276	-0.5082	Yes
ANAPC11	22777	-0.297	-0.5108	Yes
PSMC6	22963	-0.309	-0.5079	Yes
PSMB4	23227	-0.327	-0.5070	Yes
CDC23	23258	-0.330	-0.4987	Yes
PSMC3	23391	-0.339	-0.4933	Yes
AURKA	23515	-0.348	-0.4874	Yes
PSMC2	23557	-0.351	-0.4788	Yes
CCNA2	23615	-0.356	-0.4707	Yes
SEM1	23655	-0.359	-0.4619	Yes
PSMD14	23662	-0.360	-0.4520	Yes
MAD2L1	23742	-0.366	-0.4442	Yes
UBC	23849	-0.375	-0.4370	Yes
PSMD10	23850	-0.376	-0.4265	Yes
PSMF1	23978	-0.385	-0.4197	Yes
PSMD3	24007	-0.387	-0.4097	Yes
PSMD5	24019	-0.388	-0.3992	Yes
PSMD2	24040	-0.389	-0.3890	Yes
PSMC1	24201	-0.403	-0.3827	Yes
CCNB1	24596	-0.439	-0.3827	Yes
PSMA7	24747	-0.455	-0.3746	Yes
PSMC5	24901	-0.472	-0.3662	Yes
PSME3	24948	-0.478	-0.3542	Yes
PTTG1	24975	-0.482	-0.3416	Yes
PSMA5	24990	-0.484	-0.3285	Yes
PSMD9	25002	-0.485	-0.3152	Yes
UBE2C	25037	-0.489	-0.3026	Yes
PSMA3	25118	-0.499	-0.2912	Yes
BUB1B	25136	-0.501	-0.2777	Yes
PSMB7	25374	-0.530	-0.2703	Yes
PLK1	25387	-0.532	-0.2557	Yes
PSMD8	25501	-0.553	-0.2438	Yes
PSMD13	25611	-0.565	-0.2314	Yes
PSMB6	25719	-0.578	-0.2186	Yes
PSMD12	25769	-0.585	-0.2037	Yes
PSMA4	25798	-0.591	-0.1881	Yes
PSMD1	25838	-0.597	-0.1726	Yes
PSMD11	26192	-0.650	-0.1654	Yes
PSMB5	26239	-0.659	-0.1484	Yes
NEK2	26278	-0.663	-0.1310	Yes

PSME4	26326	-0.675	-0.1136	Yes
SKP1	26407	-0.701	-0.0965	Yes
PSMC4	26521	-0.728	-0.0797	Yes
UBE2S	26675	-0.775	-0.0628	Yes
PSMB3	26706	-0.785	-0.0417	Yes
CDC26	26767	-0.807	-0.0210	Yes
PSMB11	28036	-0.974	-0.0333	Yes
PSMB2	29713	-1.012	-0.0572	Yes
PSMB8	30252	-1.351	-0.0362	Yes
PSMB10	30626	-1.572	-0.0039	Yes
PSMA8	31122	-1.864	0.0328	Yes

Supplementary Table 3: REACTOME: CDT1 ASSOCIATION WITH THE CDC6 ORC ORIGIN COMPLEX.

SYMBOL	RANK IN GENE LIST	RANK METRIC SCORE	RUNNING ES	CORE ENRICHMENT
PSME2	8458	0.603	-0.2404	No
ORC6	12635	0.229	-0.3617	No
ORC3	14765	0.082	-0.4249	No
MCM8	15996	0.017	-0.4625	No
PSME1	16229	0.007	-0.4695	No
PSMB9	18460	-0.047	-0.5371	No
PSMA1	18492	-0.049	-0.5362	No
ORC2	19018	-0.077	-0.5496	No
ORC5	19394	-0.099	-0.5575	No
RPS27A	19548	-0.108	-0.5582	No
PSMA6	19723	-0.118	-0.5591	No
ORC4	20100	-0.139	-0.5656	No
PSMD4	20365	-0.154	-0.5679	No
ORC1	20730	-0.174	-0.5726	No
PSMD6	21068	-0.194	-0.5757	No
UBB	21457	-0.216	-0.5796	Yes
UBA52	21613	-0.226	-0.5758	Yes
GMNN	21883	-0.243	-0.5750	Yes
PSMD7	22047	-0.251	-0.5705	Yes
PSMA2	22129	-0.258	-0.5632	Yes
PSMB1	22427	-0.276	-0.5620	Yes
PSMC6	22963	-0.309	-0.5669	Yes
PSMB4	23227	-0.327	-0.5626	Yes
PSMC3	23391	-0.339	-0.5548	Yes
CDC6	23516	-0.348	-0.5454	Yes
PSMC2	23557	-0.351	-0.5333	Yes
SEM1	23655	-0.359	-0.5227	Yes
PSMD14	23662	-0.360	-0.5092	Yes
UBC	23849	-0.375	-0.5007	Yes

PSMD10	23850	-0.376	-0.4864	Yes
PSMF1	23978	-0.385	-0.4757	Yes
PSMD3	24007	-0.387	-0.4618	Yes
PSMD5	24019	-0.388	-0.4474	Yes
PSMD2	24040	-0.389	-0.4333	Yes
PSMC1	24201	-0.403	-0.4229	Yes
PSMA7	24747	-0.455	-0.4225	Yes
PSMC5	24901	-0.472	-0.4094	Yes
PSME3	24948	-0.478	-0.3926	Yes
CDT1	24989	-0.484	-0.3754	Yes
PSMA5	24990	-0.484	-0.3570	Yes
PSMD9	25002	-0.485	-0.3389	Yes
PSMA3	25118	-0.499	-0.3235	Yes
PSMB7	25374	-0.530	-0.3113	Yes
PSMD8	25501	-0.553	-0.2942	Yes
PSMD13	25611	-0.565	-0.2761	Yes
PSMB6	25719	-0.578	-0.2574	Yes
PSMD12	25769	-0.585	-0.2367	Yes
PSMA4	25798	-0.591	-0.2151	Yes
PSMD1	25838	-0.597	-0.1936	Yes
PSMD11	26192	-0.650	-0.1799	Yes
PSMB5	26239	-0.659	-0.1562	Yes
PSME4	26326	-0.675	-0.1332	Yes
PSMC4	26521	-0.728	-0.1116	Yes
PSMB3	26706	-0.785	-0.0875	Yes
PSMB11	28036	-0.974	-0.0918	Yes
PSMB2	29713	-1.012	-0.1055	Yes
PSMB8	30252	-1.351	-0.0709	Yes
PSMB10	30626	-1.572	-0.0227	Yes
PSMA8	31122	-1.864	0.0328	Yes

Supplementary Table 4: REACTOME: DEGRADATION OF BETA CATENIN BY THE DESTRUCTION COMPLEX.

SYMBOL	RANK IN GENE LIST	RANK METRIC SCORE	RUNNING ES	CORE ENRICHMENT
PSME2	8458	0.603	-0.2453	No
TLE2	8798	0.565	-0.2388	No
CTBP2	13034	0.199	-0.3647	No
PPP2R5B	13037	0.199	-0.3588	No
FRAT1	13213	0.186	-0.3586	No
TCF7L2	14453	0.100	-0.3942	No
APC	14621	0.091	-0.3966	No
GSK3B	14648	0.090	-0.3947	No
AMER1	14650	0.089	-0.3920	No
CUL1	14762	0.083	-0.3930	No
TLE4	15414	0.045	-0.4119	No
TLE1	15725	0.029	-0.4207	No
TLE5	15940	0.020	-0.4267	No
PSME1	16229	0.007	-0.4355	No
CTBP1	16709	-0.011	-0.4501	No
TLE3	18201	-0.036	-0.4955	No
PSMB9	18460	-0.047	-0.5021	No
PSMA1	18492	-0.049	-0.5016	No
HDAC1	19052	-0.079	-0.5166	No
BTRC	19238	-0.091	-0.5196	No
RPS27A	19548	-0.108	-0.5260	No
PPP2R5D	19662	-0.115	-0.5260	No
PSMA6	19723	-0.118	-0.5243	No
FRAT2	19884	-0.127	-0.5255	No
PSMD4	20365	-0.154	-0.5357	No
MYC	20936	-0.187	-0.5479	No
PSMD6	21068	-0.194	-0.5461	No
UBB	21457	-0.216	-0.5516	Yes
AXIN1	21582	-0.223	-0.5487	Yes
UBA52	21613	-0.226	-0.5428	Yes
PPP2CB	21701	-0.231	-0.5386	Yes
PPP2R5E	21806	-0.238	-0.5346	Yes
PSMD7	22047	-0.251	-0.5345	Yes
PPP2R5A	22079	-0.254	-0.5278	Yes
ZRANB1	22094	-0.255	-0.5205	Yes
PSMA2	22129	-0.258	-0.5138	Yes
PSMB1	22427	-0.276	-0.5147	Yes
CTNNB1	22462	-0.277	-0.5073	Yes
PPP2R1A	22938	-0.307	-0.5128	Yes
PSMC6	22963	-0.309	-0.5042	Yes
PPP2R5C	23159	-0.322	-0.5006	Yes
PSMB4	23227	-0.327	-0.4927	Yes
PPP2R1B	23273	-0.331	-0.4841	Yes

PSMC3	23391	-0.339	-0.4775	Yes
TCF7L1	23523	-0.349	-0.4710	Yes
PSMC2	23557	-0.351	-0.4615	Yes
SEM1	23655	-0.359	-0.4536	Yes
PSMD14	23662	-0.360	-0.4429	Yes
AXIN2	23808	-0.372	-0.4362	Yes
UBC	23849	-0.375	-0.4261	Yes
PSMD10	23850	-0.376	-0.4147	Yes
PPP2CA	23924	-0.381	-0.4054	Yes
PSMF1	23978	-0.385	-0.3954	Yes
PSMD3	24007	-0.387	-0.3846	Yes
PSMD5	24019	-0.388	-0.3732	Yes
PSMD2	24040	-0.389	-0.3621	Yes
PSMC1	24201	-0.403	-0.3548	Yes
PSMA7	24747	-0.455	-0.3580	Yes
PSMC5	24901	-0.472	-0.3485	Yes
PSME3	24948	-0.478	-0.3355	Yes
PSMA5	24990	-0.484	-0.3221	Yes
PSMD9	25002	-0.485	-0.3078	Yes
CSNK1A1	25032	-0.488	-0.2939	Yes
PSMA3	25118	-0.499	-0.2815	Yes
PSMB7	25374	-0.530	-0.2734	Yes
PSMD8	25501	-0.553	-0.2606	Yes
PSMD13	25611	-0.565	-0.2468	Yes
PSMB6	25719	-0.578	-0.2327	Yes
PSMD12	25769	-0.585	-0.2165	Yes
PSMA4	25798	-0.591	-0.1995	Yes
PSMD1	25838	-0.597	-0.1827	Yes
PSMD11	26192	-0.650	-0.1740	Yes
PSMB5	26239	-0.659	-0.1555	Yes
PSME4	26326	-0.675	-0.1377	Yes
SKP1	26407	-0.701	-0.1190	Yes
PSMC4	26521	-0.728	-0.1005	Yes
TCF7	26618	-0.758	-0.0806	Yes
PSMB3	26706	-0.785	-0.0595	Yes
RBX1	26801	-0.821	-0.0376	Yes
PSMB11	28036	-0.974	-0.0466	Yes
PSMB2	29713	-1.012	-0.0682	Yes
PSMB8	30252	-1.351	-0.0441	Yes
PSMB10	30626	-1.572	-0.0082	Yes
PSMA8	31122	-1.864	0.0328	Yes

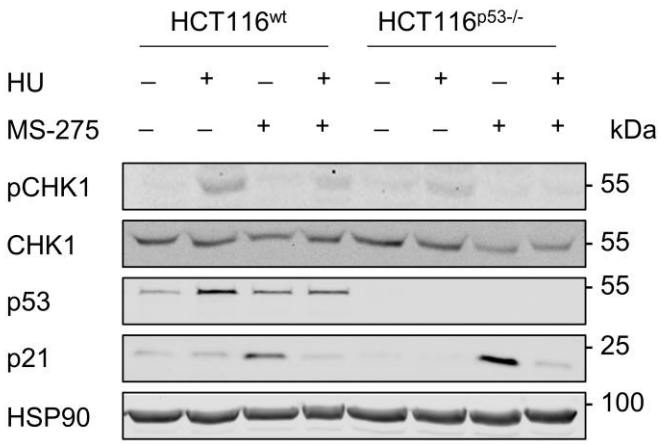

Supplementary Figure 8.4: p53-dependent expression of p21 is independent of HDACi treatment. HCT116^{wt} and HCT116$^{p53-/-}$ cells were treated with 1 mM HU ± 5 µM MS-275 for 24 h. Indicated proteins were analyzed by immunoblot. HSP90 served as loading control.

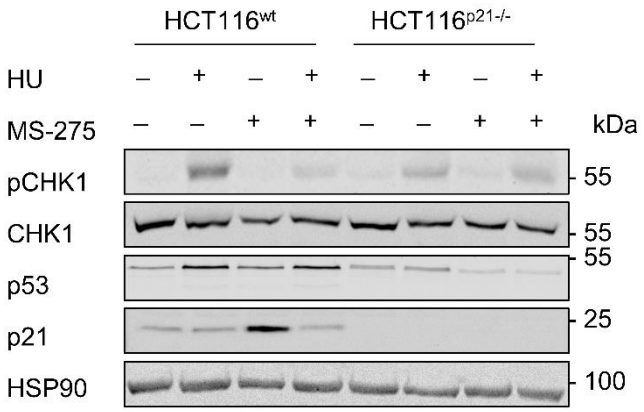

Supplementary Figure 8.5: p21 is essential for efficient CHK1 phosphorylation upon replication stress. HCT116^{wt} and HCT116$^{p21-/-}$ cells were treated with 1 mM HU ± 5 µM MS-275 for 24 h. Indicated proteins were analyzed by immunoblot. HSP90 served as loading control.

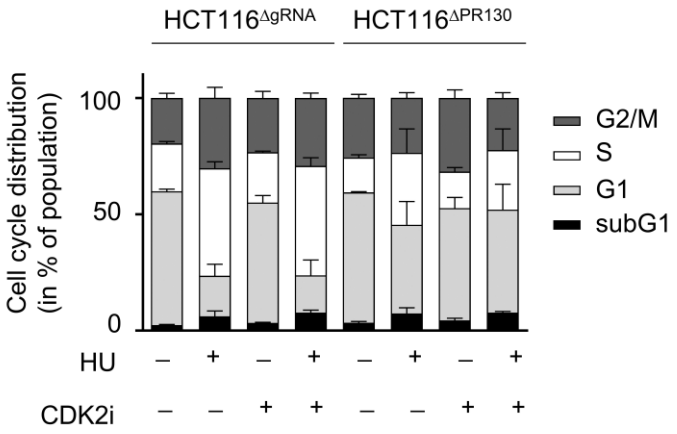

Supplementary Figure 8.6: CDK2 is essential for cell cycle regulation. HCT116$^{\Delta gRNA}$ and HCT116$^{\Delta PR130}$ cells were treated with 1 mM HU ± 5 µM CDK2i for 1 h. Cell cycle analysis of PI-stained cells was carried out on the BD FACS Canto II system (n=3)**.**

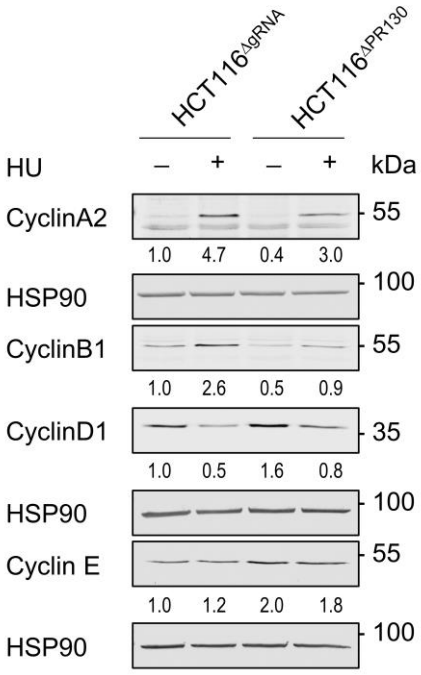

Supplementary Figure 8.7: PR130-dependent expression of cyclins. HCT116$^{\Delta gRNA}$ and HCT116$^{\Delta PR130}$ cells were treated with 1 mM HU ± 5 µM MS-275 for 24 h. Numbers beneath analyzed cyclins indicate densitometric values of the immunoblot signals relative to those of lysates from untreated wild-type cells (normalized to HSP90; loading control).

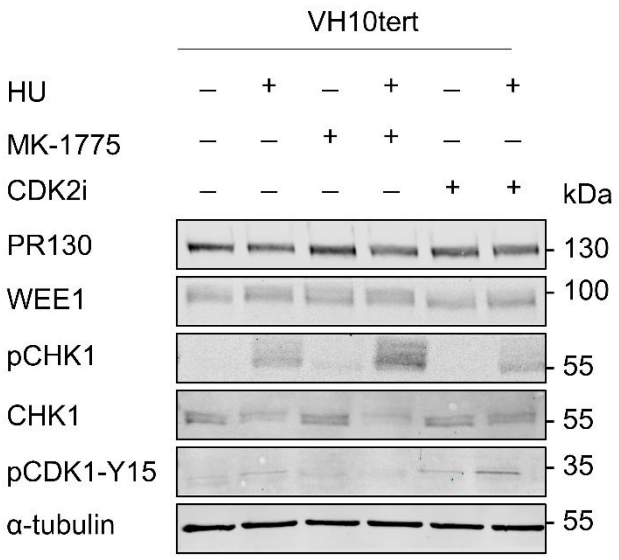

Supplementary Figure 8.8: WEE1 controls phosphorylation of CHK1 via cyclin-dependent kinase CDK2. VH10tert cells were treated with 1 mM HU for 24 h and afterwards with 500 nM MK-1775 or 5 µM CDK2i for 1 h. Indicated proteins were detected by immunoblot.

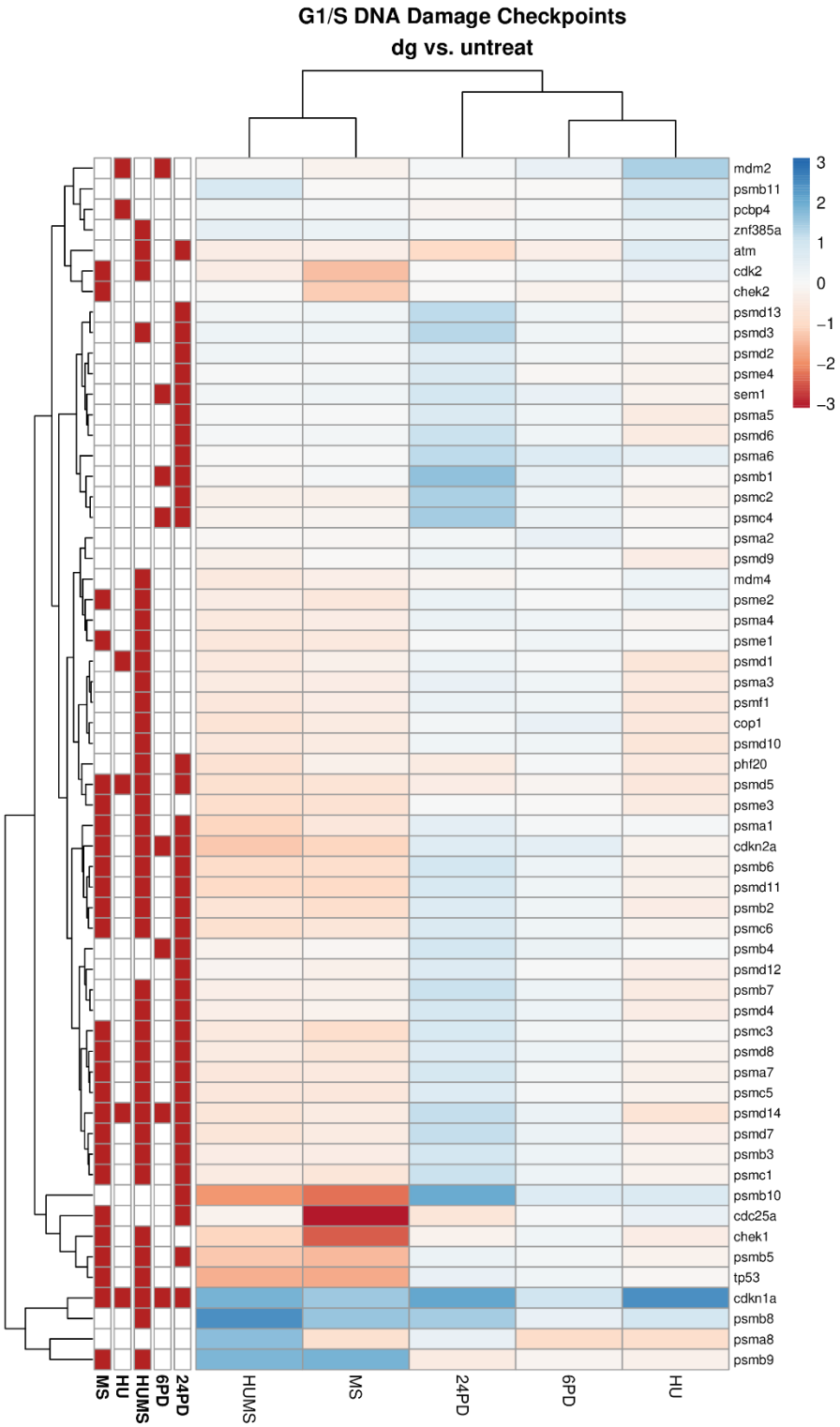

Supplementary Figure 8.9: G1/S DNA damage checkpoints in HCT$^{\Delta gRNA}$ cells upon replication stress and HDACi treatment. HCT$^{\Delta gRNA}$ cells were treated with 1 mM HU ± 5 µM MS-275 for 24 h. mRNAs were analyzed by RNA sequencing (in cooperation with [redacted]). Figure shows the most upregulated mRNAs important for G1/S DNA damage checkpoints.

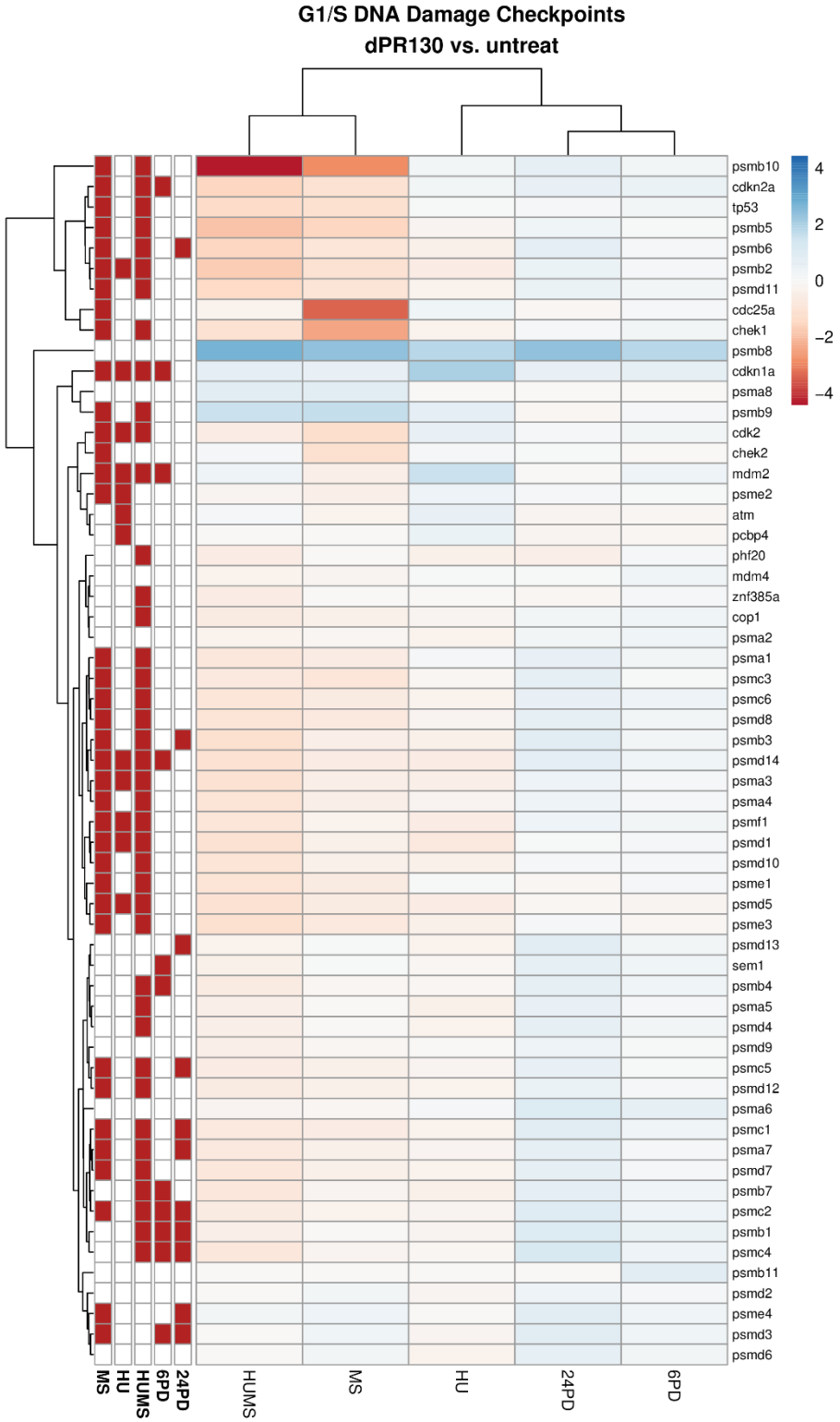

Supplementary Figure 8.10: G1/S DNA damage checkpoints in HCT$^{\Delta PR130}$ cells upon replication stress and HDACi treatment. HCT$^{\Delta PR130}$ cells were treated with 1 mM HU ± 5 µM MS-275 for 24 h. mRNAs were analyzed by RNA sequencing (in cooperation with [redacted]. Figure shows the most upregulated mRNAs important for G1/S DNA damage checkpoints.

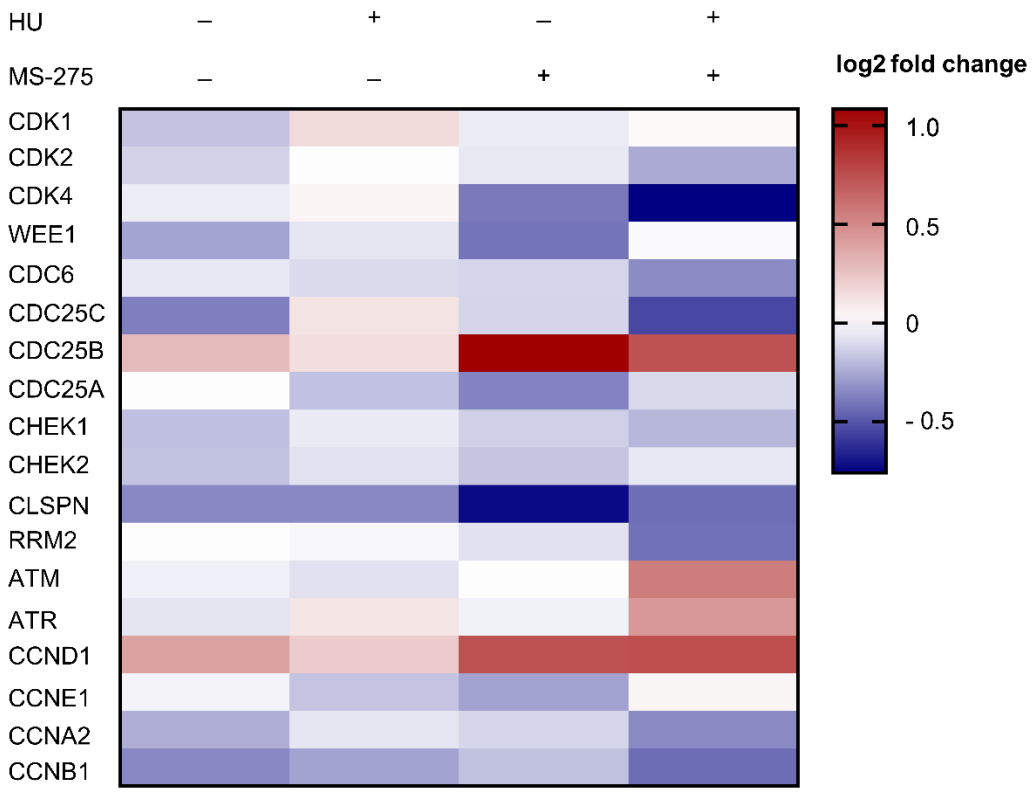

Supplementary Figure 8.11: Heatmap of cell cycle regulators. HCT116$^{\Delta gRNA}$ and HCT116$^{\Delta PR130}$ cells were treated with 1 mM HU ± 5 µM MS-275 for 24 h. RNA sequencing analysis of three independent replicates was carried out using the NextSeq500 system. Heatmap shows log2 fold changes. Shown are the differences between HCT116$^{\Delta gRNA}$ and HCT116$^{\Delta PR130}$ cells (higher expressed in PR130-deficient cells compared to wild-type cells).

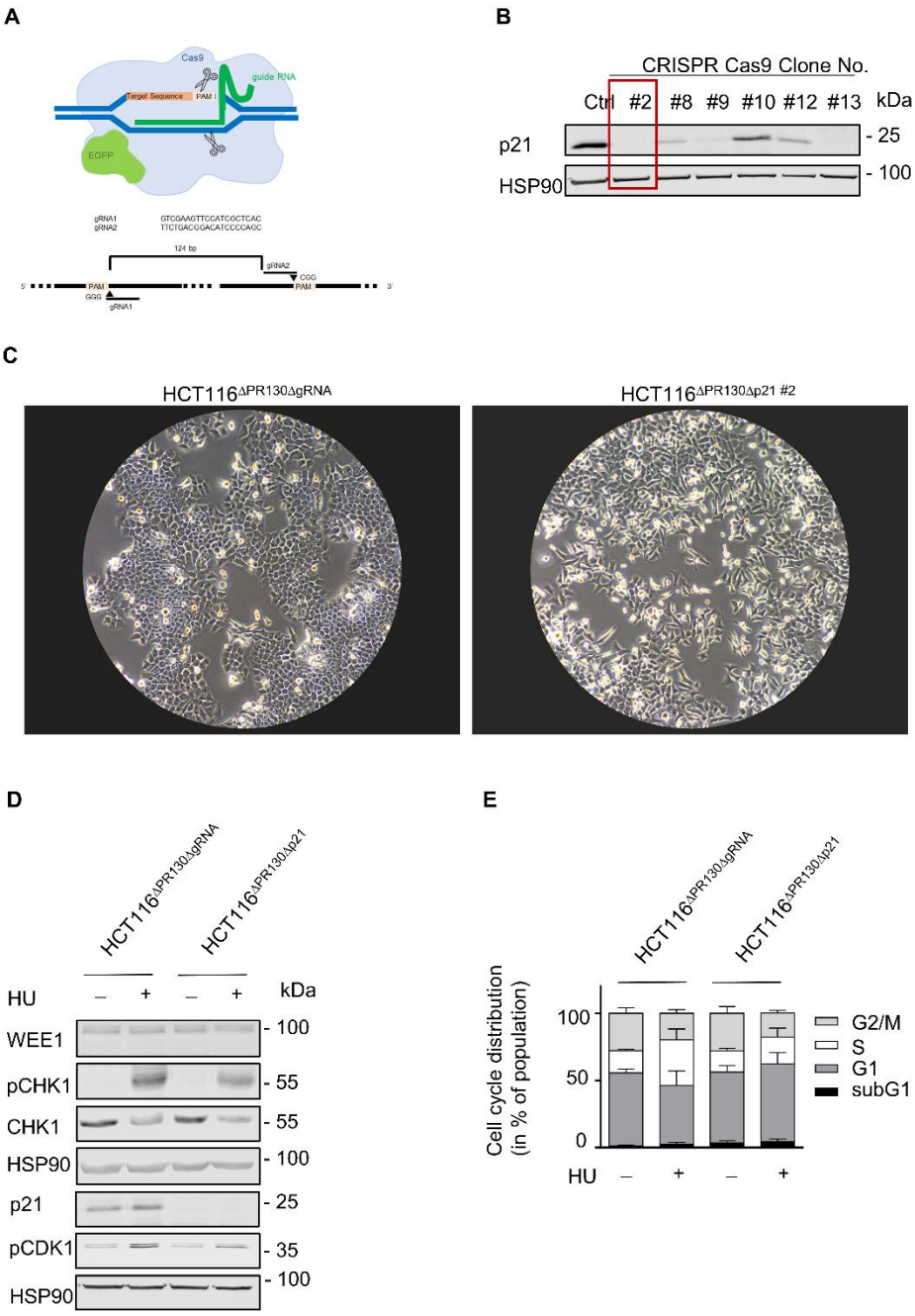

Supplementary Figure 8.12: p21 is essential for efficient checkpoint kinase phosphorylation and cell cycle regulation. A Schematic overview of GFP-Cas9-mediated knockout of p21 in HCT116$^{\Delta PR130}$ cells. Cells were transfected with GFP-Cas9 protein and the indicated gRNA1 and gRNA2. PAM sequences adjacent to the chosen sequences in the *CDKN1A* gene are marked. **B** Selection and analysis of PR130-p21-null CRISPR-Cas9 clones. Whole cell lysates were analyzed by immunoblotting. p21 and HSP90 (loading control) were measured using the Odyssey Imaging system. Clone #2 is marked in red and was chosen for following experiments. **C** Microscopic images of HCT116$^{\Delta PR130\Delta gRNA}$ (CRISPR-Cas9 control; left) and

HCT116$^{\Delta PR130\Delta p21}$ (right) cells (ECHO Rebel; x20). **D** HCT116$^{\Delta PR130\Delta gRNA}$ and HCT116$^{\Delta PR130\Delta p21}$ cells were treated with 1 mM HU for 24 h. Indicated proteins (HSP90 as loading control) were analyzed by western blot. **E** Cells were treated with 1 mM HU for 24 h, stained with PI and analyzed by flow cytometry.

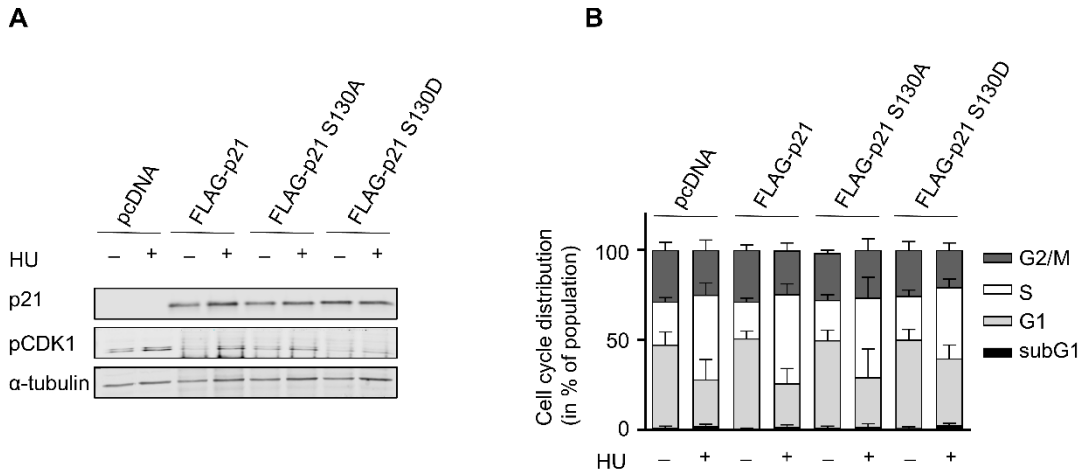

Supplementary Figure 8.13: pp21-S130 controls activity of WEE1. HCT116$^{p21-/-}$ cells were transfected with FLAG-tagged p21, p21 S130 A, p21 S130 D or a vector control (pcDNA3.1) for 24 h. Afterwards, cells were treated with 1 mM HU for 24 h. **A** Proteins were analyzed by immunoblot (HSP90 and α-tubulin = loading controls). **B** Cells were stained with PI and cell cycle was analyzed by flow cytometry.

Supplementary Table 5: p53BP1 and pRIF1 are novel targets of the PP2A-PR130 complex. HCT116$^{\Delta gRNA}$ and HCT116$^{\Delta PR130}$ cells were cultured in light, medium and heavy SILAC medium for 2 weeks. Cells were then treated with 1 mM HU for 24 h. Table shows gene sequences and detected phosphosites of 53BP1 and RIF1.

Gene	Sequence	Phospho-site
53BP1	T(0.005)S(0.005)S(0.005)VLGMS(0.925)VES(0.059)APAVEEE KGEELEQK	124; 129
53BP1	MVIQGPS(0.892)S(0.108)PQGEAMVTDVLEDQKEGR	1113; 1118
53BP1	GSGEKPVS(0.004)APGDDT(0.036)ES(0.96)LHS(1)QGEEEFD MPQPPHGHVLHR	1219; 1224
53BP1	TS(0.002)S(0.998)GTSLSAMHSSGSSGK	1317; 1322; 80
RIF1	LRELDPSLVSANDS(1)PSGMQTR	2161; 435
RIF1	TIGDLST(0.004)LT(0.031)AS(0.965)EIK	2339; 2313; 613
RIF1	ASQGLLSSIENS(0.001)ES(0.974)DS(0.02)S(0.005)EAK	1554
RIF1	KADVQAPVS(0.891)PS(0.102)ET(0.005)S(0.001)QANPYSEGQ FLDEHHSVNFHLGLK	1772; 46

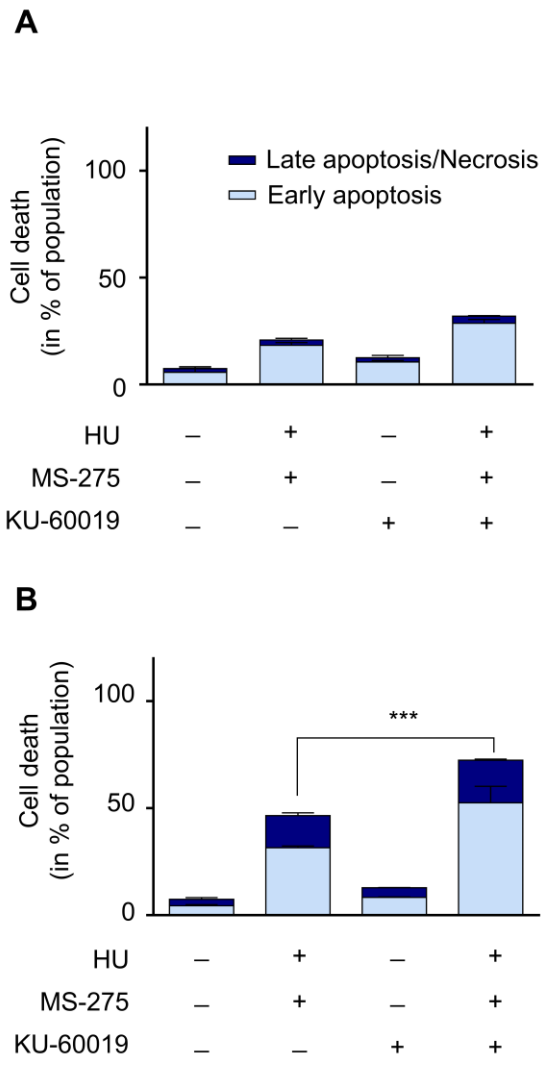

Supplementary Figure 8.14: ATM and NHEJ carry out pro-survival functions. HCT116$^{\Delta PR130}$ cells were treated with 1 mM HU ± 5 µM MS-275 ± 3 µM KU-60019 (1 h pre-treatment) for 24 h (**A**) or 48 h (**B**) and stained with annexin V/PI for cell death analysis. Statistical analysis was done using Two-way ANOVA and Tukey's Multiple Comparison Test (***p<0.001; n=3).

9 Figures

Figures

Figures

10 Tables

11 Danksagung